NEW APPROACHES TO AIRLINE RECOVERY PROBLEMS

BY

JANE LEE

DISSERTATION

Submitted in partial fulfillment of the requirements
for the degree of Doctor of Philosophy in Civil Engineering
in the Graduate College of the
University of Illinois at Urbana-Champaign, 2020

Urbana, Illinois

Doctoral Committee:

Professor Yanfeng Ouyang, Chair
Assistant Professor Lavanya Marla, Director of Research
Associate Professor Cedric Langbort
Assistant Professor Alexandre Jacquillat, Massachusetts Institute of Technology

ABSTRACT

Air traffic disruptions result in fight delays, cancellations, passenger misconnections, creating high costs to aviation stakeholders. This dissertation studies two directions in the area of airline disruption management – an area of significant focus in reducing airlines' operating costs. These directions are: (i) a joint proactive and reactive approach to airline disruption management, and (ii) a dynamic aircraft and passenger recovery approach to evaluate the long-term effects of climate change on airline network recoverability.

Our first direction proposes a joint proactive and reactive approach to airline disruption management, which optimizes recovery decisions in response to realized disruptions and in anticipation of future disruptions. Specifically, it forecasts future disruptions partially and probabilistically by estimating systemic delays at hub airports (and the uncertainty thereof) and ignoring other contingent disruption sources. It formulates a dynamic stochastic integer programming framework to minimize network-wide expected disruption recovery costs. Specifically, our Stochastic Reactive and Proactive Disruption Management (SRPDM) model combines a stochastic queuing model of airport congestion, a fight planning tool from Boeing/Jeppesen and an integer programming model of airline disruption recovery. We develop an online solution procedure based on look-ahead approximation and sample average approximation, which enables the model's implementation in short computational times. Experimental results show that leveraging partial and probabilistic estimates of future disruptions can reduce expected recovery costs by 1-2%, as compared to a baseline myopic approach that uses realized disruptions alone. These benefits are mainly driven by the deliberate introduction of departure holds to reduce expected fuel costs, fight cancellations and aircraft swaps.

Our next direction studies the impact of climate change-imposed constraints on the recoverability of airline networks. We first use models that capture the modified payload-

range curves for different aircraft types under multiple climate change scenarios, and the associated (reduced) aircraft capacities. We next construct a modeling and algorithmic framework that allows for simultaneous and integrated aircraft and passenger recovery that explicitly capture the above-mentioned capacity changes in aircraft at different times of day. Our computational results using the climate model on a worst-case, medium-case, and mild-case climate change scenarios project that daily total airline recovery costs increase on average, by 25% to 55.9% on average ; and by 10.6% to 156% over individual disrupted days. Aircraft-related costs are driven by a huge increase in aircraft swaps and cancelations; and passenger-related costs are driven by increases in disrupted passengers who need to be rebooked on the same or a different airline. Our work motivates the critical need for airlines to systematically incorporate climate change as a factor in the design of aircraft as well as in the design and operations of airline networks.

To my dad.

Contents

Chapter 1

INTRODUCTION

1.1 Motivation

The formation and propagation of operating disruptions across spatial-temporal networks create missed revenue opportunities, resource wastage, employee overtime shifts and reduced customer satisfaction, leading to financial and welfare losses in industries such as supply chains, transportation, telecommunications, and medical services. As a prime example, flight delays and cancellations create significant costs across air traffic networks.

The growth of air traffic operations worldwide has resulted in the routine occurrence of significant disruptions across airline flight networks. These disruptions materialize in the form of flight delays and cancellations, as well as passenger misconnections. Moreover, given the interconnected nature of air traffic operations, they often propagate throughout the airline's network of flights by creating additional disruptions at other airports, thus amplifying their negative impact on airline, passenger and airport operations. The resulting costs of these disruptions can be very significant for all aviation stakeholders. For instance, the overall impact of flight delays was estimated at over $30 billion in the United States in 2007 (Ball et al. 2010). The management of flight disruptions from strategic and operational viewpoints, is therefore one of the foremost objectives of air traffic management and airline

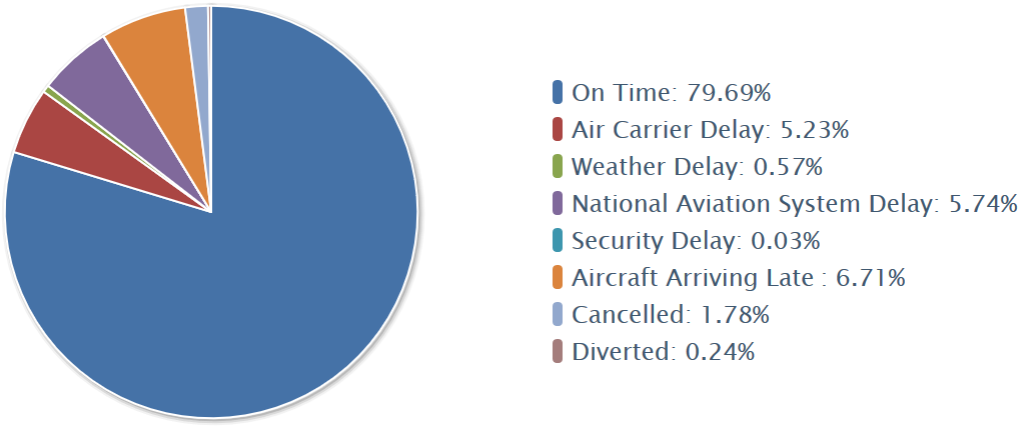

Figure 1.1: Bureau of Transportation Statistics delays by category

operations systems.

The Bureau of Transportation Statistics classifies the causes of disruptions into multiple categories: (i) air carrier delay (delays that are solely the airline's responsibility, such as ground operations,swaps or holds) , (ii) aircraft arriving late delay (due to propagation from previous aircraft), (iii) security delays, (iv) National Aviation System delay (such as airspace congestion and airport congestion), (v) extreme weather delays,(vi) flights canceled and (vii) flights diverted. In the six years spanning March 2014-March 2020, while 79.69% of flights were on time, the remaining flights that were delayed according to these above categories were 5.23%, 0.57%, 5.74%, 0.03%, 6.71%, 1.78% and 0.24% as shown in Figure 1.1.

Delays and disruptions are addressed by addressing their root causes, *before* disruptions occur, such as improved robust schedule construction through improved schedules, aircraft routes and crew pairings, management of the airspace, strategic capacity management at airports and tactical capacity changes using modified runway configurations, improved landing and takeoff policies and improved taxiing and gating policies, and proactively managing weather-induced capacity drops through Ground Delay Programs (GDPs) and Airspace Flow Programs (AFPs). Additionally, many of these methods are complemented by airlines using reactive methods of disruption management, also called recovery, *after* the occurrence

of disruptions.

The focus in this dissertation is on reactive methods of managing airline's networks, which are primarily under the control of the airline, and managed by the airline's Operating Controls Center (OCC). Measures such as aircraft flight holds, swaps, cancelations and flight holds (Marla et al. 2017b) are used to manage these disruptions. We study and propose novel ways of understanding and modifying disruption management practice to achieve greater benefits and evaluate impacts.

This thesis examines airline recovery from two perspectives: (i) a stochastic and dynamic approach to airline disruption management, and (ii) a dynamic aircraft and passenger recovery approach to evaluate the long-term effects of climate change on airline network recoverability.

The first of these modifications involves enhancing reactive disruption management measures using proactive strategic and tactical measures discussed above, which address the root causes of disruptions. Specifically, among the possible measures, we consider tactical airport congestion mitigation measures that manage airport capacities. We utilize methods developed by Jacquillat and Odoni (2015b) that model the patterns and variability of the airport delays due to flight schedule congestion. We incorporate these airport congestion models as future predictions of disruptions, into existing reactive disruption recovery approaches. We propose this problem as a stochastic dynamic programming problem and develop an efficient approximate algorithm to solve this problem in a reasonable time.

Next, we also examine the sensitivity of disruption management to factors such as climate change. As the planet continues to experience increased fluctuations in temperatures, referred to as global warming, as result of human activity (IPCC Report 2014, Santer B. D. et.al. 1996), communities and businesses around the world are expected to be increasingly challenged. The aviation industry will also need to address challenges that climate change is already beginning to inflict. An International Civil Aviation Organization ICAO Report (2016) highlights the impacts that global warming can have on airline operating

costs. The report indicates that shifting wind patterns can have an impact on the optimal flight routes along with increasing fuel consumption. Also, rising sea levels and storms can have an impact on the airports closer to these water bodies. In many instances of high temperature increase-related disruptions, airlines need to operate some aircraft at restricted take-off weights to achieve sufficient lift. This results in lower load and fuel weight allowed to be carried by the aircraft causing significant disruptions in flight schedules for the airlines. These climate change disruptions can cause re-routing and cancellations which can be very costly for airlines.

Our goal is to first estimate the impact of such disruptions on the operating costs of airlines by modeling the climate change disruptions in combination with normally occurring disruptions using real-world data. These results motivate the need to develop airline practices derived from understanding the impact of climate change, which can buffer airlines from climate damage and help make their operations more resilient and sustainable for the long term.

In the following sections, we present the context, contributions and structure for these perspectives. We discuss our stochastic and dynamic approach to recovery in Chapter 2 and passenger recovery under climate change in Chapter 3.

1.2 Thesis Contributions and Structure

1.2.1 Overview of Chapter 2: Stochastic and Dynamic Disruption Management

Airline disruption management interventions can be broadly classified into two categories: reactive and proactive interventions. Proactive interventions stem from the airline robust planning literature: they provide *a priori* operating plans (e.g., flight schedules, aircraft routing and crew pairings) that can respond effectively to future disruptions. However, they do not adjust operating plans dynamically as operating disruptions are realized. Reac-

tive interventions stem from the airline recovery literature: they provide *a posteriori* recovery plans in response to observed disruptions (e.g., whether, when and with which aircraft to operate each flight) to minimize the costs of bringing operations back to normal. However, they do not anticipate future disruptions that are likely to occur across the airline's network of flights—thus potentially resulting in sub-optimal decisions when future operations themselves depart from planned operations.

Deterministic models of airline disruption management that are commonly used in practice do not capture information about potential future state at airports, and therefore, render the recovery decisions myopic and reactive in responding to delay and disruptions. We propose an original approach to disruption management which proactively responds by also anticipating future disruptions in additional to revealed disruptions, and therefore, make decisions which reduce the expected recovery costs.

We develop a dynamic and stochastic optimization model that optimizes recovery decisions, given observed disruptions and the probability distribution of future disruptions. The proposed framework involves network-wide air traffic optimization under airport queueing stochasticity at multiple airports simultaneously, and therefore, results in a large-scale optimization problem. The size of problem increases with the scale of the network, the time horizon of recovery, and the number of potential future disruption scenarios captured.

For solving the large-scale stochastic and dynamic optimization problem, we propose an efficient algorithm that arrives at the optimal solution within reasonable computational time. We demonstrate the performance of the proposed algorithm by using real-world data for our experiments. On average a 1-2% reduction in recovery costs are observed across multiple disruption instances considered. The results demonstrate that our proactive approach provides more cost savings by using the partial information on future disruptions.

1.2.2 Overview of Chapter 3: Passenger Re-accommodation and Aircraft Recovery under Climate Change Considerations

The airline recovery problem we discussed in Chapter 2 has a focus on aircraft recovery in current operating conditions.

In this chapter, our focus is to understand the impact of disruptions due to climate change on airline recovery. To accurately estimate the impact of such disruptions, we first aim to understand how climate change causes aircraft of different sizes to operated at reduced capacities due to reduced lift. We also jointly solve for aircraft and passenger recovery, in a simultaneous rather than sequential manner, allowing us to compute the additional costs associated with passenger re-accommodations resulting from climate change-related disruptions.

First, we develop a large-scale, integrated, aircraft and passenger recovery modeling and algorithmic framework that also captures the dynamic nature of aircraft and passenger recovery at airlines. We show how our approach captures the unique constraints that climate change-related temperature increases impose on each aircraft's ability to operate in the network at specific points in time. Second, we present an algorithm for integrated aircraft and passenger recovery, that runs on a rolling horizon basis, which allows for tactical decision-making when climate change constraints become operational. Our algorithm is designed to mimic real-world airline operations, and captures airline recovery (including inter-fleet swaps), simultaneously integrated with optimally assigning re-accommodations for disrupted passengers.

Our results indicate that, climate change can impact significantly airlines' ability to recover from disruptions. Specifically, through computations on a major US airline, we demonstrate that if a similar network structure and similar load factors as today were operated in 2035 and 2050, airlines' recovery costs can be compounded significantly. Specifically, our estimates for daily airline-recovery related costs in years 2035 and 2050 (during high traffic and high climate change timeframes) range on average from $1.8 million - $2.6 million

and passenger related costs on average range from $2.0 million - $3.1 million depending on the severity of climate change in conjunction with the size of disruptions.

It is evident that global temperatures continue to rise while the aviation industry continues to grow. The combination of the aviation demand increase and climate change will play a significant impact on the global warming itself. To address the problem of climate change and its negative impact on the global economy, airline must have a long-term plan even though its impact today is very limited. Our work motivates the critical need for airlines to systematically incorporate climate change as a factor proactively, in the design of small aircraft as well as in the design and operations of airline networks.

Chapter 2

STOCHASTIC REACTIVE AND PROACTIVE DISRUPTION MANAGEMENT

2.1 Introduction

As described in Chapter 1, in this chapter, we propose an original approach to disruption management that is jointly reactive and proactive—by simultaneously responding to past disruptions and anticipating future disruptions. A major challenge is that future disruptions can only be characterized *probabilistically* and *partially*. First, air traffic operations are subject to significant uncertainty, so disruptions cannot be anticipated in advance exactly and with certainty. Second, operating disruptions stem from systemic and contingent sources. Systemic disruptions arise from congestion resulting from more flights being scheduled than available capacity at busy airports. These disruptions can be estimated by means of stochastic queuing models, as shown by Pyrgiotis et al. (2013) and Jacquillat and Odoni (2015b). Contingent disruptions include other delay sources, such as aircraft maintenance, late crews, late passenger boarding, etc. In comparison, contingent disruptions are very difficult to anticipate. This chapter integrates probabilistic forecasts of systemic disruptions across networks of operations into a dynamic and stochastic optimization framework for airline disruption recovery.

Specifically, this chapter makes the following contributions:

It develops an original approach to network-wide disruption management that proactively leverages partial and probabilistic disruption forecasts into reactive disruption recovery. The approach relies on a dynamic and stochastic optimization model that optimizes recovery decisions, given observed disruptions and the probability distribution of future systemic disruptions. This work thus integrates, for the first time to our knowledge, principles from the robust airline planning literature into the disruption recovery literatures. As compared to existing disruption recovery approaches, the proposed framework results in larger and more complex optimization problems, but can reduce expected disruption costs through more flexible and robust disruption management.

It formulates a Stochastic Reactive and Proactive Disruption Management (SRPDM) model to optimize network-wide airline disruption recovery under airport queuing stochasticity. SRPDM is formulated as a stochastic integer program using a probabilistic time-space network representation. It combines: (i) the stochastic and dynamic queuing model from Jacquillat and Odoni (2015a), which yields the probability distribution of delays over time at each hub airport; (ii) a flight planning tool from Boeing/Jeppesen, which provides routing, speed and altitude options for each flight, along with corresponding flying times and fuel costs; and (iii) the deterministic model of recovery optimization from Marla et al. (2017a). This provides the first model of network-wide air traffic optimization that applies a stochastic queuing model at multiple airports simultaneously.

It develops an efficient approximate algorithm that can solve the SRPDM within reasonable computational times, consistent with the airline disruption recovery literature and with practical implementation requirements. The size of SRPDM increases with the scale of the network, the time horizon of recovery, and the number of systemic disruption scenarios. In realistic instances, the model's sheer size makes direct implementation highly intractable. To solve it efficiently, this work develops an approximate solution algorithm based on look-ahead approximation (by optimizing recovery decisions for a restricted time window) and sample average approximation (by leveraging a sampled set of disruption scenarios). The

algorithm solves SRPDM iteratively over a rolling horizon (we use a one-hour rolling horizon in this chapter, but the proposed algorithm can be applied more or less frequently in practice). Using real-world scheduling data from Delta Air Lines, we show that, at any point in time, the proposed algorithm can solve SRPDM in 3-5 minutes—which is consistent with earlier airline recovery models and with practical requirements. Ultimately, these computational results demonstrate the model's implementability in practice.

It shows that our jointly reactive and proactive approach to disruption management can significantly enhance recovery decisions, as compared to purely reactive approaches. Since our approximate algorithm does not yield solution quality guarantees, we compare the recovery solutions obtained with our modeling and computational framework to those obtained with a myopic baseline approach that does not leverage forecasts of future disruptions. For this comparison, we use disruption realizations derived from real-world data. Results suggest that our approach reduces expected recovery costs by 1–2%. Moreover, we find no disruption instance in which our approach increases recovery costs (it performs either as well as or better than the baseline). Stated differently, our stochastic optimization approach reduces expected operating costs without introducing additional risk in airline recovery. These benefits are mainly driven by deliberately introducing departure holds at key points in the network to reduce expected fuel costs, flight cancellations and aircraft swaps. This approach is particularly beneficial for airlines with concentrated operations at hub airports and with congested hubs. Ultimately, these case study results demonstrate the benefits of proactively leveraging even partial and probabilistic information on future disruptions and applying even an approximate stochastic optimization algorithm to enhance airline recovery decisions.

We review the literatures on robust airline planning and disruption recovery in Section 3.2. We describe our dynamic decision-making approach in Section 2.3. Section 2.4 formulates SRPDM and describes our solution algorithm. Our experimental setting is detailed in Section 2.5. Section 3.5 reports computational results, showing the benefits of the proposed modeling and computational approach. Section 2.8 summarizes our findings and

outlines opportunities for future research.

2.2 Literature Review

The management of flight disruptions is one of the foremost objectives of air traffic management and airline operating systems. Major air traffic management interventions include the optimization of airport operations (Balakrishnan and Chandran 2010, Jacquillat and Odoni 2017, Simaiakis et al. 2014), air traffic flow management (Bertsimas et al. 2011, Vossen et al. 2012), and airport demand management (Jacquillat and Odoni 2015a, Ribeiro et al. 2017, Zografos et al. 2012). From an airline's perspective, minimizing disruptions comprises two main steps: (i) robust airline planning—to reduce its vulnerability to future disruptions (a proactive method) and (ii) disruption recovery—to re-allocate resources and minimize the impact of observed disruptions (a reactive approach). We review these two bodies of work in this section.

Robust airline planning involves optimizing planning decisions (such as flight schedules, fleet assignments, aircraft routings and crew schedules) to minimize the cost of operating disruptions, if and when they occur. This literature includes two main approaches: (i) those that minimize the *impact* of delays, and (ii) those that minimize the *occurrence* of (propagated) delays.

The first category designs strategic plans to respond effectively to future disruptions. Rosenberger et al. (2004) create fleet assignments with 'short cycles' to minimize the ripple effects of cancellations. Smith and Johnson (2006) restrict the number of aircraft types at airports to create swapping opportunities. Sohoni et al. (2011) formulate probabilistic service level constraints, under block-time uncertainty. Arıkan et al. (2013) propose robust scheduling and network planning strategies, under delay propagation uncertainty. Pita et al. (2012) integrate airport congestion estimates into flight scheduling and fleet assignment. Froyland et al. (2013) optimize aircraft routing, given the uncertainty of future disruptions and resulting recovery. Other studies incorporate robustness into crew pairing (Schaefer

et al. 2005, Shebalov and Klabjan 2006, Yen and Birge 2006).

The second category designs strategic plans to minimize delay propagation across flight networks. Lan et al. (2006b) distinguish primary vs. propagated delays, and propose optimization models to prevent delay propagation through aircraft routing (by allocating schedule slack where it is most critical) and schedule retimings (by adjusting flights' departure and arrival times to reduce passenger misconnections). Ahmadbeygi et al. (2010) and Borndörfer et al. (2010) optimize aircraft routings and schedule re-timings to minimize propagated delays. Cadarso and Marín (2011) optimize flight scheduling and fleet assignment to avoid passenger misconnections, by allocating schedule slack accordingly. Dunbar et al. (2012) and Dunbar et al. (2014) optimize aircraft routings and crew pairings to minimize propagated delay—assuming deterministic and stochastic primary delays, respectively. Yan and Kung (2016) use robust optimization to capture the uncertainty on primary delays into the optimization of aircraft routings. Marla et al. (2018) compare chance programming, stochastic programming and robust optimization for aircraft routing.

This chapter departs from this literature in two ways. First, robust airline planning focuses on strategic decisions, made prior to the day of operations in anticipation of future disruptions. In contrast, this chapter optimizes airline recovery decisions, made during the day of operations in response to observed disruptions. Second, the vast majority of the robust airline planning literature focuses on propagated delays (due to insufficient buffers). In this work, we further break down non-propagated (primary) delays into "systemic" and "contingent" delays, and use a queuing model of airport congestion to capture systemic disruptions—in addition to propagated delays.

Airline disruption recovery involves optimizing operating decisions in response to observed disruptions during the day of operations, in order to minimize the costs of bringing operations back to normal. The main recovery levers include, from the least to most disruptive, aircraft and crew swaps (i.e., changes in aircraft-flight assignments and crew pairings), departure holds (i.e., voluntary introduction of flight departure delays), passenger

re-accommodations, and flight cancellations (see Barnhart and Vaze 2015). Typical trade-offs involve operating flights close to their schedule to minimize delays vs. introducing departure holds to ensure connectivity.

Starting with initial aircraft recovery heuristics from Teodorović (1984), researchers have designed large-scale optimization algorithms to deal with realistic problem instances (see, e.g., Cao and Kanafani 1997, Clarke and Naryadi 1995, Jarrah et al. 1993, Yan and Yang 1996). Thengvall et al. (2000) extend basic aircraft recovery models to minimize changes in aircraft routings and to capture airlines' preferences. Rosenberger et al. (2003) jointly optimize departure holds (i.e., flight rescheduling) and aircraft reroutings. Eggenberg et al. (2010) add operational constraints to ensure that the airline can comply with aircraft maintenance, crew recovery, and passenger accommodation requirements. Other studies focused on crew recovery, following aircraft recovery decisions (Lettovský et al. 2000, Wei et al. 1997, Yu et al. 2003).

Subsequent studies integrate the problems of aircraft, crew and passenger recovery. Zhang et al. (2015) address aircraft and crew recovery in sequence. Jozefowiez et al. (2013) and Zhang et al. (2016) present three-step heuristics that sequentially solve schedule recovery, aircraft recovery and passenger recovery. Bratu and Barnhart (2006b) combine aircraft and passenger recovery. Petersen et al. (2012a) propose a fully integrated model of schedule, aircraft, passenger and crew recovery, solved with Benders decomposition, column generation and row generation. Follow-up studies have developed algorithms for large-scale integrated recovery problems, using large-scale neighborhood search (Sinclair et al. 2014a), a reduced time-band representation (Hu et al. 2015), greedy randomized adaptive search (Hu et al. 2016), and row-and-column generation (Maher 2016). Marla et al. (2017a) integrate flight planning (i.e., aircraft routing, flying altitude and speed) into aircraft and passenger recovery—showing that flight planning provides an additional recovery lever.

In contrast with this body of work, our work leverages forecasts of future systemic disruptions—and the uncertainty thereof—into recovery optimization. To our knowledge,

the literature on recovery optimization under uncertainty is limited. Abdelghany et al. (2004) propose a heuristic simulation to project flight delays and Abdelghany et al. (2008) integrate delay uncertainty into a myopic optimization model of disruption recovery. Jafari and Zegordi (2010) dynamically optimize aircraft recovery and passenger re-accommodation, on a relatively small-scale network and with two disruption scenarios. McCarty and Cohn (2018) propose a two-stage stochastic program to pre-emptively change passenger itineraries, before misconnections occur, under uncertainty on delay propagation. Our work shares similarities with this approach but also exhibits two differences: (i) we focus on aircraft recovery, as opposed to passenger recovery, and (ii) we incorporate forecasts of propagated delays as well as systemic delays resulting from airport congestion.

Summary. This chapter augments the prior literature in two major ways:

1. We propose the first jointly reactive and proactive approach to airline disruption management that optimizes aircraft recovery in response to observed disruptions, while anticipating future disruptions (partially and probabilistically). This approach differs from the airline disruption recovery literature by proactively leveraging forecasts of future disruptions. As such, it shares similarities with the robust airline planning literature, but it deals with a tactical disruption recovery problem—as opposed to a strategic planning problem.

2. We integrate probabilistic forecasts of systemic delays arising from demand-capacity imbalances at busy airports—in addition to propagated delays—into disruption management. This is achieved by embedding future disruption scenarios obtained from a stochastic queuing model of airport congestion into a prescriptive optimization framework of disruption recovery.

2.3 Modeling Framework

We now formulate our dynamic decision-making framework for aircraft recovery. The model optimizes recovery and flight planning decisions. Recovery decisions include departure times (i.e., when to operate each flight), aircraft-flight assignments (i.e., whether to "swap" aircraft or not), and flight cancellations. Flight planning decisions include aircraft routing, flying altitude and flying speed. Together, these two sets of decisions determine recovery costs (i.e., delay costs, swap costs and cancellation costs) and flight operating costs. Unlike existing approaches, our framework optimizes these decisions in response to observed disruptions as well as given forecasts of future disruptions—thus providing a jointly reactive and proactive approach to disruption management.

Specifically, disruptions observed at any point in time can be classified into three categories:

- *Propagated disruptions*: past disruptions spreading across spatial-temporal networks, due to insufficient buffers in the schedule to absorb upstream delays.
- *Systemic disruptions*: congestion at hub airports induced by demand-capacity imbalances.
- *Contingent disruptions*: other inefficiencies within airline and passenger operations (e.g., aircraft maintenance, late crews, late passenger boarding).

At any decision time, the decision-maker observes all operating disruptions. However, future disruptions are only known partially and probabilistically. First, our approach (like existing ones) captures propagated disruptions resulting from recovery decisions. Second, our approach (unlike existing ones) considers probabilistic forecasts of systemic disruptions—obtained from a stochastic and dynamic queuing model at hub airports. Third, our approach ignores future contingent disruptions in the optimization, but these still realize randomly at each decision point.

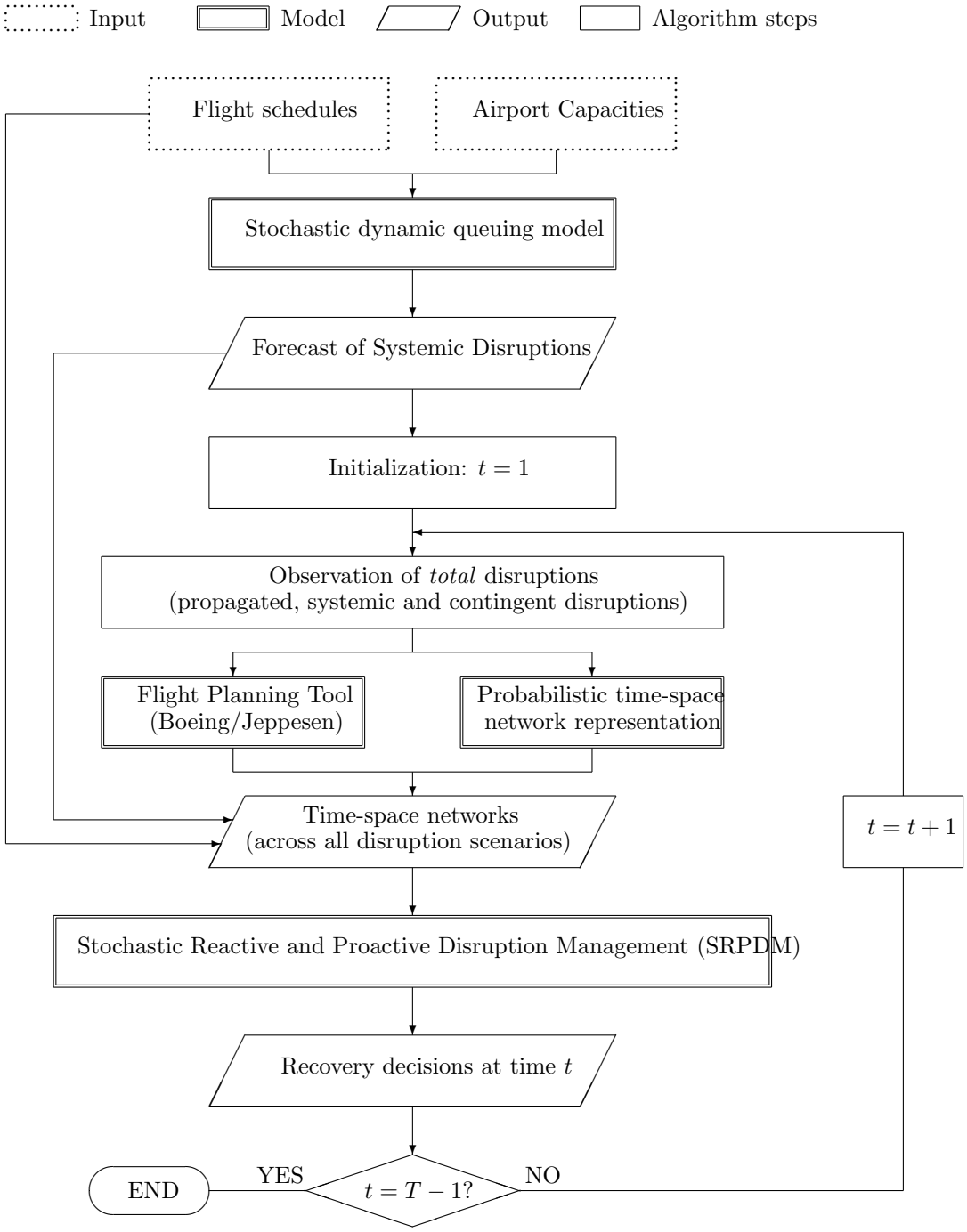

Figure 2.1: Modeling architecture.

Our modeling architecture is shown in Figure 2.1. It starts by applying the stochastic queuing model to generate probabilistic forecasts of systemic disruptions, using data on flight schedules and airport capacities (Section 2.3.1). It then optimizes recovery decisions dynamically. We divide the day into T periods, indexed by $t = 1, \cdots, T$. In each period, the

state of the system is determined from past operations and observed (propagated, systemic and contingent) disruptions. Flight planning options are generated with an engineering tool provided by Boeing/Jeppesen called JetPlan (Section 2.3.2). We represent recovery and flight planning options in a probabilistic time-space network of operations (Section 2.3.3). We then optimize airline recovery decisions to minimize expected recovery costs. This is cast as a dynamic program (Section 2.3.4). However, the size of the problem makes it intractable, so we propose in Section 2.4 a solution procedure based on look-ahead approximation and sample average approximation. This procedure relies on the Stochastic Reactive and Proactive Disruption Management (SRPDM), which optimizes recovery decisions across a sampled set of disruption scenarios for a given look-ahead window. The recovery plan is used to define the state of the system in the next period. The process is repeated until the end of the horizon.

A few observations on our problem are noteworthy. First, the approach developed in this chapter can be applied to any airline network but is likely to be most beneficial for hub-and-spoke airlines. Second, this chapter focuses on schedule and aircraft recovery. We leave the integration of other recovery decisions, such as passenger and crew recovery, into our stochastic optimization framework for future research. In practice, passenger and crew recovery can be optimized subsequently, given the aircraft recovery plan. Last, we solve the aircraft recovery problem for each fleet type independently. This is consistent with the existing literature and current practice—as aircraft swaps typically occur within each fleet to minimize interference with passenger and crew itineraries.

2.3.1 Queuing Model of Systemic Disruptions at Hub Airports

The stochastic and dynamic queuing model is applied at each hub airport to forecast future systemic disruptions. This approach characterizes the airport as a queuing system, in which service is provided by the runway system and aircraft join the system when they are ready to take off or to land. The model takes as inputs the schedule of flights and the

runway capacity at each airport. It returns the probability distribution of flight delays at each time of the day, which is then used to sample disruption scenarios and to construct our time-space networks (see Figure 2.1).

Specifically, we model arrival and departure delays at each airport by means of dynamic and stochastic $M(t)/E_3(t)/1$ queuing models. In other words, the arrival and departure demand processes are both modeled as Poisson processes, and the arrival and departure service processes are modeled as Erlang processes of order 3. The model is non-stationary, i.e., demand and service rates are time-varying to reflect changes in flight schedules and airport capacities over the day. We divide the day of operations into periods of length $S = 15$ minutes. The demand rates (λ_s in period s) are determined by the number of flights scheduled. The service rates (μ_s in period s) are constrained by the airport's capacity. To reflect air traffic operating procedures, we integrate a dynamic programming model that optimizes arrival and departure service rates, under capacity constraints, by selecting runway configurations (i.e., the set of active runways) and balancing arrivals and departures (Jacquillat et al. 2016). This approach approximates the dynamics and magnitude of delays at busy airports with good accuracy (Jacquillat and Odoni 2015b).

The state-transition diagram of the $M(t)/E_3(t)/1$ queuing system is shown in Figure 2.2. It relies on the characterization of an Erlang process of order 3 and rate μ as the succession of 3 Markovian "stages of work", each completed at rate 3μ. The state i defines the number of remaining stages of work. Let u be a time index that varies continuously, and $P_i(u)$ be the probability of being in state i at time u. Equations (2.1)–(2.5) show the system of Chapman-Kolmogorov first-order differential equations describing the evolution of $P_i(u)$ in period s, with u varying between $(s-1)S$ and sS. The practical queue capacity is denoted by N. The system is empty at the beginning of the day. We solve Equations (2.1)–(2.5) using the built-in differential equation solver ode45 in MATLAB 8.1.

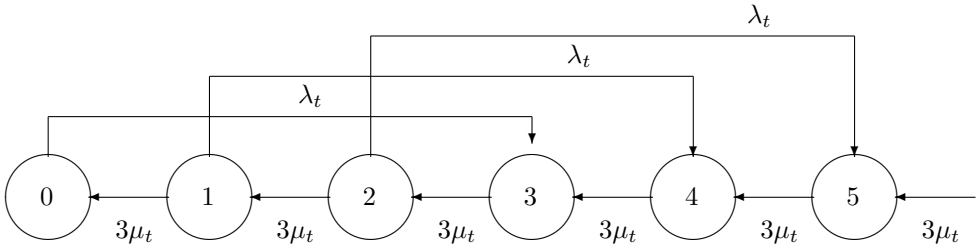

Figure 2.2: State-transition diagram of the $M(t)/E_3(t)/1$ queuing system.

$$\frac{dP_0(u)}{du} = -\lambda_t P_0(u) + k\mu_t P_1(u) \tag{2.1}$$

$$\frac{dP_i(u)}{du} = -(\lambda_t + k\mu_t)P_i(u) + k\mu_t P_{i+1}(u) \qquad \forall i \in \{1, \cdots, k\} \tag{2.2}$$

$$\frac{dP_i(u)}{du} = \lambda_t P_{i-k}(u) - (\lambda_t + k\mu_t)P_i(u) + k\mu_t P_{i+1}(u) \quad \forall i \in \{k+1, \ldots, (N-1)k\} \tag{2.3}$$

$$\frac{dP_i(u)}{du} = \lambda_t P_{i-k}(u) - k\mu_t P_i(u) + k\mu_t P_{i+1}(u) \qquad \forall i \in \{(N-1)k+1, \ldots, kN-1\} \tag{2.4}$$

$$\frac{dP_{kN}(u)}{du} = \lambda_t P_{k(N-1)}(u) - k\mu_t P_{kN}(u) \tag{2.5}$$

We denote the sample space of systemic disruption profiles by $\tilde{\mathcal{Q}}$, indexed by $\tilde{q} = 1, \cdots, \tilde{Q}$, each occurring with a probability $\xi_{\tilde{q}}$. The set $\tilde{\mathcal{Q}}$ includes all queue length combinations in all time periods and at all airports. Across T periods and in a network of K airports, the cardinality of $\tilde{\mathcal{Q}}$ is thus $(N+1)^{2TK}$ (since the arrival and departure queue lengths can each take any of the values $0, \cdots, N$ in each period and at each airport). Even for a short horizon and a small network, integrating the full range of airport congestion outcomes into recovery optimization is highly intractable. Therefore, we will proceed by Monte Carlo sampling to generate representative scenarios from this probability distribution. We denote by $\mathcal{Q}$ the set of such sampled scenarios, indexed by $q = 1, \cdots, Q$.

Two comments on this queuing model are noteworthy. First, the model is applied independently at each airport. This is motivated by the fact that airport operating stochasticity primarily stems from local factors (e.g., variations in flight operations, weather, aircraft

mix, etc.). Second, look-ahead stochastic disruption scenarios are generated once for all periods $t = 1, \cdots, T$. In practice, delays occurring from period t onward obviously depend on realized congestion at period t. However, our approach aims to capture delay forecasts that are *available to an airline*. In the current environment, the level of collaboration between traffic managers and airlines is such that information on the exact number of queuing aircraft at each airport is not publicly shared in real time. Therefore, we adopt a conservative approach that only leverages the information that is available before the day of operations (e.g., the schedule of flights) or can be estimated from historical records of operations (e.g., airport capacity estimates). In future work, this assumption can be relaxed by integrating a dynamic queuing update mechanism into the framework shown in Figure 2.1—thus identifying the benefits resulting from real-time information sharing between operating entities.

2.3.2 Flight Planning

We leverage in this dissertation the JetPlan tool from Boeing/Jeppesen—a flight planning software used by many airlines to plan their flight trajectories prior to departure. JetPlan takes as inputs the flight's scheduled departure and arrival times, anticipated weather patterns, aircraft and engine configurations, and the aircraft's payload (including cargo, passengers, luggage, and fuel). It generates flight planning options (including aircraft routing across waypoints from origin to destination, flight speeds, and flying altitudes) and estimates the resulting fuel costs and travel times. In our framework, JetPlan is used to generate flight copies in the time-space networks (see Figure 2.1).

Specifically, the flight trajectories generated by JetPlan are expressed as a function of an engineering-based metric called the cost-index (CI). CI is defined as the ratio of the flight's time-related costs (determined by the flight's duration and aircraft, passenger and crew connectivities) divided by the fuel cost. CI can be interpreted as the amount of additional fuel worth burning (relative to the minimum fuel burn to operate the flight) to save one unit of time. The most fuel-efficient flight plan is referred to as CI0. The larger the CI value,

the higher the fuel costs and the lower the flying times. Oftentimes, operating all flights at CI0 result in delays and lost connectivity, especially under disruptions; therefore, flights are planned at a slightly higher CI, typically around CI30. In our experiments, we use as discrete inputs corresponding to CI0 (a conservative flight plan), CI30 (the baseline option), CI70, CI100, and CI700 (increasingly aggressive flight plans).

2.3.3 Time-space Network Representation

In each period, we construct a time-space network for each aircraft, comprising all flights that the aircraft can operate by the end of the horizon (period T). This representation starts with the aircraft's current location, observed disruptions, probabilistic forecasts of future systemic disruptions (Section 2.3.1), and possible flight plans (Section 2.3.2). For each flight, the network defines several *copies*, each associated with departure and arrival times and with a flight plan. It is then used to formulate a multi-commodity network flow model, with each aircraft treated as a commodity—enabling to optimize flight-aircraft pairings among a huge number of options (see Figure 2.1).

Figure 2.3 shows an example of such time-space network representation in periods t (Figure 2.3(a)) and $t+1$ (Figure 2.3(b)). Let us denote by $\widehat{\mathcal{NW}}_a^t$ the time-space network in period $t = 1, \cdots, T$ for aircraft $a \in \mathcal{A}$. Each node in $\widehat{\mathcal{NW}}_a^t$ represents a combination of time and location. Each arc represents a possible flight arc (straight line in Figure 2.3) or a ground arc, that is, the aircraft's turnaround from one arrival node to a subsequent departure node at the same airport (curved line). We add a supply node n_s denoting the location and time where the aircraft is currently available, and a demand node n_d representing the end of the aircraft's operation.

Flight copies are widely used in airline recovery, but we highlight here two particular features of our approach. First, flight copies differ not only by departure time (thus capturing recovery decisions, such as departure times, aircraft-flight assignments, and cancellations) but also by flight duration (thus capturing flight planning decisions, such as route, altitude,

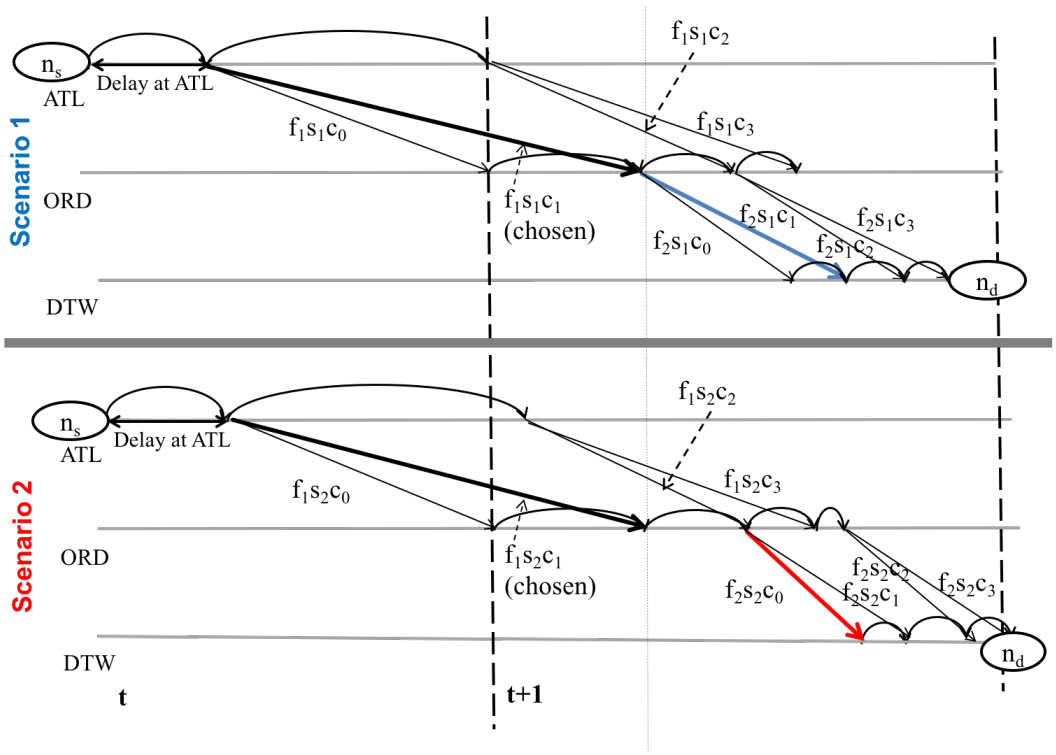

((a)) $\widehat{\mathcal{NW}}^{t}_{aq}$: f_1's operation is realized at time t

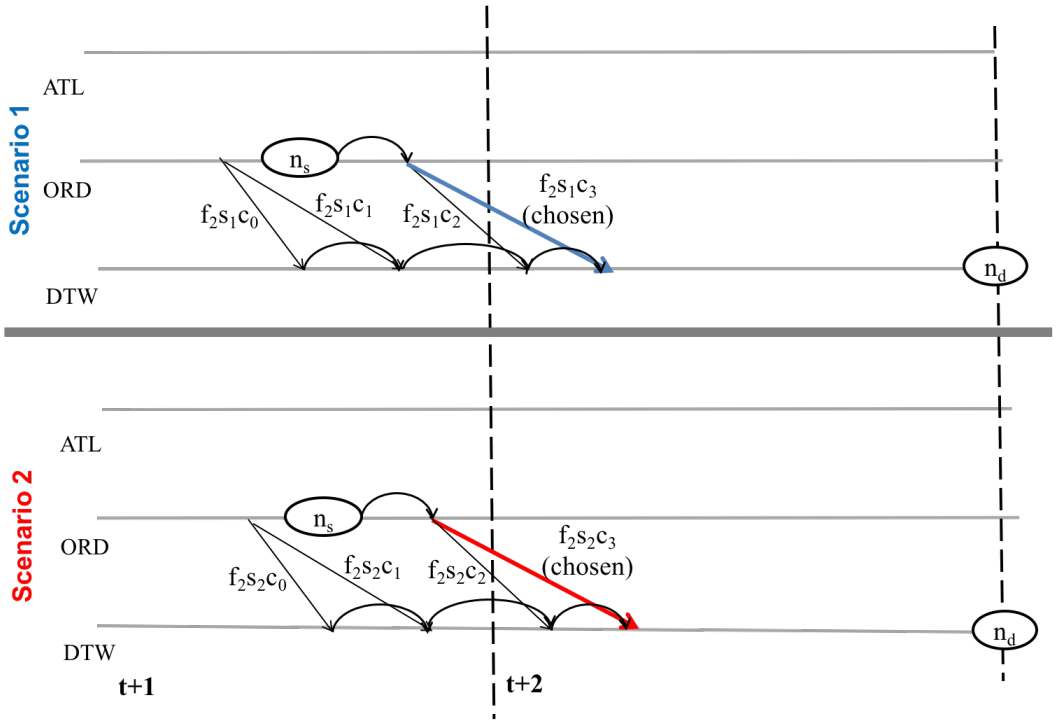

((b)) $\widehat{\mathcal{NW}}^{t+1}_{aq}$: f_2's operation is realized at time $t+1$

Figure 2.3: Example of probabilistic time-space network representation.

speed). This is consistent with the model from Marla et al. (2017a). For instance, in Figure 2.3, flight f_1 has four copies ($f_1s_1c_0$, $f_1s_1c_1$, $f_1s_1c_2$ and $f_1s_1c_3$), where $f_1s_1c_2$ and $f_1s_1c_3$ involve larger departure delays than $f_1s_1c_0$ and $f_1s_1c_1$, and $f_1s_1c_1$ and $f_1s_1c_3$ have a longer en-route time than $f_1s_1c_0$ and $f_1s_1c_2$. Second, our time-space networks are subject to uncertainty regarding future disruptions. Thus, $\widehat{\mathcal{NW}}_a^t$ represents a probabilistic time-space network at this point. In Section 2.4, we shall develop scenario-based time-space network representations. This probabilistic time-space network representation lies at the core of the stochastic approach to airline recovery and flight planning developed in this chapter.

The time-space network representation captures the evolution of the system over time by tracking each aircraft's movement over time and space and creating flight copies based on the latest (propagated, systemic and contingent) disruptions observations. To illustrate the dynamics of the system, the figure shows two scenarios, assumed to be equally probable. Flight f_1 is scheduled to operate in period t, before uncertainty is resolved. Decisions related to flight f_1 thus need to be identical across all scenarios; in our example, copy c_1 is selected. Then, the model anticipates to operate copy c_1 of flight f_2 in scenario 1 (a slower option since departure delay is small) and copy c_0 in scenario 2 (a faster option since departure delay is larger). Figure 2.3(b) shows the state of the system at time $t+1$; the supply node n_s updates the aircraft's availability, depending on prior decisions and realized disruptions. The model is solved again to optimize recovery decisions in period $t+1$—at that point, the operating decision for flight f_2 (namely, operating copy c_3) is identical in scenario 1 and in scenario 2. The process is repeated until the end of the horizon.

2.3.4 Stochastic Optimization Approach

Finally, our stochastic optimization model determines, in each period $t = 1, \cdots, T$, the airline's recovery and flight planning decisions. It takes as inputs the probabilistic time-space networks (Section 2.3.3) of all aircraft (see Figure 2.1). For each flight, it selects at most one copy across all time-space networks—thus ensuring that each flight is either covered

by one aircraft or cancelled.

We cast this problem as a finite-horizon dynamic program. We describe it in this section, and motivate our look-ahead and sample average approximations (detailed in Section 2.4).

Let $\mathcal{F}_t$ denote the set of flights scheduled to depart in period $t = 1, \cdots, T$. Let $\widehat{\mathcal{K}}^t_{fa}$ be the set of copies in the time-space network $\widehat{\mathcal{NW}}^t_a$ associated with flight $f \in \mathcal{F}_t$. Let ρ_k be the fuel cost associated with copy $k \in \widehat{\mathcal{K}}^t_{fa}$ (obtained from the flight plan). Let δ_k be its delay cost (obtained from its departure time). Let σ_k be its swap cost, incurred if aircraft a is different from the one that was originally planned to operate flight f. Let γ_f be the cost of cancelling flight $f \in \mathcal{F}_t$. Note that these cost parameters can capture non-linearities (e.g., non-linear costs of delays).

State variable: The state variable tracks the physical state of the airline's fleet and observed disruptions. The physical state can be represented by two vectors $\boldsymbol{\theta^t}$ and $\boldsymbol{l^t}$, each defined over $a \in \mathcal{A}$. For each aircraft $a \in \mathcal{A}$, θ^t_a and l^t_a denote, respectively, its latest arrival time and its arrival airport. Note that θ^t_a can either correspond to a past time stamp (if aircraft a is on the ground at time t) or a future one (if aircraft a is in the air at time t). Observed disruptions are represented by a vector $\boldsymbol{D^t}$ defined over $f \in \mathcal{F}_t$, where D^t_f denotes the departure delay of flight $f \in \mathcal{F}_t$ observed at time t. The state variable, denoted by $\boldsymbol{R^t}$, is thus given by:

$$\boldsymbol{R^t} = \left(\boldsymbol{\theta^t}, \boldsymbol{l^t}, \boldsymbol{D^t}\right). \tag{2.6}$$

The vector $\boldsymbol{R^t}$ is used to construct the time-space networks $\widehat{\mathcal{NW}}^t_a$ for all $a \in \mathcal{A}$.

Decision variables: All recovery and flight planning decisions are captured by the set of copies selected across all time-space networks $\widehat{\mathcal{NW}}^t_a$ for $a \in \mathcal{A}$. We capture them with two decision vectors $\hat{\boldsymbol{x}}^{\boldsymbol{t}}$ and $\hat{\boldsymbol{z}}^{\boldsymbol{t}}$, where $\hat{\boldsymbol{x}}^{\boldsymbol{t}}$ is defined over $a \in \mathcal{A}$ and $k \in \cup_{f \in \mathcal{F}_t} \widehat{\mathcal{K}}^t_{fa}$ and $\hat{\boldsymbol{z}}^{\boldsymbol{t}}$ is defined over $f \in \mathcal{F}_t$. Specifically, $\hat{x}^t_{ka}$ is equal to 1 if copy k is selected and flown by aircraft

a, and 0 otherwise; and $\hat{z}_f^t$ is equal to 1 if flight f is cancelled, and 0 otherwise. Our decision variable, denoted by $\boldsymbol{U^t}$ given by:

$$\boldsymbol{U^t} = \left(\hat{\boldsymbol{x}}^{\boldsymbol{t}}, \hat{\boldsymbol{z}}^{\boldsymbol{t}}\right). \tag{2.7}$$

Recovery and flight planning decisions are subject to a set of constraints (detailed in Section 2.4). We denote here the decision space by $\boldsymbol{\mathcal{U}^t}$.

Objective function. Our cost function, denoted by $C_t(\boldsymbol{R^t}, \boldsymbol{U^t})$, is defined as the total cost of recovery across all flights $f \in \mathcal{F}_t$, including fuel, delay, swap and cancellation costs. It is given by:

$$C_t(\boldsymbol{R^t}, \boldsymbol{U^t}) = \sum_{a \in \mathcal{A}} \sum_{f \in \mathcal{F}_t} \sum_{k \in \widehat{\mathcal{K}}_{fa}^t} \left(\rho_k + \delta_k + \sigma_k\right) \hat{x}_{ka}^t + \sum_{f \in \mathcal{F}_t} \gamma_f \hat{z}_f^t. \tag{2.8}$$

Transition function: The transition function describes the recovery process and the dynamic realization of disruptions between t and $t+1$. It can be represented by a function f_t as follows:

$$\boldsymbol{R^{t+1}} = f_t\left(\boldsymbol{R^t}, \boldsymbol{U^t}\right). \tag{2.9}$$

The recovery process updates the arrival airport and arrival time of each aircraft a. For example, if a flight is operated by aircraft a from airport K to airport L, then l_a^t is updated to airport L and θ_a^t is updated to its planned arrival time at airport L. Conversely, if an aircraft is not assigned to any departing flight at time t, then its availability remains unchanged. Specifically, we have:

$$(\theta_a^{t+1}, l_a^{t+1}) \quad = \quad \begin{cases} (\theta_a^t, l_a^t), & \text{if } \hat{x}_{ka}^t = 0, \text{ for all } k \in \cup_{f \in \mathcal{F}_t} \widehat{\mathcal{K}}_{fa}^t, \\ (\overline{\theta}_k, \overline{l}_k), & \text{if } \hat{x}_{ka}^t = 1, \text{ for some } k \in \cup_{f \in \mathcal{F}_t} \widehat{\mathcal{K}}_{fa}^t, \end{cases}$$

where $\overline{\theta}_f^k$ and $\overline{l}_f^k$ denote the time and location of arrival of flight copy k, respectively.

Realized disruptions are written as the sum of propagated, systemic and contingent disruptions, denoted respectively by $\overline{\boldsymbol{PD}}^{\boldsymbol{t+1}}$, $\overline{\boldsymbol{SD}}^{\boldsymbol{t+1}}$ and $\overline{\boldsymbol{CD}}^{\boldsymbol{t+1}}$. Specifically, we have:

$$\boldsymbol{D}^{\boldsymbol{t+1}} = \overline{\boldsymbol{PD}}^{\boldsymbol{t+1}} + \overline{\boldsymbol{SD}}^{\boldsymbol{t+1}} + \overline{\boldsymbol{CD}}^{\boldsymbol{t+1}}, \text{ with: } \begin{cases} \overline{\boldsymbol{PD}}^{\boldsymbol{t+1}} \text{ realized from disruption decisions,} \\ \overline{\boldsymbol{SD}}^{\boldsymbol{t+1}} \text{ realized from } \xi \text{ (Section 2.3.1),} \\ \overline{\boldsymbol{CD}}^{\boldsymbol{t+1}} \text{ realized from an unknown distribution.} \end{cases} \tag{2.10}$$

Bellman Equation: Let $J_t(\boldsymbol{R}^{\boldsymbol{t}})$ be the optimal cost-to-go in period t. The terminal cost in period $T+1$ is 0. Therefore, the Bellman equation is given as follows, where the expectation of the future cost-to-go is taken over the probability distribution ξ of future systemic disruptions (Section 2.3.1):

$$J_t(\boldsymbol{R}^{\boldsymbol{t}}) = \min_{\boldsymbol{U}^{\boldsymbol{t}} \in \boldsymbol{\mathcal{U}}^{\boldsymbol{t}}} \left\{ \sum_{a \in \mathcal{A}} \sum_{f \in \mathcal{F}_t} \sum_{k \in \widehat{\mathcal{K}}^t_{fa}} (\rho_k + \delta_k + \sigma_k)\, \hat{x}^t_{ka} + \sum_{f \in \mathcal{F}_t} \gamma_f \hat{z}^t_f + E_\xi \left[J_{t+1} \left(f_t \left(\boldsymbol{R}^{\boldsymbol{t}}, \boldsymbol{U}^{\boldsymbol{t}} \right) | \boldsymbol{R}^{\boldsymbol{t}} \right) \right] \right\}, \tag{2.11}$$

$$J_{T+1}(\boldsymbol{R}^{\boldsymbol{T+1}}) = 0. \tag{2.12}$$

Unfortunately, this Bellman equation is too complex to be solved exactly by backward induction. Indeed, the state space grows exponentially as a function of the number of aircraft and the sample space of systemic disruptions (itself exponentially large), and the decision space grows exponentially as a function of the number of flights, the number of recovery options and the number of flight plans. The dynamic program can thus quickly become computationally intractable for real-sized instances—a well-known "curse of dimensionality" (Powell 2007).

2.4 Solution Approach and SRPDM Formulation

We propose a solution procedure based on *look-ahead approximation* and *sample average approximation* to solve the decision-making problem from Section 2.3. Look-ahead approximation involves estimating the cost-to-go function using a restricted time window, rather than the full horizon (Bertsekas 2005, 2012, Powell 2007). Sample average approximation involves estimating the cost-to-go function using a sampled set of scenarios of future systemic disruptions, rather than their full probability distribution (Kleywegt et al. 2002). At each decision point, we apply our Stochastic Reactive and Proactive Disruption Management (SRPDM) model, formulated as a stochastic integer program in Section 2.4.1. SRPDM optimizes recovery decisions for the look-ahead horizon based on the sampled disruption scenarios. Similar solution approaches have been applied to such problems as vehicle routing (Secomandi 2001) and job shop scheduling (Meloni et al. 2004).

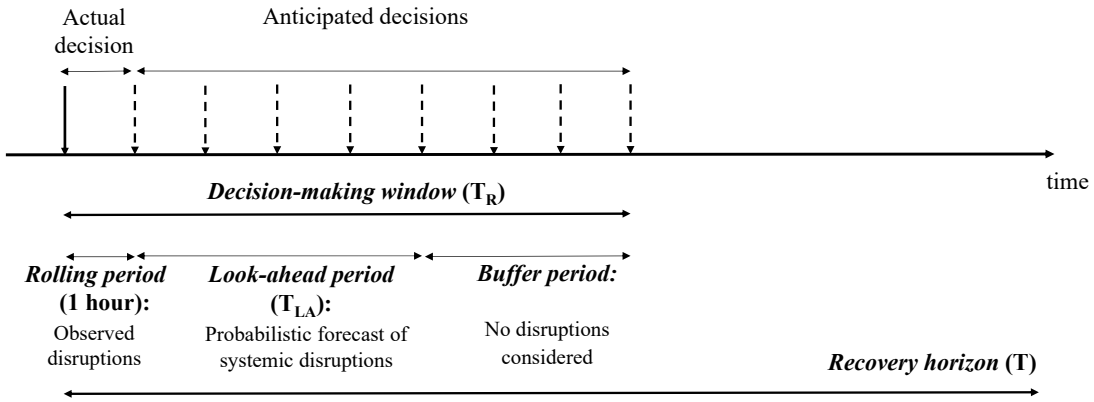

Figure 2.4: Look-ahead framework for dynamic disruption management.

Our look-ahead procedure is shown in Figure 2.4, with decision points indexed by $t = 1, \cdots, T$. The interval between periods t and $t + 1$ is referred to as the *rolling period*. At each decision point, we observe realized disruptions for the rolling period and derive scenarios of systemic disruptions for a given *look-ahead period*. SRPDM is applied to derive disruption recovery and flight planning decisions for the rolling and look-ahead periods. We add a *buffer period* to handle cases in which the disruptions are too large to accommodate all

flights within the look-ahead period. The buffer period also ensures consistency of near-term operating decisions with flight schedules beyond the look-ahead window. We denote by T_R the length of the decision-making window and by $T_{LA}(< T_R)$ the length of the look-ahead period. The objective at time t is given by:

$$\min_{\substack{\boldsymbol{U^t}\in\boldsymbol{\mathcal{U}^t}\\ \cdots \\ \boldsymbol{U^{t+T_R}}\in\boldsymbol{\mathcal{U}^{t+T_R}}}} \sum_{\tau=t}^{t+T_R} E_\xi \left(\sum_{a\in\mathcal{A}} \sum_{f\in\mathcal{F}_\tau} \sum_{k\in\widehat{\mathcal{K}}^\tau_{fa}} (\rho_k + \delta_k + \sigma_k)\, \hat{x}^\tau_{ka} + \sum_{f\in\mathcal{F}_\tau} \gamma_f \hat{z}^\tau_f \right) \tag{2.13}$$

We now use our sample average approximation to approximate Equation (2.13). As mentioned in Section 2.3.1, we proceed by Monte Carlo sampling to approximate the expectation operator, using the set $\mathcal{Q}$ of disruption scenarios. As detailed in the next section, we define a time-space network for each aircraft $a \in \mathcal{A}$ in each scenario q, and denote by $\mathcal{K}^t_{faq}$ be the set of copies in the corresponding time-space network associated with flight $f \in \mathcal{F}_t$. We also introduce variables x^t_{kaq} and z^t_{fq} as the counterparts of $\hat{x}^t_{ka}$ and $\hat{z}^t_f$ in scenario q. These decision variables are scenario-dependent, thus capturing the flexibility of adapting future recovery and flight planning decisions as a function of the scenario realization. We also define non-anticipativity constraints in Section 2.4.1 to ensure the consistency of near-term decisions across all scenarios. The objective function becomes:

$$\min_{\substack{\boldsymbol{U^t}\in\boldsymbol{\mathcal{U}^t}\\ \cdots \\ \boldsymbol{U^{t+T_R}}\in\boldsymbol{\mathcal{U}^{t+T_R}}}} \sum_{\tau=t}^{t+T_R} \frac{1}{Q} \sum_{q\in\mathcal{Q}} \left(\sum_{a\in\mathcal{A}} \sum_{f\in\mathcal{F}_\tau} \sum_{k\in\mathcal{K}^\tau_{faq}} (\rho_k + \delta_k + \sigma_k)\, x^t_{kaq} + \sum_{f\in\mathcal{F}_\tau} \gamma_f z^t_{fq} \right) \tag{2.14}$$

We now use Equation (2.14) to develop the mathematical formulation of our SR-PDM. We calibrate our look-ahead and sample average approximations in Section 2.6.1. Like any approximation scheme, our algorithm induces a trade-off between speed and solution quality. In our implementation, we strive to obtain solutions within a few minutes of computation—consistently with practical requirements and with earlier studies in airline recovery (see, e.g., Maher 2016, Marla et al. 2017a, Petersen et al. 2012a). Note, moreover,

that our solution algorithm does not provide solution quality guarantees. We shall thus compare in Section 3.5 its solution to that of a myopic baseline (defined in Section 2.4.3)—underscoring the benefits of our modeling approach and approximate algorithm as compared to existing recovery approaches that do not leverage forecasts of future disruptions.

2.4.1 Stochastic Reactive and Proactive Disruption Management (SRPDM)

SRPDM builds upon the model from Marla et al. (2017a), but extends it to capture partial and probabilistic forecasts of future disruptions. SRPDM optimizes disruption recovery decisions (i.e., departure holds, aircraft swaps, flight cancellations) and flight planning decisions (i.e., flying altitude, speed and route) to minimize *expected* recovery costs across all disruption scenarios (Equation (2.14)). It is formulated as a stochastic integer program, based on non-anticipativity constraints for first-stage decision variables and scenario-dependent constraints for subsequent periods.

Sets

$\mathcal{F}_\tau$: Set of flights scheduled to depart in period $\tau = t, \cdots, t + T_R$

$\mathcal{A}$: Set of available aircraft

$\mathcal{Q}$: Set of sampled disruption scenarios

$\mathcal{NW}^t_{aq}$: Time-space network corresponding to aircraft a in scenario q at time t

$\mathcal{K}^t_{faq}$: Set of copies of flight $f \in \mathcal{F}^R_t$ in network $\mathcal{NW}^t_{aq}$ from aircraft a in scenario q at time t

$\mathcal{G}^t_{aq}$: Set of ground arcs connecting pairs of nodes in $\mathcal{NW}^t_{aq}$

$\mathcal{N}^t_{aq}$: Set of nodes in $\mathcal{NW}^t_{aq}$

$\mathcal{I}^t_{naq}$: Set of incoming arcs to node $n \in \mathcal{N}^t_{aq}$ in $\mathcal{NW}^t_{aq}$

$\mathcal{O}^t_{naq}$: Set of outgoing arcs to node $n \in \mathcal{N}^t_{aq}$ in $\mathcal{NW}^t_{aq}$

We define here a time-space network $\mathcal{NW}^t_{aq}$ in each scenario $q \in \mathcal{Q}$ for each aircraft $a \in \mathcal{A}$. The earlier probabilistic network representation $\widehat{\mathcal{NW}}^t_a$ is equivalent to the collec-

tion $\left(\mathcal{NW}^t_{aq}\right)_{q\in\mathcal{Q}}$. The same observation applies to $\mathcal{K}^t_{faq}$. By construction, the time-space networks coincide for all flights in the rolling period across scenarios, i.e., $\mathcal{K}^t_{f,a,q_1} = \mathcal{K}^t_{f,a,q_2}$ for all $f \in \mathcal{F}_t$, $a \in \mathcal{A}$ and $q_1, q_2 \in \mathcal{Q}$. However, the networks may differ for the flights scheduled in the look-ahead and buffer periods to reflect the various operating conditions across disruption scenarios.

Parameters

δ_k : Delay cost associated with copy $k \in \mathcal{K}^t_{faq}$, over all $f \in \cup_{\tau=1,\cdots,T_R}\mathcal{F}_\tau, a \in \mathcal{A}, q \in \mathcal{Q}$

ρ_k : Fuel cost associated with copy $k \in \mathcal{K}^t_{faq}$, over all $f \in \cup_{\tau=1,\cdots,T_R}\mathcal{F}_\tau, a \in \mathcal{A}, q \in \mathcal{Q}$

σ_k : Aircraft swap cost associated with copy $k \in \mathcal{K}^t_{faq}$, over all $f \in \cup_{\tau=1,\cdots,T_R}\mathcal{F}_\tau, a \in \mathcal{A}, q \in \mathcal{Q}$

γ_f : Cost of cancellation of flight $f \in \cup_{\tau=1,\cdots,T_R}\mathcal{F}_\tau$

$$s^t_{naq} = \begin{cases} 1 & \text{if aircraft } a \in \mathcal{A} \text{ starts in } \mathcal{NW}^t_{aq} \text{ at node } n \\ -1 & \text{if aircraft } a \in \mathcal{A} \text{ ends in } \mathcal{NW}^t_{aq} \text{ at node } n \\ 0 & \text{otherwise} \end{cases}$$

The swap cost σ_k depends only on which aircraft is used to operate copy k. Specifically, we have $\sigma_{k_1} = \sigma_{k_2}$ for $k_1, k_2 \in \mathcal{NW}^t_{aq}$ for all a and q; and $\sigma_k = 0$ if $k \in \mathcal{NW}^t_{a_0q}$ for all $q \in \mathcal{Q}$, if the flight was originally planned to be operated by a_0. Moreover, $s^t_{naq} = 1$ (or -1) indicates that node n is the supply (or demand) node for aircraft a in $\mathcal{NW}^t_{aq}$, and $s^t_{naq} = 0$ means node n is an intermediate airport location. These parameters will be used to formulate the flow balance constraints.

Decision Variables

$$x^t_{kaq} = \begin{cases} 1 & \text{if copy } k \in \cup_{\tau=1,\cdots,T_R} \cup_{f\in\mathcal{F}_\tau} \mathcal{K}^t_{faq} \text{ is selected with aircraft } a \text{ in scenario } q \text{ at time } t \\ 0 & \text{otherwise} \end{cases}$$

$$y^t_{gaq} = \begin{cases} 1 & \text{if ground arc } g \text{ in } \mathcal{NW}^t_{aq} \text{ of aircraft } a \text{ is selected in scenario } q \text{ at time } t \\ 0 & \text{otherwise} \end{cases}$$

$$z_{fq}^t = \begin{cases} 1 & \text{if } f \in \cup_{\tau=1,\cdots,T_R} \mathcal{F}_\tau \text{ is cancelled in scenario } q \text{ at time } t \\ 0 & \text{otherwise} \end{cases}$$

The decision variables include first-stage variables, which are determined at time t before any scenario is realized, and scenario-dependent variables throughout the look-ahead and buffer periods. This structure enables different decisions to be made across scenarios in periods $t+1, \cdots, t+T_R$. But decisions made for the rolling period (period t) will be subject to non-anticipativity constraints. Only those decisions in the rolling period are to be executed at time t.

Formulation

$$\min_{x,y,z} \quad \sum_{\tau=t}^{t+T_R} \frac{1}{|\mathcal{Q}|} \sum_{q\in\mathcal{Q}} \left(\sum_{a\in\mathcal{A}} \sum_{f\in\mathcal{F}_\tau} \sum_{k\in\mathcal{K}_{faq}^t} (\rho_k + \delta_k + \sigma_k) x_{kaq}^t + \sum_{f\in\mathcal{F}_\tau} \gamma_f z_{fq}^t \right) \tag{2.15}$$

$$\text{s.t.} \quad x_{k,a,q_1}^t = x_{k,a,q_2}^t \qquad \forall k \in \mathcal{K}_{f,a,q_1}^t, \forall f \in \mathcal{F}_t, \forall q_1, q_2 \in \mathcal{Q}, \forall a \in \mathcal{A} \tag{2.16}$$

$$z_{f,q_1}^t = z_{f,q_2}^t \qquad \forall f \in \mathcal{F}_t, \forall q_1, q_2 \in \mathcal{Q} \tag{2.17}$$

$$\sum_{a\in\mathcal{A}} \sum_{k\in\mathcal{K}_{faq}^\tau} x_{kaq}^t + z_{fq}^t = 1 \qquad \forall f \in \mathcal{F}_t \cup \cdots \cup \mathcal{F}_{t+T_R}, \forall q \in \mathcal{Q} \tag{2.18}$$

$$\sum_{g\in\mathcal{I}_{naq}^t \cap \mathcal{G}_{aq}^t} y_{gaq}^t + \sum_{k\in\mathcal{I}_{naq}^t \setminus \mathcal{G}_{aq}^t} x_{kaq}^t + s_{naq}^\tau = \sum_{g\in\mathcal{O}_{naq}^t \cap \mathcal{G}_{aq}^t} y_{gaq}^t + \sum_{k\in\mathcal{O}_{naq}^t \setminus \mathcal{G}_{aq}^t} x_{kaq}^t$$
$$\forall n \in \mathcal{N}_{aq}^t, \forall a \in \mathcal{A}, \forall q \in \mathcal{Q} \tag{2.19}$$

$$x_{kaq}^t \in \{0,1\} \qquad \forall k \in \mathcal{K}_{faq}^t, \forall f \in \mathcal{F}_\tau, \forall a \in \mathcal{A}, \forall q \in \mathcal{Q}, \forall \tau = t, \cdots, t+T_R \tag{2.20}$$

$$y_{gaq}^t \in \{0,1\} \qquad \forall g \in \mathcal{G}_{aq}^t, \forall a \in \mathcal{A}, \forall q \in \mathcal{Q} \tag{2.21}$$

$$z_{fq}^t \in \{0,1\} \qquad \forall f \in \mathcal{F}_\tau, \forall q \in \mathcal{Q}, \forall \tau = t, \cdots, t+T_R \tag{2.22}$$

The objective function (3.1) minimizes expected recovery costs, averaged across all $|\mathcal{Q}|$ sampled scenarios. Constraints (2.16) and (2.17) are non-anticipativity constraints that ensure that first-stage decisions in the rolling period are identical across all scenarios. Constraints (3.2) ensure that a copy of each flight is selected or the flight is cancelled. Con-

straints (3.3) maintain flow conservation: if an aircraft is incoming to a node, it must also be outgoing from that node—except at the source and destination, which have an outgoing and an incoming aircraft, respectively. This formulation also ensures that each aircraft reaches its final destination by the end of the day—in high-disruption instances where this would lead to infeasibility, this formulation could be easily modified by imposing aggregate constraints ensuring, for instance, that a minimal number of aircraft would end their routes at each given airport. Constraints (3.7)–(3.8) define the domains of all variables.

2.4.2 Rolling Algorithm

We synthesize our dynamic solution procedure in Algorithm 1. The algorithm iterates over the recovery horizon $\{1, \cdots, T\}$. At each time period t, it generates the time-space networks $\mathcal{NW}^t_{aq}$, and solves SRPDM. From one period to the next, our state variable $\boldsymbol{R^t} = (\boldsymbol{\theta^t}, \boldsymbol{l^t}, \boldsymbol{D^t})$ is updated based on prior recovery decisions and revealed disruptions. We discuss below the creation of the time-space networks and other steps ensuring the feasibility and practicality of the solution.

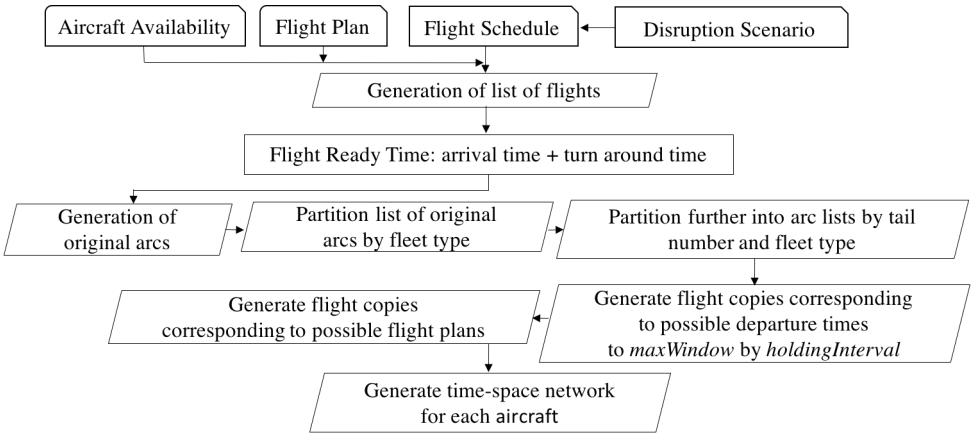

Figure 2.5: Process used to create time-space networks $\mathcal{NW}^t_{aq}$.

Time-space network generation. The process underlying the creation of the time-space networks $\mathcal{NW}^t_{aq}$ is shown in Figure 3.4. It starts by reading the flight schedule, the flight

Algorithm 1 Solution algorithm.

get R_1;
for each $t \in \{1, 2, \dots T\}$ **do**
  get $\mathcal{F}_t, \cdots, \mathcal{F}_{t+T_R}$
  maxWindow = initialHoldingWindow;
  holdingInterval = 10 minutes;
  set feasibleSolution = false;
  while feasibleSolution = false *and* maxWindow$\leq$ maxWindowLimit **do**
    for each $a \in \mathcal{A}$, each $q \in \mathcal{Q}$ **do**
      Generate $\mathcal{NW}^t_{aq}$; ▷ See Figure 3.4
    end for
    Solve *SRPDM*, (see Equations (3.1) to (3.8)) ▷ See Section 2.4.1
    if SRPDM feasible and less than Γ cancellations **then**
      feasibleSolution = true;
      for each $a \in \mathcal{A}$, each $f \in \mathcal{F}_t$, each $q \in \mathcal{Q}$, each $k \in \widehat{\mathcal{K}}^t_{faq}$ **do**
        if $x^t_{kaq} \forall q \in \mathcal{Q} \equiv x^t_{ka} = 1$ **then**
          Update $\boldsymbol{R^t}$ with new location and time of all aircraft $a \in \mathcal{A}$;
        end if
      end for
    else
      maxWindow=maxWindow+δ
    end if
  end while
  if feasibleSolution = false **then**
    $\tilde{A}$ = set of aircraft that cause infeasibility
    maxWindow = initialHoldingWindow;
    for each $a \in \mathcal{A} \setminus \tilde{A}$, each $q \in \mathcal{Q}$ **do**
      Generate $\mathcal{NW}^t_{aq}$; ▷ See Figure 3.4
    end for
    Solve *SRPDM* ▷ See Section 2.4.1
    for each $a \in \mathcal{A}$, each $f \in \mathcal{F}_t$, each $q \in \mathcal{Q}$, each $k \in \widehat{\mathcal{K}}^t_{faq}$ **do**
      if $x^t_{ka} = 1$ **then**
        Update $\boldsymbol{R^t}$ with new location and time of aircraft a;
      end if
    end for
  end if
end for

planning options, the latest availability of each aircraft (which depend on its past flight assignments, past disruptions, and turnaround times), and the disruption scenario considered. This information is used to generate a set of flight copies that can be operated by the aircraft in the decision-making window. For each flight, the first copy departs at the flight's scheduled departure time shifted by its delay observed at time t, or at the time when the aircraft becomes available—whichever comes later. The additional copies correspond to added departure delays and/or alternative flight plans.

Generating flight copies requires assumptions on the granularity and scope of the time-space network. Granularity refers to the interval between consecutive copies, named *holding interval*. The smaller the holding interval, the larger the decision space but the better the solution. We use a holding interval of 10 minutes. Scope refers to the largest allowed departure hold, named *maximum holding window*. For instance, a maximum holding window of 1 hour implies that at most 7 copies of each flight can be created for a given flight plan (associated with holds of $0, 10, \cdots, 60$ minutes). This information is used to generate the flight arcs and ground arcs across the network.

Ensuring global feasibility. Under large disruptions, the flow balance constraints in SRPDM may lead to infeasibility or result in inadequately large numbers of flight cancellations, due to the maximum holding window. This happens when no aircraft is available until the end of the allowed holding window for a given flight, thereby violating the flow balance constraint at the supply node. In practice, airlines need to balance objectives of minimizing the largest flight delays (captured by the maximum holding window) and of minimizing the number of cancellations. For this reason, we impose an upper bound Γ to the number of cancellations, and increase the maximum holding window iteratively until a solution with fewer than Γ cancellations is obtained. In our computations, we use a value Γ equal to 5% of the total number of flights in SRPDM at each time t.

We initialize the maximum holding window value and, if a feasible solution that

cancels fewer than Γ flights is found, we update the state variable and proceed to the next period. If the problem is infeasible or results in more than Γ cancellations, we increase the maximum holding window by increments of δ. As soon as a feasible solution that cancels fewer than Γ flights is found, we update the state variable and proceed to the next period. If no such solution is found after the maximum holding window reaches a pre-specified upper bound, we remove the restriction on the number of cancellations and re-solve the model. We report these parameters in Section 2.6.1.

2.4.3 Myopic Baseline

Before proceeding to the computational implementation of the modeling and computational framework developed in this chapter, we outline the baseline approach used as a benchmark. Specifically, we consider a baseline that optimizes recovery decisions myopically, without considering future disruptions, which follows the approach from Marla et al. (2017a). This approach is then extended to be solved dynamically on a rolling basis, under which the decision-maker observes disruptions at time t, and optimizes recovery decisions over the full planning horizon. It does capture propagated disruptions, but ignores the creation of future primary (systemic or contingent) disruptions. Since the baseline approach is less computationally complex than our stochastic optimization approach, it can be solved as a single integer program from period t up to the terminal period T at each decision point. We still implement it on a rolling basis to capture the realizations of (systemic and contingent) disruptions—observed at each period.

This myopic baseline relies on a single time-space network for each aircraft, captured by sets $\tilde{\mathcal{K}}^t_{fa}$—analogous to $\mathcal{K}^t_{faq}$. Similarly, the decision variables are written as $\tilde{x}^t_{ka}$ and $\tilde{z}^t_f$, defined for all flights $f \in \mathcal{F}_t \cup \cdots \cup \mathcal{F}_T$ (or their copies). The variables $\tilde{x}$ and $\tilde{z}$ are subject

to similar constraints as Equations (2.16)–(3.8). The objective function becomes:

$$\min_{x,z} \quad \sum_{\tau=t}^{T} \left(\sum_{a\in\mathcal{A}} \sum_{f\in\mathcal{F}_\tau} \sum_{k\in\tilde{\mathcal{K}}^\tau_{fa}} (\rho_k + \delta_k + \sigma_k)\tilde{x}^t_{ka} + \sum_{f\in\mathcal{F}_\tau} \gamma_f \tilde{z}^t_f \right). \tag{2.23}$$

2.5 Experimental Setup

We now implement our approach computationally to quantify the benefits of SR-PDM, as compared to the myopic baseline. All models are implemented in the Java programming language interfaced with IBM ILOG CPLEX 12.6.1 on a workstation running at 1.8 GHz with 80 GB RAM.

2.5.1 Network Description

We consider the network of flights of Delta Air Lines, a major US hub-and-spoke airline. This choice is arbitrary, and does not reflect Delta's operating practices. While our model is expected to bring stronger benefits for hub-and-spoke carriers, it can be applied to any airline network. Delta Air Lines leverages six airports as hubs of operations (New York's LaGuardia (LGA) and John F. Kennedy (JFK), Atlanta (ALT), Detroit (DTW), Minneapolis-Saint Paul (MSP), and Salt Lake City (SLC)). We obtain flight schedules and fleet assignments from the Aviation System Performance Metrics (ASPM) database maintained by the Federal Aviation Administration (FAA). We consider 3 fleet types: Airbus 319 (A319), Airbus 320 (A320), and Boeing 757-200 (B752).

We consider the schedule of flights on four weekdays in July 2014. Table 2.1 reports characteristics of each fleet's network, and the corresponding percentile of the distribution of the number of daily flights from Delta Air Lines in 2014. Note, first, that our experimental setup captures the variability in Delta Air Lines' schedules: the four days under consideration range from the 33^{th} percentile to the 100^{th} percentile for the A319 fleet, from the 30^{th}

Table 2.1: Summary statistics for each network.

	July 15			July 16			July 17			July 18		
Metric	A319	A320	B752	A319	A320	B752	A319	A320	B752	A319	A320	B752
# flights	256	260	306	266	247	312	279	254	311	276	262	314
percentile (2014)	33	80	40	80	30	60	100	50	60	95	80	65
# arr. – JFK	2	3	20	4	3	21	4	4	4	4	3	24
# arr. – LGA	19	9	1	20	9	2	23	10	4	23	8	2
# arr. – ATL	24	25	122	25	21	121	26	23	91	24	21	128
# arr. – MSP	26	38	27	27	37	27	28	38	24	28	34	29
# arr. – SLC	19	41	21	20	39	22	22	39	21	22	38	22
# arr. – DTW	36	25	16	38	22	18	37	22	16	37	22	16
Total	126	141	207	134	131	211	140	136	160	138	126	221
# dep. – JFK	2	3	20	4	3	24	4	4	7	4	3	24
# dep. – LGA	20	9	1	20	9	2	23	10	4	22	10	2
# dep. – ATL	24	25	117	26	21	123	26	22	89	24	22	124
# dep. – MSP	26	38	25	27	37	31	28	38	24	28	38	27
# dep. – SLC	19	40	22	21	39	21	22	38	20	22	38	22
# dep. – DTW	37	24	16	37	24	18	33	21	16	38	21	17
Total	128	139	204	135	133	219	136	137	160	137	132	216
less than 1 hour	9	2	0	10	0	0	9	0	0	9	0	0
1–2 hours	157	100	105	160	93	104	165	89	103	169	97	98
2–3 hours	54	72	75	57	64	74	63	65	71	57	71	78
3–4 hours	34	56	38	35	58	45	40	63	41	39	57	43
4–5 hours	2	25	42	4	27	42	2	28	48	2	29	49
5–6 hours	0	5	32	0	4	33	0	7	32	0	6	30
6+ hours	0	0	14	0	0	14	0	0	16	0	0	16
avg. flight time (min)	119	153	184	120	155	186	120	161	189	119	157	189

percentile to the 80$^{\text{th}}$ percentile for the A320 fleet, and from the 40$^{\text{th}}$ percentile to the 65$^{\text{th}}$ percentile for the B752 fleet. In terms of spatial concentration, the airline's network is tightly connected to the six hub airports—with around 50% of the arrivals and departures operated a hub. Finally, the A319, A320 and B752 fleets cover increasingly long flights on average—thus offering different recovery opportunities.

2.5.2 Stochastic Model Inputs

We generate disruption scenarios at each of the six hubs (see Section 2.3.1). We use capacity data from Simaiakis (2012) and the Federal Aviation Administration (2004). We

capture weather variations by means of a two-state Markov chain with "Visual Meteorological Conditions" and "Instrumental Meteorological Conditions" states (used as proxies of "good" and "poor" weather, respectively). We estimate the transition probabilities from historical data.

Figure 2.6 plots the number of flights scheduled at each of the six hub airports under consideration on July 17, 2014 per 15-minute period of the day. Note that, at some airports, the schedule of flights is relatively evenly distributed over the day, whereas other airports operate a strongly "peaked" schedule. JFK and LGA are the most congested airports and SLC is the least congested one, with ATL, DTW and MSP lying in-between. At one extreme, New York's LaGuardia (LGA) airport faces strong local demand and schedule limits (or "flight caps"), resulting in high scheduling levels and limited schedule variability throughout the day. At the other extreme, Detroit (DTW) operates arrival "banks" immediately followed by departure "banks" to enable passenger connections, resulting in a sequence of peaks and valleys. Similar scheduling patterns are observed at Salt Lake City (SLC) and, to a lesser extent, at Minneapolis Saint Paul (MSP). The remaining two airports (New York's John F. Kennedy (JFK) airport and Atlanta's (ATL) airport) fall in-between: the schedule exhibits peaks and valleys but milder variations than at DTW, SLC and MSP. These scheduling patterns are the primary determinants of the expected delay patterns at each of the six hub airports, for each 15-minute period of the day, shown in Figure 2.7. As expected, congestion levels exhibit significant variability from one airport to another, due to differences in underlying scheduling and capacity patterns. Airports with strongly "peaked" schedules, with alternating arrival and departure banks—resulting in a sequence of periods with high delays and periods with low delays. At other airports (e.g., LGA), the schedule of flights is relatively evenly distributed over the day, resulting in more steady congestion levels throughout the day. These different patterns underscore the potential value of capturing the dynamics of formation and propagation of delays by means of our queuing model for disruption recovery.

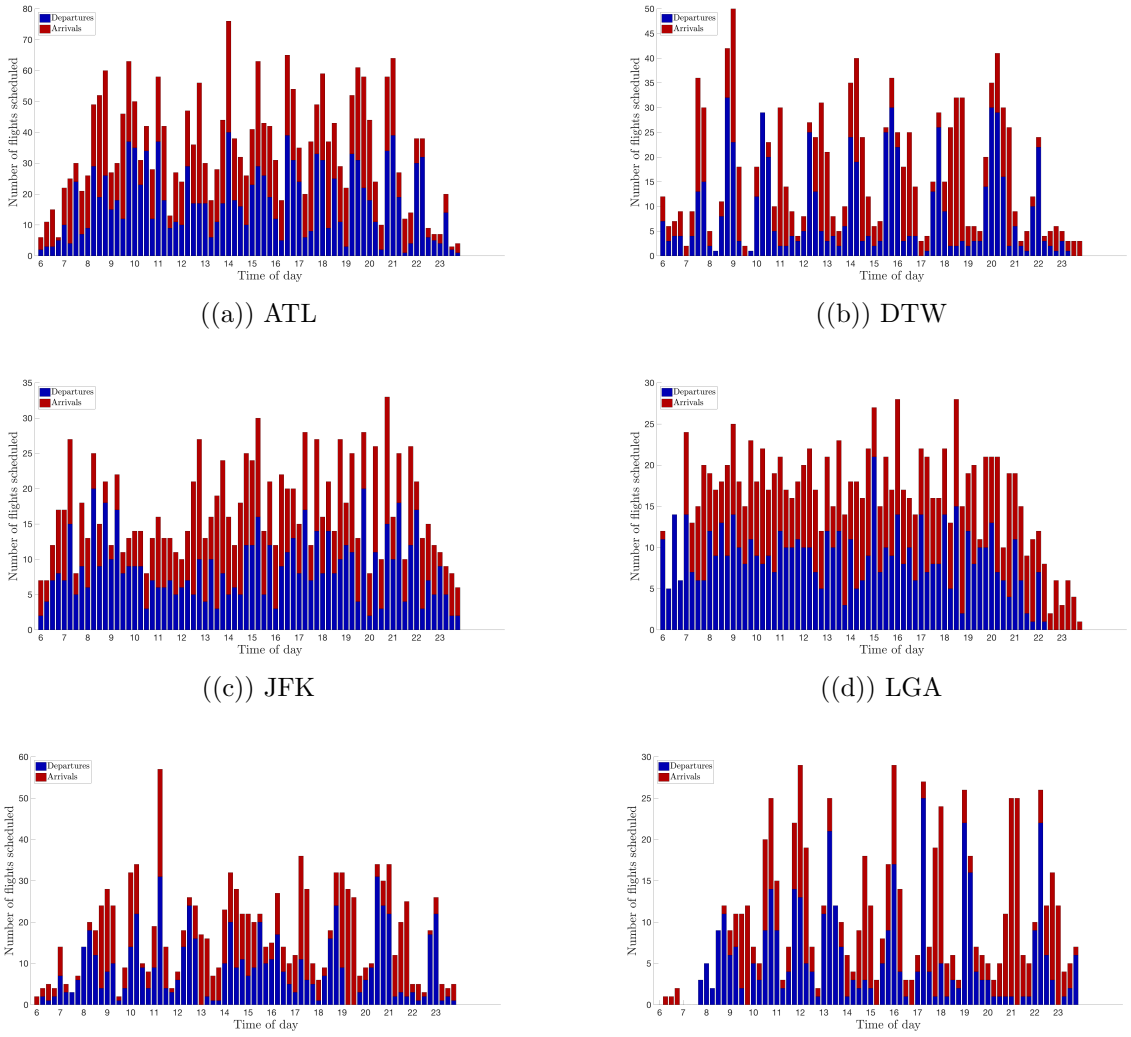

((a)) ATL

((b)) DTW

((c)) JFK

((d)) LGA

((e)) MSP

((f)) SLC

Figure 2.6: Schedule of flights at each airport on July 17, 2014.

2.5.3 Generation of Disruption Instances

In each period $t = 1, \cdots, T$, we generate disruption instances (i.e., the departure delay of each flight $i \in \mathcal{F}_t$). We aim here to replicate the dynamics of the system (captured by the variable $\boldsymbol{D^t}$) and assess the performance of our modeling and computational framework against the myopic baseline. For unbiased comparisons, we do *not* sample disruptions among the set of systemic disruption scenarios considered in our stochastic optimization framework, but instead we generate disruption realizations from real-world data. This procedure cap-

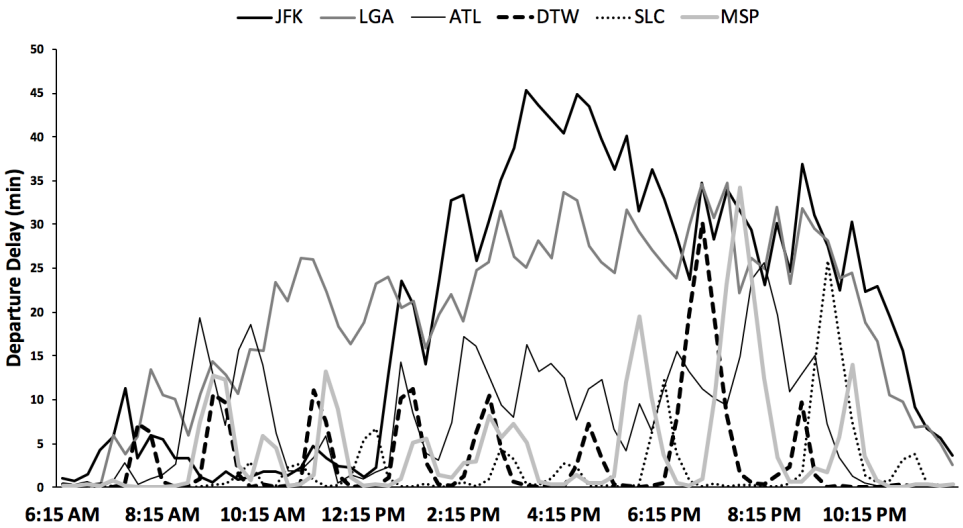

Figure 2.7: Expected departure delay at the six hubs.

tures *all* disruptions: we optimize recovery decisions based on delay propagation dynamics and probabilistic forecasts of systemic disruptions, but assess the resulting decisions against all (propagated, systemic *and* contingent) disruptions.

We use the departure delays from the Bureau of Transportation Statistics (BTS) database. But these delays result from combined propagated, systemic and contingent disruptions, so using them directly would result in double-counting propagated disruptions (which would carry over from previous time periods as well as appear in the newly generated disruptions). We thus need to infer the "new" (systemic and contingent) disruptions by subtracting propagated disruptions.

To this end, we use the inference method from Lan et al. (2006b). We first sort the sequence of flight legs operated by each aircraft. We assume a minimum turnaround time of 30, 35 and 40 minutes for A319, A320 and B752 aircraft, respectively. For every pair of consecutive flights i and j operated by the same aircraft, we define the *slack* between i and j as the difference between the planned and minimum turnaround times between the two flights. The propagated delay of flight j is then computed as max(Arrival Delay of Flight i $-$ Slack, 0). By subtracting this propagated delay from total delays, we obtain the newly created delays (from systemic and contingent disruptions).

Finally, for interpretability, we classify all disruption instances into "small", "medium" and "large" disruptions. The procedure is detailed in Section 2.6.

2.6 Disruption Classification

We classify each disruption instance (see Section 3.4.2) into "small", "medium" and "large" disruption categories. We use a multinomial logistic regression with two independent variables: total delay and maximum delay occurring in the network. Our model is trained with selected scenarios that are *a priori* classified into the three categories, as a training step. We then perform a validation step, to predict the groups for all remaining scenarios. The proportional log-odds of a disruption scenario belonging to the small and medium category, versus the large category, is defined as the logarithm of the ratio of the two probabilities. The logistic regression model is provided in Equations (2.24) and (2.25), where P_s, P_m and P_l denote the probabilities of belonging to the large, medium and small delay categories, respectively.

$$\log\left(\frac{P_s}{P_l}\right) = \beta_0 + \beta_1^s \text{ total delay} + \beta_2^s \text{ max delay} \tag{2.24}$$

$$\log\left(\frac{P_m}{P_l}\right) = \beta_0 + \beta_1^m \text{ total delay} + \beta_2^m \text{ max delay} \tag{2.25}$$

The model's coefficients for each fleet type are reported in Table 2.2. First, all coefficients are negative: the larger the total delays and/or the maximum delays, the less likely the scenario under consideration is to be classified in the small or medium category, as compared to the large category. Second, all coefficients are smaller for the small delay category than for the medium delay category: all else being equal, the larger the total delays and/or the maximum delays, the less likely the scenario is to be classified in the small category, as opposed to the medium category. Third, all but one p-values are lower than 0.05, thus suggesting that the classification model is statistically significant. Last, we

perform a cross-validation on a test set, and confirm zero misclassification. The number of scenarios into each category is reported in Table 2.3.

Table 2.2: Parameter estimates for multinomial logistic regression.

		small (vs. large)			medium (vs. large)		
Fleet	Predictor	Coef.	Std. err.	p-value	Coef.	Std. err.	p-value
A319	constant	16.729	2.488	0.000	8.485	2.068	0.000
	total delay	-0.007	0.001	0.000	-0.002	0.001	0.001
	max delay	-0.016	0.005	0.000	-0.013	0.004	0.001
A320	constant	22.054	3.138	0.000	10.361	2.406	0.000
	total delay	-0.008	0.001	0.000	-0.002	0.001	0.002
	max delay	-0.036	0.008	0.000	-0.016	0.005	0.001
A320	constant	21.968	2.902	0.000	11.464	2.293	0.000
	total delay	-0.002	0.001	0.006	0.000	0.000	0.130
	max delay	-0.078	0.013	0.000	-0.026	0.006	0.000

Table 2.3: Number of disruption instances in each category.

Fleet	A319	A320	B752
Small disruptions	3	16	12
Medium disruptions	12	11	17
Large disruptions	10	7	8

2.6.1 Additional Settings and Parameters

In Algorithm 1, we use a rolling period of 1 hour and a decision-making window T_R of 7 hours. At each time period t, disruptions are observed for the one-hour rolling period. Systemic disruptions are forecasted for a look-ahead period T_{LA}, ranging from 0 to 4 hours. The remainder of the decision-making window is the buffer period, for which no new disruptions are considered.

Note that the hourly time discretization only plays a minor role computationally. As we shall see, the main driver of the problem's complexity is the look-ahead period T_{LA}, which impacts the set of flights $\mathcal{F}_t$ and the resulting number of scenario-dependent decision

variables. The one-hour rolling period (which impacts the number of scenario-agnostic decision variables) restricts the number of iterations required to simulate the recovery dynamics over the full day of operations. In practice, however, an airline could implement the proposed model on a more frequent basis.

As described in Section 2.4.2, the departure holding window is set to an initial value and extended, in case of infeasibility, up to a maximum possible holding window. Table 2.4 reports the initial and maximum departure holding windows for each fleet type, used to balance computational runtimes and solution quality. This results in longer holding windows for B752, intermediate ones for A320, and shorter ones for A319—similar to the process applied at airlines' Operations Control Centers.

Table 2.4: Initial and maximum holding window by fleet type.

Fleet	Initial Holding Window	Maximum Holding Window
A319	30–40 minutes	90–360 minutes
A320	30–60 minutes	120–480 minutes
B752	50–110 minutes	400–550 minutes

Aircraft swap costs (σ_k) are set to \$500. Cancellation costs (γ_f) are estimated as the cost of re-accommodating passengers on the next available flight—assuming 129, 155 and 291 seats for A319, A320 and B752 aircraft respectively, a load factor of 85%, and a cost of \$37.5 per hour of passenger delays (Cook and Tanner 2008b). Fuel costs (ρ_k) are set to \$0.53–\$0.73 per lb (International Air Transport Association 2010). We use a baseline value for the flight delay cost (δ_k) of \$10 per minute. This captures the direct costs of delays *to the airline*. We conduct sensitivity analyses by varying the parameter δ_k from its baseline value of \$10 per minute to a maximum value of \$77 per minute—obtained by fully internalizing the cost of passenger inconvenience, calculated as the product of the number of passengers on the flight and a value of time of \$37.5 per hour. This setup considers linear delay costs, consistent with the airline recovery literature (Maher 2016, Marla et al. 2017a). However, delay costs may have increasing penalties (Ball et al. 2010, Cook and Tanner 2008a). We

thus also consider a non-linear delay cost function in Section 2.7.4 to capture this.

2.7 Computational Results

We now evaluate the performance of SRPDM, as compared to the myopic baseline from Section 2.4.3. Unless otherwise specified, we implement the model with data from July 17, 2014, using 30 scenarios capturing delays at all six hubs for a look-ahead window of $T_{LA} = 4$ hours. First, we show that the proposed approach significantly reduces expected recovery costs (Section 2.7.1). We then demonstrate that, to be beneficial, the proposed approach needs to capture disruption forecasts over the full-scale network of operations and over an extended time horizon (Section 2.7.2). In Section 2.7.3, we discuss the computational performance of our approximate solution approach, showing that SRPDM is solved in reasonable computational times that are consistent with practical requirements. Section 2.7.4 then shows the robustness of the model's benefits to the schedule of flights and to the specification of the objective function. We synthesize the main insights in Section 2.7.5.

Before proceeding further, Table 2.5 shows outputs in three disruption instances to highlight the three main recovery mechanisms employed by SRPDM—and the various trade-offs. Instance 1 illustrates the *speed change* mechanism: if subsequent flights are likely to be delayed, SRPDM may deliberately slow down earlier flights to reduce fuel burn without impacting connectivity—albeit at a higher delay cost. Conversely, SRPDM can speed up some aircraft to maintain connectivity or facilitate swaps. Instance 2 illustrates the *departure hold* mechanism: SRPDM can deliberately delay departing flights (in conjunction with speed ups) to preserve connectivity. Instance 3 illustrates the *aircraft swap avoidance* mechanism. While aircraft swaps may be myopically less costly than departure holds, they can also lead to cancellations at later times; the SRDPM can avoid this situation by anticipating future disruptions earlier, resulting in lower cancellation and swap costs.

Table 2.5: Experimental results of SRPDM vs. baseline in three disruption instances.

Experiments	Model	Total # Cancellations	Total Fuel Burn (lb.)	Total # of Swaps	Total Dep. Delay (min)	Total Arr. Delay (min)	Cost Savings Per Day (%)
Instance 1	Baseline	2	**1,511,000**	0	**556**	1,418	–
	SRPDM	2	**1,508,025**	0	**586**	1,476	0.16%
Instance 2	Baseline	**14**	1,457,276	6	**714**	1,313	–
	SRPDM	**10**	1,457,276	6	**950**	1,433	6.16%
Instance 3	Baseline	**13**	1,424,447	**4**	1,312	1,320	–
	SRPDM	**11**	1,446,258	**2**	1,318	1,335	3.60%

2.7.1 SRPDM Benefits

Table 2.6 reports the results of SRPDM and the myopic baseline across all disruption instances and fleet types. Note that SRPDM yields significant improvements over the myopic baseline: SRPDM reduces expected recovery costs by 1.5%, 1.8% and 1.9% for the A319, A320 and B752 fleets, respectively. These expected savings can result in large financial gains for major airlines, underscoring the benefits of anticipating future disruptions into disruption recovery—even with partial and probabilistic forecasts of future disruptions and even with an approximate solution algorithm.

Under small disruptions, the strongest benefits are derived for the B752 fleet and, to a smaller extent, for the A320 fleet. In contrast, SRPDM does not lower costs of recovery for the A319 network. This mainly stems from the fact that the A319 network primarily consists of short-haul flights, which limits flexibility in terms of flight speed changes. Moreover, the A319 network is significantly smaller than the A320 and B752 ones, and thus less sensitive to disruptions.

When it comes to medium and large disruptions, SRPDM reduces expected recovery costs for all fleet types—from 1% to 2.5%. Note, again, the variability across disruption instances: SRPDM yields the same costs as the myopic baseline in some instances but large cost reductions in other instances. Such variability underscores the importance of capturing

Table 2.6: Comparison of SRPDM over myopic baseline, for each fleet type and each disruption category.

Disruption Category	Fleet	Model	Total Cost ($)	Dep. Delay (min)	Arr. Delay Delay (min)	Fuel Burn ($)	Num. Speed Change	Num. Cancel.	Num. Swaps	Savings
Small	A319	Baseline (avg.)	310,587	951	543	257,608	15	11	0.25	–
		Baseline (min.)	255,425	604	410	257,261	15	6	0	–
		Baseline (max.)	352,312	1,245	688	258,647	15	15	1	–
		SRPDM (avg.)	310,587	951	543	257,608	15	11	0.25	0%
		SRPDM (min.)	255,425	604	410	257,261	15	6	0	0%
		SRPDM (max.)	352,312	1,245	688	258,647	15	15	1	0%
	A320	Baseline (avg.)	1,169,750	1,015	1,540	1,502,723	72	3	0.6	–
		Baseline (min.)	1,117,555	574	1,314	1,457,276	70	0	0	–
		Baseline (max.)	1,279,491	1,783	1,925	1,523,659	74	10	6	–
		SRPDM (avg.)	1,149,427	1,073	1,578	1,503,788	72	2	0.6	2%
		SRPDM (min.)	1,117,555	574	1,314	1,457,276	70	0	0	0%
		SRPDM (max.)	1,279,491	1,783	1,925	1,523,659	74	10	6	6.2%
	B752	Baseline (avg.)	982,914	1,517	1,334	1,658,401	50	2.4	0.25	–
		Baseline (min.)	928,083	579	1,009	1,657,556	49	1	0	–
		Baseline (max.)	1,114,213	2,616	1,910	1,662,632	50	6	2	–
		SRPDM (avg.)	943,657	1,575	1,367	1,658,401	50	1.3	0.08	3.9%
		SRPDM (min.)	928,083	579	1,043	1,657,556	49	1	0	0%
		SRPDM (max.)	1,008,525	2,750	1,972	1,662,632	50	3	1	19.7%
Medium	A319	Baseline (avg.)	500,281	1,929	1,284	458,580	23.8	7.2	1.4	-
		Baseline (min.)	314,116	727	585	281,761	16	0	0	-
		Baseline (max.)	1,174,571	3,900	3,134	1,502,174	73	14	4	-
		SRPDM (avg.)	490,556	1,978	1,331	457,260	23.7	6.7	1.3	2.4%
		SRPDM (min.)	314,116	727	602	296,284	17	0	0	0%
		SRPDM (max.)	1,174,571	3,900	3,134	1,502,174	73	14	4	27.1%
	A320	Baseline (avg.)	1,211,508	1,880	1,909	1,492,283	72	5	0.8	-
		Baseline (min.)	1,124,625	850	1,404	1,256,011	60	0	0	-
		Baseline (max.)	1,499,232	3,998	2,944	1,523,437	74	28	5	-
		SRPDM (avg.)	1,185,928	1,942	1,939	1,495,583	72	3.7	0.47	2.2%
		SRPDM (min.)	1,124,625	850	1,404	1,256,011	60	0	0	0%
		SRPDM (max.)	1,499,232	3,998	2,944	1,523,437	74	28	5	16.3%
	B752	Baseline (avg.)	1,033,625	2,452	1,694	1,658,712	50	3.53	1	-
		Baseline (min.)	930,693	1,219	1,061	1,657,556	48	1	0	-
		Baseline (max.)	1,605,263	4,042	3,080	1,665,240	50	19	9	-
		SRPDM (avg.)	1,020,740	2,464	1,702	1,658,613	50	3.2	1	1.1%
		SRPDM (min.)	930,693	1,239	1,122	1,657,556	48	1	0	0%
		SRPDM (max.)	1,495,119	4,042	3,080	1,665,240	50	16	8	7.4%
Large	A319	Baseline (avg.)	536,473	2,718	1,165	366,123	19.8	11.9	2.2	-
		Baseline (min.)	338,946	1,796	691	306,153	17	2	0	-
		Baseline (max.)	859,662	4,526	2,155	377,477	21	30	7	-
		SRPDM (avg.)	527,945	2,771	1,179	366,123	19.8	11.4	2.1	2.0%
		SRPDM (min.)	338,946	1,796	691	306,153	17	2	0	0%
		SRPDM (max.)	859,662	4,526	2,155	306,153	21	30	7	9.5%
	A320	Baseline (avg.)	1,241,417	2,679	2,273	1,483,771	72	6.4	1.7	-
		Baseline (min.)	1,143,749	1,208	1,320	1,424,447	69	2	0	-
		Baseline (max.)	1,339,418	4,710	3,236	1,524,743	74	14	4	-
		SRPDM (avg.)	1,223,880	2,744	2,307	1,486,887	72	5.4	1.4	1.4%
		SRPDM (min.)	1,143,749	1,182	1,335	1,446,258	70	2	0	0%
		SRPDM (max.)	1,293,446	4,710	3,236	1,524,743	74	11	4	6.4%
	B752	Baseline (avg.)	1,203,155	5,026	2,590	1,597,024	48	8.3	4	-
		Baseline (min.)	946,623	1,610	942	1,491,546	45	1	0	-
		Baseline (max.)	1,688,686	1,610	4,966	1,657,556	50	20	13	-
		SRPDM (avg.)	1,191,148	5,278	2,708	1,590,140	47	8	4.4	1.0%
		SRPDM (min.)	946,623	1,556	931	1,491,546	45	1	0	0%
		SRPDM (max.)	1,659,628	13,419	5,818	1,657,556	50	19	15	5.6%

stochastic airport delays in airline recovery in instances where future disruptions at hub airports can be significant.

These results also highlight that the performance improvements from SRPDM mainly stem from an increased number and magnitude of departure holds—reflected by larger departure delays than with the myopic baseline. These departure holds result in fewer cancellations and swaps (especially for the medium- and long-haul flights in the A320 and B752 networks, which offer stronger flight planning flexibility). Moreover, as long as disruptions remain relatively small, the airline can maintain network connectivity through departure holds. Ultimately, these results emphasize that SRPDM can reduce expected recovery costs through more flexible and robust recovery.

Table 2.7 details the distribution of the SRPDM benefits across disruptions instances, for each fleet and disruption category. Except for the three small-disruption instances with the A319 fleet, the SRPDM reduces recovery costs in 8% to 43% of disruption instances but never increases them. This can be explained as follows. First, the SRPDM adds robustness into airline recovery through departure holds and slower flight plans—which are only applied if they markedly reduce the future likelihood of flight cancellations or aircraft swaps. In other words, the SRPDM plans for scenarios in the lower tail of the delay distribution. Second, in any time period, realized disruptions (which account for propagated, systemic and contingent disruptions) are unlikely to be much smaller than forecasted ones (which ignore contingent disruptions). Third, realized disruptions are even less likely to be much smaller than forecasted ones throughout the recovery horizon. So even if in a certain time period the SRPDM costs are higher than baseline costs, the added robustness resulting from SRPDM can be exploited at later decision points. From a practical standpoint, this result shows that our approach not only reduces expected recovery costs without increasing worst-case recovery costs—thus enhancing the average recovery efficiency without introducing additional risk.

Table 2.7: SRPDM results statistics.

	Small disruptions			Medium disruptions			Large disruptions		
Fleet	Num. Worse	Num. Better	Total instances	Num. Worse	Num. Better	Total instances	Num. Worse	Num. Better	Total instances
A319	0	0	3	0	1	12	0	2	10
	(0%)	(0%)	–	(0%)	(8.3%)	–	(0%)	(20%)	–
A320	0	7	16	0	3	11	0	2	7
	(0%)	(44%)	–	(0%)	(27%)	–	(0%)	(29%)	–
B752	0	3	12	0	5	17	0	2	8
	(0%)	(25%)	–	(0%)	(28%)	–	(0%)	(25%)	–

2.7.2 Impact of Spatial and Temporal Scale

We now show the importance of capturing systemic disruptions at scale in space (i.e., across the full networks of the airline's operations) and time (i.e., for sufficiently long look-ahead windows). Table 2.8 reports SRPDM results from the A320 fleet when future disruptions are captured (i) at a subset of three hubs (at JFK, ATL and MSP, but not at LGA, DTW and SLC); (ii) for a 2-hour look-ahead window (rather than a 4-hour look-ahead window); and (iii) for the full set of six hubs and a 4-hour look-ahead window (referred to as "full size").

First, the benefits of SRPDM increase significantly as stochastic disruptions forecasts are developed at 6 hub airports, as compared to a subset of 3 hubs. Around 25% of flights in the A320 network depart from or arrive at the subset of three hubs (JFK, ATL and MSP), while about 50% of flights depart from or arrive at the full set of six hubs. The results show that SRPDM provides minimal improvements over the myopic baseline when disruptions are only forecasted at the subset of three hubs—with average cost reductions of 0.05%. In contrast, SRPDM reduces expected costs by 1.8% on average when delays are

Table 2.8: Performance of SRPDM, for different spatial and temporal scopes of disruptions predictions.

Model	Total Cost ($)	Dep. Delay (min)	Arr. Delay (min)	Fuel Burn (lb.)	# Speed Change	# Cancel.	# Swaps	Savings
Baseline (avg.)	1,212,395	1,975	1,960	1,491,618	72	5	1	–
Baseline (min.)	1,117,555	574	1,314	1,256,011	60	0	0	–
Baseline (max.)	1,499,232	4,710	3,236	1,524,743	74	28	6	–
SRPDM, 3 hubs (avg.)	1,191,783	2,679	2,402	1,508,036	73	11	4	0.05%
SRPDM, 3 hubs (min.)	1,117,555	1,015	1,284	458,580	24	2	0	0.00%
SRPDM, 3 hubs (max.)	1,499,232	4,710	3,236	1,524,743	74	13	4	1.54%
SRPDM, $T_{LA} = 2$ hrs (avg.)	1,191,783	2,342	2,230	1,498,243	72	7	2	0.46%
SRPDM, $T_{LA} = 2$ hrs (min.)	1,117,555	574	1,281	458,580	24	0	0	0.00%
SRPDM, $T_{LA} = 2$ hrs (max.)	1,319,100	4,710	3,236	1,524,743	74	13	6	6.17%
SRPDM, full size (avg.)	1,191,764	2,037	1,994	1,494,200	72	4	1	1.8%
SRPDM, full size (min.)	1,117,555	574	1,314	1,256,011	60	0	0	0.0%
SRPDM, full size (max.)	1,499,232	4,710	3,236	1,524,743	74	28	6	16.3%

predicted at the full set of six hubs, with reductions of up to 16% in some instances. These results demonstrate the value of capturing *network-wide disruptions*, and their stochasticity, by applying the queuing model at several hub airports simultaneously.

Recall, also, that each look-ahead disruption scenario relied on independent disruption forecasts across airports—ignoring potential network-wide correlations. But this restriction is conservative, as any benefits obtained with independent scenarios (as compared to the myopic baseline) can also be achieved with correlated scenarios. This is because we test the model on real-world disruption instances, which contain any correlations observed in practice. Ultimately, our results provide a lower bound of the benefits that could be obtained with correlated disruptions.

Finally, developing scenarios over extended time periods can further reduce recovery costs. Indeed, the benefits of SRPDM are larger with a longer look-ahead window of 4 hours than with a smaller look-ahead window of 2 hours (1.8% vs. 1.54% on average). This difference mainly stems from the much lower recovery costs in the largest disruption instances—with a maximum cost reduction of 16.3% over the baseline with a 4-hour look-ahead, as opposed to 6.17% with a 2-hour look-ahead. By anticipating broader ranges of future disruptions, longer look-ahead windows T_{LA} mitigate expected recovery costs through added flexibility and robustness in decision-making.

2.7.3 Computational Performance

The main determinants of the model's size—and hence, of its computational performance—are the scope of the flight plans (determined by the maximum holding window and the holding interval, as described in Section 2.4.2) and the number of scenarios. Note that the size of SRPDM remains unchanged as disruptions are forecasted at more airports and/or over longer look-ahead windows.

Figure 2.8 shows the sensitivity of the solution quality and the runtimes as a function of the number of scenarios, over five randomly-generated disruption instances. The runtimes are given here for each iteration of the algorithm—thus reflecting its relevant computational requirements for the airline at any decision point. Figure 2.8(a) indicates that solution quality improves with 30 vs. 10 scenarios, but remains unchanged with 30 vs. 70 scenarios. At the same time, computational requirements increase non-linearly at each iteration with the number of scenarios (Figure 2.8(b))—from 3–5 minutes with 30 scenarios to over 15 minutes with more scenarios. This indicates a "sweet spot" in the model's implementation with 30 scenarios, which yields a sample space that is large enough to ensure high solution qualities and small enough to derive solutions in reasonable runtimes.

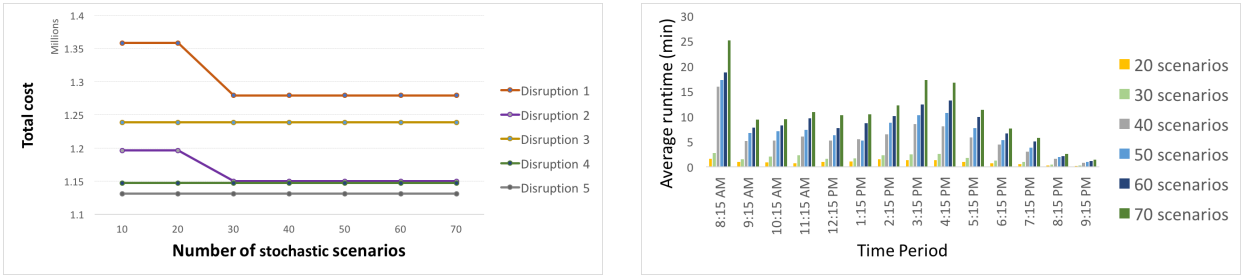

((a)) SRPDM performance

((b)) Average computation times per time period

Figure 2.8: SRPDM performance vs. computation times over increasing numbers of scenarios.

Ultimately, SRPDM can be implemented in short computational times—consistent with earlier models of disruption recovery and with airline requirements. This strong computational performance would enable the implementation of SRPDM in practice. Moreover, in

full-scale software implementations within airline systems, a number of acceleration strategies could also be applied—including parallelization, advanced software engineering, and the use of high-speed computing machines. Our model could also provide close-to-optimal solution in shorter runtimes, should the airline need to (e.g., by considering a smaller scenario set, or by imposing a maximum runtime).

2.7.4 Robustness

At this point, we have shown that the proposed modeling and computational framework can mitigate expected recovery costs by 1–2%, as compared to the myopic baseline. We now establish the robustness of these findings. We first vary the schedule of flights by considering inputs from different days in July 2014. We then vary the delay cost parameter, thus changing the weights attributed to the different components of the objective function.

Impact of Flight Schedule.

First, we consider flight schedules for four weekdays of July 2014 (July 15–18)—which are representative of the distribution of flight schedules over the entire year of operations (see Table 2.1). For each day, we generate the disruption instances from historical delays (Section 3.4.2) and future scenarios at each of the six hubs (Section 2.5.2).

Table 2.9 reports the outputs of SRPDM and the myopic baseline for July 15, 16 and 18 (the corresponding results for July 17 are shown in Table 2.6). The results confirm that SRPDM reduces expected recovery costs by 1–2%, as compared to the myopic baseline. As earlier, SRPDM increases departure delay to reduce the number of aircraft swaps, the number of cancellations and, in some cases, fuel burn. The largest recovery cost reduction, over all disruption instances, is lower than the corresponding one for July 17. This stems from the difference in realized disruptions: the benefits of SRPDM tend to be higher when realized disruptions occur in peak periods, resulting in higher delays at hub airports and higher downstream impacts throughout the network. In such instances, the myopic baseline

Table 2.9: Results for the A320 fleet and a 4-hour look-ahead for multiple weekdays in July.

Day in July	Model	Total Cost ($)	Dep. Delay (min)	Arr. Delay (min)	Fuel Burn ($)	# Swaps	# Cancel.	# Speed Changes	Savings
15th	Baseline (avg.)	908,701	467	719	815,755	1	3	42	–
	Baseline (min)	864,396	185	582	800,320	0	2	38	–
	Baseline (max)	971,778	865	944	832,796	3	4	54	–
	SRPDM (avg.)	896,457	511	745	821,671	1	2	42	1.4%
	SRPDM (min)	858,852	223	582	799,903	0	0	38	0.0%
	SRPDM (max)	971,778	865	962	832,796	3	4	54	4.6%
16th	Baseline (avg.)	901,364	774	725	735,552	3	5	35	–
	Baseline (min)	814,419	140	514	695,086	0	2	32	–
	Baseline (max)	994,649	1,747	1,095	760,847	5	8	36	–
	SRPDM (avg.)	890,434	811	719	735,306	3	5	35	1.3%
	SRPDM (min)	787,796	278	539	695,086	0	0	32	0.0%
	SRPDM (max)	994,649	1,747	1,120	760,461	5	8	37	3.4%
18th	Baseline (avg.)	1,378,449	1,531	1,335	1,069,890	3	10	56	–
	Baseline (min)	1,333,659	830	1,109	1,038,907	1	7	52	–
	Baseline (max)	1,429,588	2,421	1,523	1,094,065	4	14	68	–
	SRPDM (avg.)	1,358,686	1,566	1,351	1,069,263	3	9	57	1.5%
	SRPDM (min)	1,314,221	918	1,133	1,038,907	1	7	53	0.0%
	SRPDM (max)	1,410,578	2,431	1,523	1,093,679	4	13	68	3.0%

tends to increase aircraft speeds to ensure connectivity, while SRPDM leverages information on future disruptions to strategically introduce departure holds. As it turns out, July 17 had a higher incidence of such large peak-hour disruptions than other days. Nonetheless, the average recovery cost savings are consistent across all days—thus highlighting that our approach does not solely provide benefits during the busiest or least busy days of the year.

Impact of Delay Costs.

Next, we establish the robustness of the benefits of SRPDM with respect to the objective function. Recall that SRPDM and the myopic baseline are formulated as multi-objective optimization problems that trade off fuel, delay, aircraft swap, and flight cancellation costs (Equation (3.1) and (2.23)). We keep all cost parameters unchanged, but vary the unit delay cost from \$10 to \$77 per minute (as described in Section 2.6.1). Table 2.10 reports the results of these experiments, for a random subset of "small" disruption instances.

We also consider non-linear (convex) delay costs: following Cook and Tanner (2008a), we set, for each copy $k \in \mathcal{K}^t_{faq}$, $\delta_k = C \times D_k \times \ln(D_k)$, where C is a constant and D_k is the delay (in minutes) of copy k. We choose C such that the average delay cost is equal to

$10/minute when applied to the solution obtained with a linear delay cost of $10/minute—so that we change the distribution of delay costs but not their overall magnitude. These results are also presented in Table 2.10.

These results show that the relative reduction in recovery costs achieved by SRPDM, as compared to the baseline, is remarkably consistent across all (linear or non-linear) delay cost functions—ranging from 2.3% to 3.1% on average. As delay costs increase, both models reduce the incidence of departure holds—reducing average delays but increasing the number of flight cancellations and aircraft swaps. But regardless of the delay cost function, SRPDM results in higher departure and arrival delays than the myopic baseline but in fewer cancellations and (with one exception) fewer aircraft swaps. Ultimately, these results confirm that SRPDM reduces recovery costs by introducing strategic departure holds, over the full range of delay cost functions under consideration.

2.7.5 Summary

Our results suggest that the SRPDM can enhance airline disruption recovery decisions—by reducing recovery costs by 1–2% on average, as compared to a myopic baseline that does not anticipate future disruptions. These results are driven by reductions in flight cancellations and aircraft swaps, partially offset by increases in flight delays. In other words, SRPDM leverages information on a range of disruption scenarios by strategically introducing departure holds and adjusting flight plans, to avoid resorting to flight cancellations and aircraft swaps in subsequent time periods.

Moreover, the benefits of SRPDM increase with the scope of the disruptions under consideration: capturing systemic disruptions—and their stochasticity—from more hub airports and over longer look-ahead windows increases the value of SRPDM. This underscores the benefits of the framework developed in this chapter, which proposes a multi-stage decision-making under uncertainty approach combining, for the first time, a predictive queuing model—applied at several airports of the network simultaneously—into a prescriptive

combinatorial optimization model of airline disruption recovery.

2.8 Conclusion

This chapter proposes a jointly reactive and proactive approach to airline disruption management. This approach optimizes disruption recovery decisions while leveraging a partial and probabilistic forecast of future disruptions—by characterizing probabilistically future systemic disruptions (i.e., congestion at hub airports) but ignoring other contingent disruption forecasts (e.g., aircraft maintenance, late crews, late passenger boarding). We formulate a Stochastic Reactive and Proactive Disruption Management (SRPDM) that combines a stochastic queuing model of congestion (applied at several airports within a network), a flight planning tool from Boeing/Jeppesen, and an optimization model of airline disruption recovery. We design an efficient solution procedure based on look-ahead approximation and sample average approximation, which enables the model's implementation at any decision point in reasonable computational times—consistent with earlier recovery models and with practical airline requirements. Results suggest that leveraging even partial and probabilistic information on future disruptions and an approximate algorithm can enhance recovery decisions: SRPDM consistently performs as well as or better than a myopic baseline, ultimately reducing expected disruption costs without creating additional risk in airline recovery.

The implications of these results are threefold. First, airline recovery can be improved through more flexible and robust decision-making—by deliberately introducing departure holds and speed changes to mitigate the incidence of flight cancellations and aircraft swaps at later points in time. Second, airline operations can benefit from the elicitation of systemic disruption scenarios, especially in instances where flight networks are concentrated at hub airports and where hub airports are highly congested. Such scenarios can be constructed from information available offline, including flight schedules, historical records of airport operations, and weather forecasts. Last, further cost savings could potentially be

achieved through online sharing of operating information between airline operators, airport operators, and air traffic managers. Most notably, continuous alignment on operating conditions, real-time congestion and delay forecasts could reduce system-wide uncertainty on future operations, thus permitting more effective recovery.

These results motivate future work on airline recovery optimization under uncertainty. First, this chapter has relied on a simple prediction of future disruptions by applying the queuing model independently at each hub airport; future research could generate disruption scenarios that capture cross-airport correlations. Moreover, further research could investigate how to incorporate dynamic updates of delay predictions into recovery optimization—in line with the real-time information sharing paradigm mentioned above. Second, this chapter has focused on aircraft recovery. An important extension would involve developing a jointly reactive and proactive approach to the integrated problem of aircraft, passenger and crew recovery. Third, the approximate solution algorithm considered in this chapter could be augmented with exact algorithms for multi-stage recovery optimization under uncertainty. The framework, model and algorithm proposed in this chapter provide the foundations to explore these questions—toward more efficient, reliable and robust recovery.

Table 2.10: Experimental results for different delay cost parameters.

Delay Cost ($/min)	Model	Total Cost ($)	Dep. Delay (min)	Arr. Delay (min)	Fuel Burn (lb.)	# Swaps	# Cancel.	# Speed Changes	Savings
$10	Baseline (min)	1,133,878	556	1,313	1,449,264	0	2	69	-
	Baseline (max)	1,358,403	1,202	1,599	1,523,785	6	14	73	-
	Baseline (avg.)	**1,205,434**	**895**	**1,463**	**1,495,607**	**1.1**	**5.1**	**72**	**-**
	SRPDM (min)	1,121,481	586	1,433	1,457,276	0	0	70	0.03%
	SRPDM (max)	1,279,491	1,222	1,750	1,522,769	6	10	74	6.2%
	SRPDM (avg.)	**1,167,328**	**1,002**	**1,535**	**1,497,605**	**1**	**3**	**72**	**2.8%**
$20	Baseline (min)	1,146,048	536	1,277	1,443,010	0	2	68	-
	Baseline (max)	1,366,260	1,192	1,566	1,524,265	6	14	72	-
	Baseline (avg.)	**1,214,304**	**864**	**1,412**	**1,489,390**	**1.1**	**5.4**	**70**	**-**
	SRPDM (min)	1,131,292	566	1,315	1,443,010	0	0	68	0.02%
	SRPDM (max)	1,289,708	1,212	1,717	1,523,511	6	10	73	5.9%
	SRPDM (avg.)	**1,177,269**	**971**	**1,484**	**1,491,388**	**1.1**	**3.4**	**71**	**3.1%**
$30	Baseline (min)	1,158,625	496	1,180	1,443,770	0	2	64	-
	Baseline (max)	1,373,611	1,162	1,451	1,526,435	6	14	68	-
	Baseline (avg.)	**1,223,163**	**820**	**1,318**	**1,484,522**	**1.1**	**5.6**	**67**	**-**
	SRPDM (min)	1,140,885	526	1,287	1,443,770	0	0	64	0.0%
	SRPDM (max)	1,299,419	1,162	1,520	1,525,214	6	10	68	5.7%
	SRPDM (avg.)	**1,187,198**	**923**	**1,376**	**1,486,723**	**1.1**	**3.6**	**67**	**3.0%**
$40	Baseline (min)	1,164,992	436	1,028	1,399,814	0	2	58	-
	Baseline (max)	1,363,486	1,102	1,261	1,529,358	5	14	63	-
	Baseline (avg.)	**1,229,222**	**758**	**1,168**	**1,478,142**	**1**	**5.9**	**61**	**-**
	SRPDM (min)	1,149,774	456	1,173	1,421,097	0	0	59	0.0%
	SRPDM (max)	1,272,351	1,112	1,402	1,528,129	7	9	64	7.2%
	SRPDM (avg.)	**1,191,866**	**867**	**1,246**	**1,479,936**	**1.3**	**3.8**	**62**	**3.1%**
$50	Baseline (min)	1,170,381	386	889	1,404,649	0	2	51	-
	Baseline (max)	1,370,553	1,052	1,120	1,534,742	5	14	57	-
	Baseline (avg.)	**1,238,187**	**710**	**1,005**	**1,483,210**	**1.1**	**5.9**	**54**	**-**
	SRPDM (min)	1,160,776	406	1,026	1,405,701	0	0	52	0.0%
	SRPDM (max)	1,301,195	1,062	1,206	1,534,214	5	11	58	5.3%
	SRPDM (avg.)	**1,207,499**	**815**	**1,073**	**1,482,628**	**1.3**	**4.1**	**55**	**2.5%**
$60	Baseline (min)	1,174,241	386	879	1,384,418	0	2	51	-
	Baseline (max)	1,395,891	1,032	1,099	1,535,943	6	16	57	-
	Baseline (avg.)	**1,253,596**	**698**	**988**	**1,481,443**	**1.5**	**6.4**	**55**	**-**
	SRPDM (min)	1,169,464	406	1,024	1,405,701	0	0	52	0.0%
	SRPDM (max)	1,328,993	1,042	1,185	1,535,415	6	11	58	5.8%
	SRPDM (avg.)	**1,218,281**	**806**	**1,062**	**1,483,390**	**1.4**	**4.3**	**56**	**2.8%**
$77	Baseline (min)	1,180,803	386	879	1,384,418	0	2	51	-
	Baseline (max)	1,404,425	1,032	1,099	1,536,319	6	16	57	-
	Baseline (avg.)	**1,265,439**	**697**	**987**	**1,481,550**	**1.5**	**6.4**	**55**	**-**
	SRPDM (min)	1,180,485	406	1,024	1,405,701	0	0	52	0.0%
	SRPDM (max)	1,341,709	1,042	1,185	1,535,791	6	11	58	5.5%
	SRPDM (avg.)	**1,231,967**	**805**	**1,060**	**1,483,496**	**1.4**	**4.3**	**56**	**2.6%**
non-linear cost (equivalent to $10)	Baseline (min)	1,142,595	556	1,418	1,447,980	0	2	71	-
	Baseline (max)	1,193,108	1,372	1,772	1,523,785	7	4	73	-
	Baseline (avg.)	**1,157,004**	**959**	**1,529**	**1,503,547**	**1**	**2.9**	**72**	**-**
	SRPDM (min)	1,111,532	586	1,471	1,447,980	0	0	71	0.0%
	SRPDM (max)	1,152,517	1,372	1,772	1,522,892	7	4	74	3.8%
	SRPDM (avg.)	**1,131,204**	**1,034**	**1,582**	**1,502,920**	**1**	**1.6**	**72**	**2.3%**

Chapter 3

PASSENGER RE-ACCOMMODATION AND AIRCRAFT RECOVERY UNDER CLIMATE CHANGE

3.1 Introduction

In this chapter, we further expand the discussion in Chapter 2, which focused on aircraft recovery in current operating conditions, to consider disruptions occurring from a different source – namely, climate change, and their impact on both aircraft and passenger recovery. Globally increasing temperatures due to climate change, especially in summers, have resulted in some aircraft being impacted negatively, by grounding aircraft or having them operate at lowered capacities. As temperatures increase in the coming decades due to climate change, these impacts are expected to only increase.

Recent disruptions in high temperature areas like Arizona in the United States, have highlighted the impact of high temperatures on grounding several flights (Wired 2017). The combination of temperature, engine thrust and runway length (or runway configuration) results in small or mid-sized aircraft not being able to gather enough thrust to take off, or to be able to operate only at reduced capacities. As a consequence, these aircraft can be grounded or taking off only with part of its load (including passengers), necessitating

recovery actions to be implemented for nearly all of the day of operations or beyond.

It is noteworthy that high temperatures typically occur during and after the afternoon peak of operations at many hub airports. It is also well known that propagation of disruptions from the morning towards the evening on a day of operations results in higher cascading effects during the latter half of the day. These two effects, in combination, can significant compounding the cascading effects of disruptions for both the airline's resources (aircraft and crew) and passengers. In fact, passenger itineraries can be significantly impacted, more so than individual flights because each passenger itinerary can consist of multiple flight legs (possibly of multiple fleet types) and passenger delays can be non-linearly correlated with flight delays (Bratu and Barnhart 2006a). In this increasingly relevant context, we are interested in an integrated view of the impacts of climate change-related disruptions, inclusive of not only aircraft delays and disruptions, but also passenger itinerary delays and disruptions. Particularly, we focus on *integrated and simultaneous* aircraft and passenger disruption management at airlines – specifically, passenger *re-accommodation* – under these severe disruptions.

3.1.1 Our Approach

The objective of this work is to evaluate the impact of climate-change-*induced* constraints on disruption management and airline operations. To this end, we construct a large-scale, climate-change-tailored, integrated aircraft and passenger recovery modeling and algorithmic framework. First, this framework allows us to capture the unique constraints that climate change-related temperature increases impose on each aircraft's ability to operate in the network at specific points in time. Specifically, it captures the change in capacity of each aircraft type as a function of high temperatures and airport runway lengths, during each hour of the day. Second, this framework incorporates these capacity constraints into rolling horizon recovery models that solve for cost-minimizing aircraft re-routing/re-scheduling and passenger re-accommodations. Thus, this frameworks allows for dynamic network design

and management of both the demand (aircraft and passengers), and associated supply (the capacity available on each re-scheduled aircraft at that point in time). We implement this framework on real data from a major airline to estimate the increase in recovery costs induced by climate change, and discuss the operational and practice implications for airlines.

3.1.2 Contributions and Outline

The contributions of our work are as follows.

We present an original modeling framework for incorporating climate change constraints caused by temperature increases, into airline recovery. To the extent of our knowledge, this is the first work that explicitly models the climate change-induced capacity reductions of aircraft, at the granularity of each airport and using multiple climate change models, into *simultaneous* aircraft and passenger recovery.

We present a rolling horizon (dynamic) algorithm for integrated aircraft and passenger recovery under climate change-imposed constraints become operational. Our dynamic rolling horizon algorithm is designed to mimic real-world airline operations by which disruptions are handled as they are revealed, and captures airline recovery (including inter-fleet swaps) simultaneously integrated with optimally assigning re-accommodations for disrupted passengers. This framework solves for recovery actions under 'normal' airline disruptions upon which climate change-related capacity constraints have been imposed.

Our results indicate that climate change can significantly impact airlines' ability to recover from disruptions occurring during normal operations. Specifically, we construct a testbed comprising of regularly occurring disruptions of different magnitudes on a major airline's network, and compare recovery costs under different cases of climate change in 2035 and 2050. Our computational results demonstrate that if a similar network structure with similar load factors as today were operated in 2035 or 2050, we would find that airlines' recovery costs can increase between 25% to 55.9% on average, with the actual costs depending on the climate change case of interest.

Our work provides important policy and practical operational implications. We find that airline recovery under climate change conditions will necessarily need to account for many aircraft being located at unplanned locations at the completion of each day of operations. This implies that improving inter-operability of aircraft fleet and locating reserve aircraft at overnighting airports may aid recoverability, especially from a passenger-centric perspective. We also find that engine design over the next decade should focus on enabling smaller aircraft to be operated even at reduced capacities without being grounded, even under high temperatures.

Outline. In Section 3.2, we discuss relevant background from two streams - (i) climate change impacts on operations over the coming decades, and (ii) methods for integrated aircraft and passenger recovery in the literature. Section 3.3 discusses our modeling and algorithmic framework that explicitly incorporates constraints imposed by climate change into simultaneous aircraft and passenger recovery. Section 3.4 presents the testbed for our real-world computational experiments. We discuss our experimental results in Section 3.5 and conclude in Section 3.6.

3.2 Background

3.2.1 Climate Change and its Impacts on Aircraft Operations

While there is a large literature about the effects of aviation on climate change, there has been less in-depth analysis on the effect of climate change on aviation. The U.S. National Climate Assessment, citing work by Coffel and colleagues (Coffel et al. 2017) says, "Air transport is sensitive to extreme heat because hotter air makes it more difficult for airplanes to generate lift (the force required for an airplane to take flight), especially at higher elevations, requiring weight reductions and/or longer takeoff distances that may require runway extensions" (Reidmiller et al. 2018). As this assessment suggests, the effect depends on runway lengths, on the aircraft's engine capabilities (smaller aircraft are more

adversely affected), and on the observed increase in temperature.

The literature on the impacts of climate change typically refers to four standard *scenarios* (called RCP2.6, RCP4.5, RCP6.0, and RCP8.5, where RCP stands for Representative Concentration Pathway) that result in different levels of radiative forcing; that is, the imbalance between the rate at which solar energy is incident on earth and the rate at which the earth radiates energy back into space (Moss et al. 2010). These different levels of forcing obtain mainly from different assumptions about the trajectory of anthropogenic emissions of greenhouse gasses, which in turn produce four different trajectories of radiative forcing for each year. These trajectories are then used as inputs to a series of climate models, each of which may make different assumptions about initial state of the atmosphere at the moment at which the model is initiated, and about the physics of the earth's climate. The Coupled Model Intercomparision Project, currently in its fifth iteration (CMIP5) (Meehl et al. 2000), uses these emissions trajectories as in input to a large ensemble of climate models, each of which produces predictions of temperature, precipitation, and a large number of other climate variable for each scenario. The predictions are typically made at a spatial resolution of about 1 degree x 1 degree, and temporal resolutions of at least several hours. A combination of higher resolution models or statistical techniques are then used to make predictions at finer spatial and temporal resolutions. In this analysis, we consider the effect on aircraft dispatch and airline operations of the temperatures that result from the RCP8.5 scenario (Riahi et al. 2011). The temperature changes emerge from 20 climate models within the RCP8.5 scenario, downscaled to a resolution of 1/8 degree x 1/8 degree and one hour[1]. The predictions of each model can be treated as a separate, plausible scenario. Potential flight restrictions or disruptions are calculated for the temperatures that emerge from each model; the process is then repeated for the predictions of the other models. In Section 3.4, we describe how we determine the restrictions on flight take-off weights and payloads, given the temperature and

[1]These data were produced by Yifan Chang and Prof. Bart Nijssen of the Department of Civil and Environmental Engineering at the University of Washington. They were made available to the authors by Francisco Ralston Fonseca and Prof. Paulina Jaramillo, of the Department of Engineering and Public Policy at Carnegie Mellon University.

airport characteristics. Among the 20 climate models, we select three models or *cases* that represent mild, medium and severe climate change temperature changes, and compute the projected temperatures for the years 2035 and 2050. We conduct experiments that compare the disruption costs for 2035 and 2050 against the costs in 2014 to understand the projected increase in costs over the next three decades.

3.2.2 Integrated Aircraft and Passenger Re-accommodation

The objective of this chapter is to study the impact of climate change on recoverability, with a perspective of integrated aircraft and passenger recoverability. We now review literature on integrated aircraft and passenger recovery, which typically falls under two categories. The first category is sequential recovery, in which aircraft recovery is followed by passenger recovery; and the second is simultaneous recovery, with both aircraft and simultaneous recovery being solved together. It is clear that the sequential approach can result in higher costs, often resulting in passenger misconnections and delays that can be avoided by the simultaneous recovery problem. On the other hand, solving the simultaneous recovery problem is significantly more complex algorithmically and computationally.

Lettovsky (1997) estimates the cost of losing passenger goodwill by incorporating the costs associated with re-booking passengers, meals and hotel costs into the cost of flight cancellation. Barnhart et al. (2002) design the Itinerary-Based Fleet Assignment Model that approximates spill and recapture cost of passengers, formulating it as a multi-commodity network flow problem. Lan et al. (2006a) present passenger-centric approaches to minimize delay propagation and passenger delays, by redesigning aircraft routings and retiming flights, though passenger re-accommodation is not explicitly modeled.The above works do not either explicitly consider passengers, solve for passenger misconnections instead of explicitly re-accommodating misconnected passengers on alternate itineraries.

Later works model passenger delay and re-accommodation explicitly. Bratu and Barnhart (2006a) explicitly consider disrupted passengers and crews, and develop a flight-

leg based aircraft recovery model to minimize recovery costs, including re-accommodation costs of passengers and crews, re-routing cost of aircraft, and cancellation costs, but with some relaxations on the constraints and variables. Zhang and Hansen (2008) consider recovery decisions on flight holding, cancellations, and substitution by other transportation modes specifically when weather causes many flight delays, minimizing the airline's disruption cost, including passenger delay-related costs. Jafari and Zegordi (2011) develop a model to solve for aircraft and passenger recovery simultaneously using rotation-based modeling instead of flight-based modeling, where the length of recovery period is determined after comparing the all possible aircraft rotations. However, due to its high computational complexity, the model can only handle small-scale disruptions with 13 aircraft, 2 fleet types, and 8 itineraries. Petersen et al. (2012b) solve the integrated recovery problem for schedule recovery, aircraft rotations, crew schedule, and passenger itineraries using Benders decomposition combined with column generation approach. The relaxed master problem is the schedule generation problem; with aircraft recovery, crew recovery and passenger recovery modeled as subproblems. Maher (2015) considers the integrated airline recovery problem with passenger reallocation for the schedule, aircraft, and crew recovery problem while also explicitly considering costs of re-accommodating passengers on the same airline's flights, other airlines' flights or not re-accommodating passengers; and models this problem as a stochastic programming problem. Bisaillon et al. (2011) introduce a large-scale neighborhood search heuristic to combine aircraft re-routing and passenger reassignment (recovery), with the objective of minimizing the costs of operation and impact on passengers. The construction, repair and improvement phases of their heuristic first prioritize aircraft routing decisions, and then re-allocate passenger itineraries. Extra phases of improvement were added by Sinclair et al. (2014b) to improve the local search solution by delaying each flight one at a time by certain interval in order to accommodate new passengers.

These existing works do not capture two aspects: (i) the capacity constraints imposed by climate change, resulting in reduced capacity for some flights given the payload and range

of the flight, and (ii) the *dynamic* nature of airline (aircraft and passenger) recovery. While works such as Marla et al. (2017b) and Lee et al. (2020) capture the dynamic nature of recovery through rolling horizon algorithms, they do not explicitly perform passenger re-accommodation, and do not also capture climate change-related constraints.

3.3 Mathematical Models

We now present our rolling horizon modeling framework for integrated and simultaneous aircraft and passenger recovery, which also incorporates capacity constraints introduced by climate change.

3.3.1 Aircraft Flow Network with Inter-fleet Swaps

Our modeling framework is based on a multi-commodity flow model constructed on a time-space network, where each aircraft is treated as a commodity. We create a time-space network, $\mathcal{NW}_a$, for each aircraft a, consisting of flights that can be operated by aircraft a and ground arcs representing connections. Figure 3.1 shows an example of such a time-space network representation. Each arc in $\mathcal{NW}_a$ represents a possible flight movement and each node represents a possible time and airport location for an arrival or a departure. We add a supply node n_s to denote the initial location of the aircraft at the beginning of the time horizon, and a demand node n_d at the end of the time horizon to signify that the aircraft has completed its last flight in the network. The location of n_d in $\mathcal{NW}_a$ is at the airport that the aircraft was originally planned to have been located at the end of the time horizon. We denote the set of nodes in $\mathcal{NW}_a$ (including n_s and n_d) as $\mathcal{N}_a$. We construct ground arcs in $\mathcal{NW}_a$ that represent a feasible (satisfying minimum turn time requirements) aircraft turnaround time at an airport, that connect one arrival node to an immediately subsequent node at the same airport. We refer to the set of ground arcs in $\mathcal{NW}_a$ as $\mathcal{G}_a$.

In most recent work, such as Lee et al. (2020), aircraft swaps are allowed only within

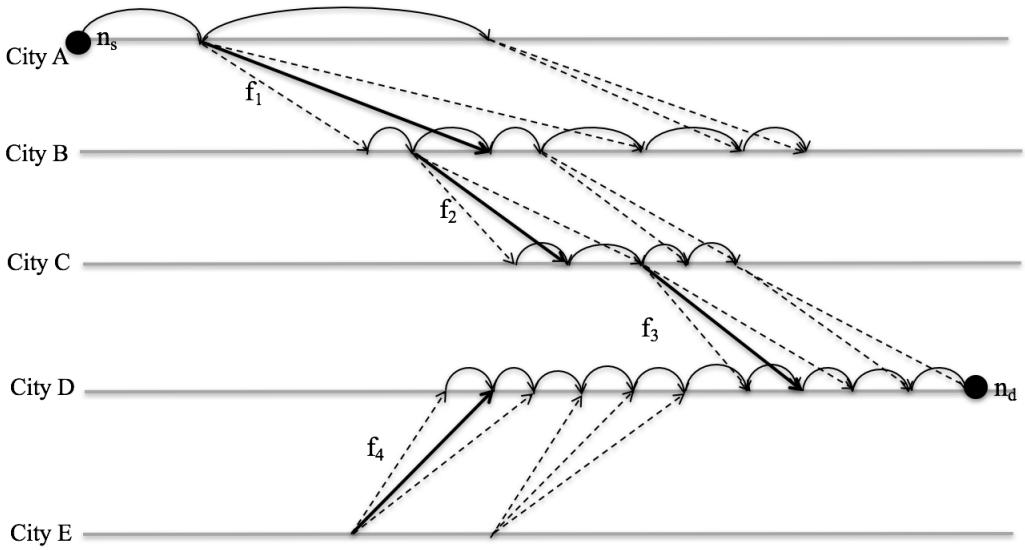

Figure 3.1: Aircraft flow network $\mathcal{NW}_a$ for aircraft a

a fleet type and thus $\mathcal{NW}_a$ contains only the flights in the schedule to which an aircraft of the same fleet type as a is assigned. However, under climate change conditions, certain fleet types cannot be operated (or operate at lower capacity) for several hours and it might be beneficial to use other aircraft types to operate the flight so as to allow passenger itineraries to be preserved. For example, an aircraft belonging to a smaller-sized fleet type can be swapped with a larger-sized aircraft if the smaller one is unable to take off because of high temperature. Hence, we now allow for aircraft swaps between multiple fleet types, and the aircraft flow network $\mathcal{NW}_a$ contains all flights in the schedule (as long as the range of the aircraft allows it to operate that flight), as the aircraft a can operate any of the flights in the schedule.

3.3.2 Generating Passenger Itineraries using Depth First Search

We replicate the network $\mathcal{NW}_a$ to create the passenger flow network $\mathcal{PN}_p$ to find feasible alternative itineraries for passengers. As shown in Figure 3.2, for each originally scheduled copy of flight f in an itinerary, there are also flight copies similar to $\mathcal{NW}_a$. For simplicity of discussion, we assume each originally booked passenger itinerary in this work

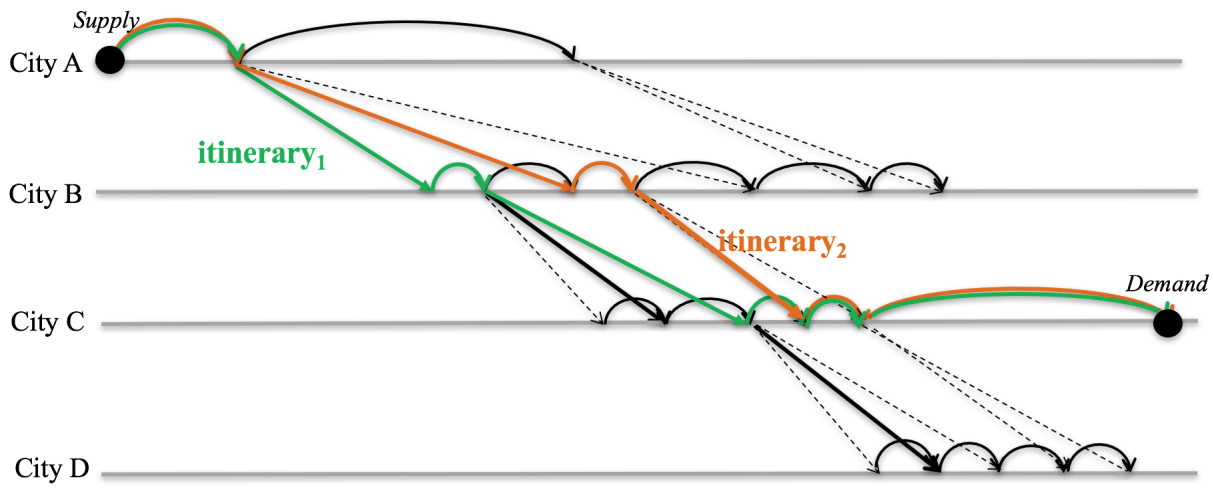

Figure 3.2: Passenger flow network $\mathcal{PN}_{\mathcal{P}}$ capturing all passenger itineraries $p \in \mathcal{P}$

consists of one or two flight legs. It is straightforward to extend the model to the case with multiple flight legs. We first add a supply node at the origin airport at the start time of each booked passenger itinerary. We also add a demand node at the itinerary destination airport with its time set to the latest allowed ending for that itinerary. Ground arcs are added between each supply node and corresponding origin node of the first flight leg of the passenger's originally booked itinerary. We also add ground arcs between the destination nodes of the last leg of the booked itinerary and the corresponding demand nodes.

We describe each passenger itinerary not only by the flights included in the itinerary but also the specific flight copies used in the itinerary. A flight leg f followed by flight leg g corresponds to several potential itineraries, each with different combinations of copies of flight legs f and g. For example, $(f_1, k_1), (f_2, k_2)$ represents an itinerary where copy k_1 of flight f_1 is feasibly (with sufficient connection time) succeeded by copy k_2 of flight f_2. Therefore, $(f_1, k_1), (f_2, k_3)$ would be called a different itinerary in our model. We use $\mathcal{P}$ to denote the original set of booked itineraries, that is, they consist of the first set of copies of flights in the itinerary, with the originally scheduled flying times.

We now generate a list of candidate recovery itineraries $R(p)$, including the planned itinerary, recovery itineraries, and a virtual itinerary that models passengers re-accommodated

by other airlines.We create a possible itinerary for each pair of supply and demand nodes for $p \in \mathcal{P}$ using the recursive depth-first search function as shown in Algorithm 2. The supply node for each itinerary is created at the departure location of the original departure of the first flight in p, with its time equal to the disruption of the first flight. The demand node for p is created at the destination airport of p, with a time equalling the latest possible arrival time allowed considering disruption. There is a feasible alternative itinerary for any given original (booked) itinerary if there exists a direct flight leg or two flight leg copies with a feasible connection (with positive slack between them). If such connections exist, we use Algorithm 2 to generate alternative itineraries. $R(p)$ is thus obtained by running Algorithm 2 on this modified network $\mathcal{NW}_p$.

3.3.3 Model Formulation

Our model simultaneously optimizes for aircraft recovery decisions (fuel cost, departure holding cost, swap costs, cancellation costs) and passenger recovery costs (re-accommodation costs, delay costs and re-accommodation on another airline), all incurred *by the airline*. Our model extends the passenger recovery components of Bratu and Barnhart (2006a) and Marla et al. (2017b), and combines them with the aircraft recovery components of Lee et al. (2020) over a rolling horizon.

Further, we extend all these models to explicitly account for the payload-range capabilities of different aircraft and the resulting seat capacity, in the passenger re-accommodation constraints. The following is our formulation for combined aircraft recovery and passenger re-accommodation including flight planning opportunities.

Sets :

$\mathcal{F}_t$: Set of flights scheduled to depart in time period $[t, T_R]$

$\mathcal{A}$: Set of available aircraft

$\mathcal{NW}_a^t$: Time-space network corresponding to aircraft a at time t

Algorithm 2 Recursive depth-first function for generating all recovery itineraries

graph ← A hash-map used to represent $\mathcal{PN}_{\mathcal{P}}$ as an adjacency list, with nodes as keys and list of connected nodes as values
origin ← The supply node
destination ← The demand node
itinerary := A list of nodes representing the itinerary
itineraryList := A list of itineraries
maxFlightlegs :=maximum length of itinerary
function DFS(*graph*, *origin*, *destination*, *itinerary* =empty, *itineraryList* =empty)
    if *itinerary* is empty **then**
        itinerary ← [*origin*]
    end if
    if *origin*.location equals *destination*.location **then**
        Add copy of *itinerary* to the list *itineraryList*
        return
    end if
    if number of flight legs in *itinerary* == *maxFligtlegs* **then**
        return
    end if
    for each *next* ∈ *graph*(*origin*) **do**
        itinerary ← *itinerary* + *next*
        DFS(*graph*, *next*, *destination*, *itinerary*, *itineraryList*)
        itinerary ← *itinerary* − *next*
    end for
end function
for each *itinerary* ∈ *itineraryList* **do**
    Remove nodes associated with ground arcs in *itinerary*
end for

$\mathcal{PN}^t_{\mathcal{P}}$: Passenger flow network that captures all passenger itineraries in time period t.

$\mathcal{P}_t$: Set of passenger itineraries considered in time period $[t, T_R]$

$\mathcal{R}_t(p)$: Set including original itinerary as well as list of candidate itineraries on the passenger flow network from the origin of p to its destination, with each starting after p's original departure, by at least the amount of disruption of p. As described in Section 3.3.2, each $r \in \mathcal{R}_t(p)$ is described by a flight as well as the a copy of that flight; and includes only feasible itineraries.

$\mathcal{K}^t_f$: Set of flight copies of flight $f \in \mathcal{F}_t$, where these copies are generated from either flight holding, or using alternate flight plans or both. Note that these copies can be operated by any aircraft.

$\mathcal{G}^t_a$: Set of ground arcs connecting every two consecutive nodes in time at the same airport in $\mathcal{NW}^t_a$

$\mathcal{N}^t_a$: Set of nodes in $\mathcal{NW}^t_a$

$\mathcal{N}^-_{nat}$: Set of incoming arcs to node $n \in \mathcal{N}^t_a$

$\mathcal{N}^+_{nat}$: Set of outgoing arcs to node $n \in \mathcal{N}^t_a$

Parameters :

δ^k_f : Delay cost of copy k of flight f, for $f \in \mathcal{F}_t$

ρ^k_f : Fuel cost associated with copy k of flight f, for $f \in \mathcal{F}_t$

σ^k_f : Aircraft swap cost of operating flight f's copy $k \in \mathcal{K}^t_f$, for $f \in \mathcal{F}_t$ by aircraft other than the one originally schedule to operate this flight.

γ_f : Cost of cancellation of flight f, for $f \in \mathcal{F}_t$

χ_{pr} : Passenger-related costs for using itinerary r to accommodate passenger p. If the passengers who cannot be accommodated on any alternative itinerary are booked on another airline's flight (using virtual itinerary r), the cost is higher, to reflect the penalty given for losing out to the competition.

n_p : Number of passengers on itinerary $p \in \mathcal{P}$

Cap_{fka} : min (number of seats available determined by payload-range capabilities of aircraft a for flight f's copy $k \in \mathcal{K}_f^t$, aircraft capacity) For each aircraft type, the payload-range equation depicts the relationship between distance of flight (*Range* in x-axis) and payload capacity (*Payload* in y-axis) with a piecewise linear curve as shown in Figure 3.3 and is modeled as a set of following constraints:

$\alpha_j * m_f + \beta_j * t_a \leq \mu_j$, for $m_{fa} \in [d_{j-1}, d_j], \forall j \in [1, 2, ..., N]$

,where m_f is the miles of flight distance for a flight f, t_a is the tonnes of aircraft a's payload, d_j is the j^{th} cut-off point in *Range*, and α_j, β_j, and μ_j are the coefficients of linear function in $[d_{j-1}, d_j]$.

Cap_{fka} is calculated as a function of m_f based on the flight leg's miles.

(e.g. $Cap_{fka} \leq \frac{(\mu_j - \alpha_j * m_f)}{\beta_j * \text{average passenger weight}}$)

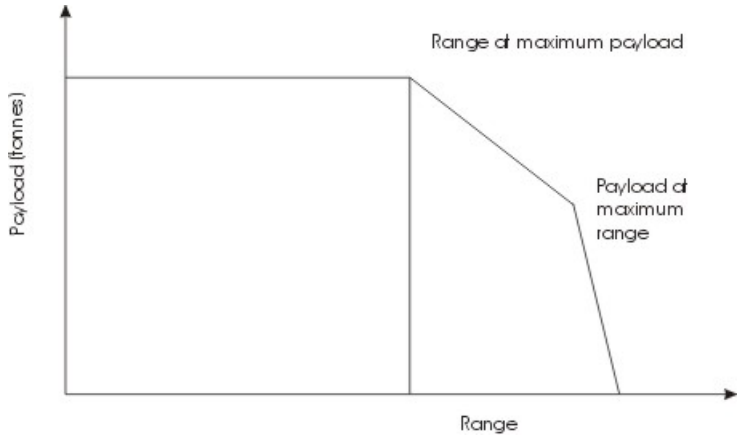

Figure 3.3: Payload capacity curve over flight distances for a given aircraft type

β_a^n : Penalty cost for aircraft a ending at a station other than the originally scheduled arrival airport in time period t

$$\theta_{fk}^{r} = \begin{cases} 1 & \text{if flight } f\text{'s copy } k \in \mathcal{K}_f^t \text{ is on itinerary } r \\ 0 & \text{otherwise} \end{cases}$$

$$s_a^n = \begin{cases} 1 & \text{if aircraft } a \in \mathcal{A} \text{ starts at node } n \text{ in } \mathcal{NW}_a^t \\ -1 & \text{if aircraft } a \in \mathcal{A} \text{ can potentially end its journey at node } n,\ n \in \mathcal{NW}_a^t \\ 0 & \text{if node } n \text{ is neither a start nor potential destination node} \end{cases}$$

Note that multiple nodes n at the end of the timeline of $\mathcal{NW}_a^t$ could be candidates for aircraft a's destination in $\mathcal{NW}_a^t$ at the end time of $\mathcal{NW}_a^t$.

$$u_f^{ka} : \begin{cases} 0 & \text{if copy } k \in \mathcal{K}_f^t \text{ cannot be operated by aircraft } a \text{ due to higher temperature} \\ 1 & \text{otherwise} \end{cases}$$

Variables :

$$x_f^{ka} = \begin{cases} 1 & \text{if copy } k \in \mathcal{K}_f^t \text{ is selected and operated by aircraft } a \\ 0 & \text{otherwise} \end{cases}$$

$$y_{ga} = \begin{cases} 1 & \text{if ground arc } g \text{ in } \mathcal{NW}_a^t \text{ of aircraft } a \text{ is selected} \\ 0 & \text{otherwise} \end{cases}$$

$$z_f = \begin{cases} 1 & \text{if } f \in \mathcal{F}_t \text{ is cancelled} \\ 0 & \text{otherwise} \end{cases}$$

v_{pr} = Number of passengers originally on itinerary p who are re-accommodated on itinerary r (v_{pp} equals the number of non-disrupted passengers traveling on their originally scheduled itinerary)

$$e_a^n = \begin{cases} 1 & \text{if aircraft } a \in \mathcal{A} \text{ starts at node } n \text{ or can potentially end at node } n \text{ in } \mathcal{NW}_a^t \\ 0 & \text{otherwise} \end{cases}$$

Note that e_n^a is known deterministically and equals 1 for the node at the beginning of $\mathcal{NW}_a^t$ where the aircraft starts its operations. e_n^a is known because of the solution to (3.1)-(3.11) at time $t-1$.

Formulation :

$$\min_{x,z} \left[\sum_{a\in\mathcal{A}} \sum_{f\in\mathcal{F}_t} \sum_{k\in\mathcal{K}_f^t} (\rho_f^k + \delta_f^k + \sigma_f^k) \cdot x_f^{ka} + \sum_{f\in\mathcal{F}_t} \gamma_f \cdot z_f + \sum_{p\in\mathcal{P}_t} \sum_{r\in\mathcal{R}_t(p)} \chi_{pr} \cdot v_{pr} + \sum_{a\in\mathcal{A}} \sum_{n\in\mathcal{N}_a^t} \beta_a^n \cdot e_a^n \right] \tag{3.1}$$

$$\sum_{a\in\mathcal{A}} \sum_{k\in\mathcal{K}_f^t} x_f^{ka} + z_f = 1 \qquad \forall f \in \mathcal{F}_t \tag{3.2}$$

$$\sum_{g\in(\mathcal{N}_{nat}^-\cap\mathcal{G}_a^t)} y_{ga} + \sum_{(f,k)\in(\mathcal{N}_{nat}^-\setminus\mathcal{G}_a^t)} x_f^{ka} + s_a^n \cdot e_a^n = \sum_{g\in(\mathcal{N}_{nat}^+\cap\mathcal{G}_a^t)} y_{ga} + \sum_{(f,k)\in(\mathcal{N}_{nat}^+\setminus\mathcal{G}_a^t)} x_f^{ka} \qquad \forall n \in \mathcal{N}_a^t, \forall a \in \mathcal{A} \tag{3.3}$$

$$\sum_{p\in\mathcal{P}_t} \sum_{r\in\mathcal{R}_t(p)} \theta_{fk}^r v_{pr} \leq \sum_{a\in\mathcal{A}} Cap_{fka} \cdot x_f^{ka} \qquad \forall k \in \mathcal{K}_f^t, \forall f \in \mathcal{F}_t \tag{3.4}$$

$$\sum_{r\in\mathcal{R}_t(p)} v_{pr} = n_p \qquad \forall p \in \mathcal{P}_t \tag{3.5}$$

$$x_f^{ka} \leq u_f^{ka} \qquad \forall k \in \mathcal{K}_f^t, \forall f \in \mathcal{F}_t, \forall a \in \mathcal{A} \tag{3.6}$$

$$x_f^{ka} \in \{0,1\} \qquad \forall k \in \mathcal{K}_f^t, \forall f \in \mathcal{F}_t, \forall a \in \mathcal{A} \tag{3.7}$$

$$z_f \in \{0,1\} \qquad \forall f \in \mathcal{F}_t \tag{3.8}$$

$$y_{ga} \in \{0,1\} \qquad \forall g \in \mathcal{G}_a^t \forall a \in \mathcal{A} \tag{3.9}$$

$$e_a^n \in \{0,1\} \qquad \forall n \in \mathcal{NW}_a^t, \forall a \in \mathcal{A} \tag{3.10}$$

$$v_{pr} \in \mathbb{Z}^+ \qquad \forall p \in \mathcal{P}_t \tag{3.11}$$

The objective function (3.1) minimizes the costs of recovery, expressed as the sum of fuel, departure holding delay and swap costs (coefficients of x_f^{ka}), cancellation (coefficient of z_f), passenger re-accommodation costs (coefficient of v_{pr}) and aircraft location costs (coefficient of e_a^n). The last term of the objective function penalizes any aircraft that ends the day at a different location that that planned, resulting in potentially unbalanced aircraft for operations and maintenance in the future. Constraints (3.2) ensure that every flight is either operated by one of the copies created over time-space networks, or canceled. Constraints (3.3)

are flow conservation constraints. They ensure the balance of incoming and outgoing flows at each node; i.e., if an aircraft is incoming to a node in a network, it must be outgoing from that node (except at the source node in each network, which only has an outgoing aircraft, and at the destination node in each network, which only has an incoming aircraft). Constraints (3.4) ensure that all passengers are assigned to a flight leg, and restrict the number of passengers assigned to a flight leg f to the number of seats available, as determined by the range of the flight f and the corresponding payload-range capabilities of each aircraft a that can operate f. Constraints (3.5) ensure that all passengers reach their destinations either on their original itinerary or an alternate one (including a virtual itinerary, representing re-accommodation on another airline's network). Constraints (3.6) enforce that the aircraft cannot operate the flights in the duration when they are disrupted due to high temperatures. Constraints (3.7), (3.8), (3.9), (3.10), and (3.11) restrict variable values to appropriate binary or integer values.

3.3.4 Dynamic Rolling Model of Passenger Recovery

We solve the above formulation as a finite-horizon dynamic program, approximated as a rolling horizon integer program. We now define the state, decisions, transition, objective and Bellman equation.

State variable: The state variable tracks the physical state of the airline's fleet as well as the state of the each passenger's itinerary based on past decisions and operations, and observed disruptions. The physical state of the airline's fleet is represented by two vectors $\boldsymbol{\theta^t}$ and $\boldsymbol{l^t}$, each defined over $a \in \mathcal{A}$. For each aircraft $a \in \mathcal{A}$, θ_{at} and l_{at} denote, respectively, its latest arrival time and its arrival airport. Note that θ_{at} can either correspond to a past time stamp (if aircraft a is on the ground at time t) or a future one (if aircraft a is in the air at time t). The state of each passenger's itinerary is represented by two vectors $\boldsymbol{pl^t}$ and $\boldsymbol{\kappa^t}$, each defined over $p \in \mathcal{P}$. For each itinerary $p \in \mathcal{P}$, pl_{pt} and κ_{pt} denote, respectively, the

location of a passenger p at time t and the remaining flights in each passenger itinerary p at time t.

Observed disruptions are represented by a vector $\boldsymbol{D^t}$ defined over $f \in \mathcal{F}^t$, where D_{ft} denotes the departure delay of flight $f \in \mathcal{F}^t$ observed at time t. The state variable, denoted by $\boldsymbol{R^t}$, is thus given by:

$$\boldsymbol{R^t} = \left(\boldsymbol{\theta^t}, \boldsymbol{l^t}, \boldsymbol{pl^t}, \boldsymbol{\kappa^t}, \boldsymbol{D^t}\right). \tag{3.12}$$

The vector $\boldsymbol{R^t}$ is used to construct the time-space networks $\mathcal{NW}_a^t$ for all $a \in \mathcal{A}$ and the passenger flow networks $\mathcal{PN}_p^t$ for all $p \in \mathcal{P}$.

Decision variables: All recovery decisions are captured by the set of copies selected across all time-space networks $\mathcal{NW}_a^t$ for $a \in \mathcal{A}$. The passenger re-accommodation decisions are captured by the list of itineraries across he passenger flow networks $\mathcal{PN}_p^t$ for $p \in \mathcal{P}$. We capture them with two decision vectors $\hat{\boldsymbol{x}}^{\boldsymbol{t}}$, $\hat{\boldsymbol{z}}^{\boldsymbol{t}}$ and $\hat{\boldsymbol{v}}^{\boldsymbol{t}}$, where $\hat{\boldsymbol{x}}^{\boldsymbol{t}}$ is defined over $a \in \mathcal{A}$ and $k \in \cup_{f \in \mathcal{F}_t} \widehat{\mathcal{K}}_{fa}^t$, $\hat{\boldsymbol{z}}^{\boldsymbol{t}}$ is defined over $f \in \mathcal{F}_t$ and $\hat{\boldsymbol{v}}^{\boldsymbol{t}}$ is defined over $p \in \mathcal{P}$ and $r \in \mathcal{R}(p)$. Specifically, $\hat{x}_{ka}^t$ is equal to 1 if copy k is selected and flown by aircraft a, and 0 otherwise; and $\hat{z}_f^t$ is equal to 1 if flight f is cancelled, and 0 otherwise. $\hat{v}_{pr}^t$ is the number of passengers on original itinerary p who are re-accommodated on itinerary r. Our decision variable, denoted by $\boldsymbol{U^t}$ given by:

$$\boldsymbol{U^t} = \left(\hat{\boldsymbol{x}}^{\boldsymbol{t}}, \hat{\boldsymbol{z}}^{\boldsymbol{t}}, \hat{\boldsymbol{v}}^{\boldsymbol{t}}\right). \tag{3.13}$$

Recovery decisions and re-accommodation decisions are subject to a set of constraints (detailed in Section 3.3.3). We denote here the decision space by $\boldsymbol{\mathcal{U}^t}$.

Objective function. Our cost function, denoted by $C_t(\boldsymbol{R^t}, \boldsymbol{U^t})$, is defined as the total cost of recovery across all flights $f \in \mathcal{F}_t$, including fuel, delay, swap and cancellation costs.

It is given by:

$$C_t(\boldsymbol{R^t}, \boldsymbol{U^t}) = \sum_{a \in \mathcal{A}} \sum_{f \in \mathcal{F}_t} \sum_{k \in \widehat{\mathcal{K}}^t_{fa}} (\rho_k + \delta_k + \sigma_k)\, \hat{x}^t_{ka} + \sum_{f \in \mathcal{F}_t} \gamma_f \hat{z}^t_f + \sum_{p \in \mathcal{P}} \sum_{r \in \mathcal{R}(p)} \pi^r_p \hat{v}^t_{pr}. \tag{3.14}$$

Transition function: The transition function describes the recovery process and the dynamic realization of disruptions between t and $t+1$. It can be represented by a function f_t as follows:

$$\boldsymbol{R^{t+1}} = f_t\left(\boldsymbol{R^t}, \boldsymbol{U^t}\right). \tag{3.15}$$

The recovery process updates the arrival airport and time of each aircraft a. For example, if a flight is operated by aircraft a from airport K to airport L, then l_{at} is updated to airport L and θ_{at} is updated to its scheduled arrival time at airport L. Conversely, if an aircraft is not assigned to any departing flight at time t, then its availability remains unchanged. Specifically, we have:

$$(\theta^{t+1}_a, l^{t+1}_a) \;=\; \begin{cases} (\theta^t_a, l^t_a), & \text{if } \hat{x}^t_{ka} = 0, \text{ for all } k \in \cup_{f \in \mathcal{F}_t} \widehat{\mathcal{K}}^t_{fa}, \\ (\overline{\theta}_k, \overline{l}_k), & \text{if } \hat{x}^t_{ka} = 1, \text{ for some } k \in \cup_{f \in \mathcal{F}_t} \widehat{\mathcal{K}}^t_{fa}, \end{cases}$$

where $\overline{\theta}_k$ and $\overline{l}_k$ denote the time and location of arrival of flight copy k, respectively. The passenger re-accommodation process updates the current airport and remaining flights of each passenger p. For example, let's say a passenger has an original itinerary p that consists of the first flight, f_1, from airport K to airport L and the second flight, f_2, from airport L to airport M. If an airline has a set of alternative itineraries and if r is one such itinerary that consists of the first flight, f'_1, from airport K to airport N, the second flight, f'_2, from airport N to airport O, and the third flight f'_3, from airport O to airport M. Two possible scenarios can happen for a passenger; either a passenger is served by an original itinerary p or one of the alternative itineraries, r. In the first case, pl_{pt} is updated to airport L and k_{pt} is updated to $\{f_2\}$. In the second case, pl_{pt} is updated to airport N and k_{pt} is updated to

$\{f'_2, f'_3\}$.

$$(pl_p^{t+1}, \kappa_p^{t+1}) \quad = \quad \begin{cases} (pl_{p_i}^t, \kappa_p^t \setminus (f_1 \cup f_2 \cup ... f_i)), & \text{if } \hat{v}_{pp}^t > 0 \\ (pl_{r_j}^t, \kappa_r^t \setminus (f'_1 \cup f'_2 \cup ... f'_j)), & \text{if } \hat{v}_{pr}^t > 0 \end{cases}$$

where $pl_{p_i}^t$ and $pl_{r_j}^t$ denote the location of arrival of flight f_i and f'_j respectively and $(f_1 \cup f_2 \cup ... f_i)$ and $(f'_1 \cup f'_2 \cup ... f'_j)$ denote the set of flights that are realized in $[t, t+1]$.

3.3.5 Dynamic Rolling Algorithms for Passenger Itineraries and Aircraft recovery

We now present our dynamic approach for passenger recovery in Algorithm 3. The algorithm loops over the full recovery horizon $\{1, ..., T\}$, and involves, at each time period t. From one period to the next, our state variable R_t is updated based upon the recovery decisions on passenger itineraries and the realized state transitions. In the remainder of this section, we first describe the procedure developed to dynamically update the passenger itineraries at at each period in Algorithm 3. Then we discuss the rolling algorithm for the aircraft recovery in Algorithm 4, which is based on the procedure developed to dynamically create the time-space network at the beginning of each period.

We use the following notation for Algorithm 3. Let $IT(p)$ be the set of flight legs in itinerary p and $IT(p, l)$ the l^{th} flight leg in itinerary p ($l \in 1, 2$). $IT(p, 2)$ is null if it is a one leg itinerary. Let p_d, p_d^l, p_a, p_a^l denote the departure time, departure location, arrival time and arrival location for the itinerary p. Let $IT(p, l)_d$, $IT(p, l)_a$ denote the departure and arrival times of $IT(p, l)$ respectively. Also let $IT(p, l)_d^l$, $IT(p, l)_a^l$ denote the departure and arrival locations of $IT(p, l)$ respectively. Define $\mathcal{P}_c$ as the set of completed itineraries. At each period t, the process checks if a flight($IT(p, 1)$) of $IT(p)$ is present in the recovery window, $[t, t + T_r]$, for each p. The process further check if a chosen flight is realized in $[t, t+1]$ and then it replaces the updated itineraries for the second flight if it is not null (We

say that a flight is realized if after solving the model, the departure time of the chosen flight is within $[t, t+1]$). Otherwise, the itinerary is complete at $[t, t+1]$ and removed from the list of itineraries to be considered for the next time period (line 3-22 in Algorithm 3). Similarly, the process also checks another condition that both of the flights($IT(p,1)$, $IT(p,2)$) of $IT(p)$ are present in the recovery window, $[t, t+T_r]$. In this case, if the chosen decision for the first flight is realized in $[t, t+1]$, the nested condition in the process checks again if the second flight is also realized or not. If so, the itinerary is complete at $[t, t+1]$ and removed from the list of itineraries to be considered for the next time period. Otherwise, it updates the realized location and time of the itineraries for the second flight if it is not null (line 23-37 in Algorithm 3).

We now present our rolling algorithm used for the Aircraft Recovery Problem(ARP) in Algorithm 4. At each period t, one time-space network is generated for each aircraft $a \in \mathcal{A}$. The process used to generate the time-space networks $\widehat{NW}_a^t$ is shown in Figure 3.4. As a starting point, the process reads the flight plans, the flight schedule, the latest availability of each aircraft, and the disruption scenario considered (see line 1-3 of Algorithm 4). This information is then used to generate a set of flight legs that can be operated by the aircraft under consideration in the decision-making window. The time at which each flight can be operated is then set to the flight's scheduled departure time or the time when the aircraft becomes available (which, itself, depends on its past flight assignments, past realized disruptions, and the aircraft's turnaround time), whichever comes last.

Next, we create a set of flight copies for each individual flight, including an "original arc", which correspond to its planned schedule, as well as additional copies that correspond to added departure holds and/or alternative flight plans. The creation of available flight plans for the aircraft considered leverages the flight planning tool from Jeppesen Commercial and Military Aviation. Note that the creation of flight copies requires assumptions on the granularity and scope of the time-space network. The granularity of the network refers to the time interval between two successive copies, referred to as *holding interval*. The smaller

Algorithm 3 Solution algorithm for Passenger Recovery Problem (PRP).

for each $t \in \{1, 2, \ldots T\}$ **do**
  for each $p \in \mathcal{P}_t$ **do**
    if $IT(p,1)_d \in$[t,t+T$_R$] AND ($IT(p,2)$ is null OR $IT(p,2)_d \in$[t+T$_R$, T]) **then**
      $\varphi \leftarrow IT(p,1)$
      Let $\varphi_{selected}$ be the selected itinerary after solving the model for φ.
      if $IT(\varphi_{selected},1)_d \in [t, t+1]$ **then**
        $\kappa \leftarrow IT(\varphi_{selected},1)$
      end if
      if $IT(\varphi_{selected},2)$ is not null and $IT(\varphi_{selected},2)_d \in [t, t+1]$ **then**
        $\kappa = IT(\varphi_{selected},2)$.
      end if
      if κ is not null **then**
        if $IT(p,2)$ is not null **then**
          $p_d \leftarrow \kappa_a$, $p_d^l \leftarrow \kappa_a^l$
          $p_a \leftarrow IT(p,2)_a$, $p_a^l \leftarrow IT(p,2)_a^l$
          $P_{t+1} \leftarrow P_{t+1} \cup p$
        else
          $\mathcal{P}_c \leftarrow \mathcal{P}_{t+1} \cup p$
        end if
      else
        $P_{t+1} \leftarrow P_{t+1} \cup p$
      end if
    else if $IT(p,1)$ *and* $IT(p,2)$ are in $[t, t+T_R]$ **then**
      Let $p_{selected}$ be the selected itinerary.
      if $IT(p_{selected},1) \in [t, t+1]$ AND ($IT(p_{selected},2)$ is null OR $IT(p_{selected},2)_d \in [t, t+1]$) **then**
        $P_c \leftarrow P_c \cup p$
      end if
      if $IT(p_{selected},1)_d \in [t, t+1]$ AND $IT(p_{selected},2)_d \notin [t+1, T]$ **then**
        $p_d \leftarrow IT(p_{selected},1)_a$, $p_d^l \leftarrow IT(p_{selected},1)_a^l$
        $p_a \leftarrow IT(p,2)_a$, $p_a^l \leftarrow IT(p,2)_a^l$
        $P_{t+1} \leftarrow P_{t+1} \cup p$
      else
        $P_{t+1} \leftarrow P_{t+1} \cup p$
      end if
    end if
  end for
end for

the holding interval, the larger the decision space, so the larger the model's computational complexity, but the better the solution might be. In our computational experiments, we use a holding interval of 10 minutes. The scope of the network refers to the *maximum holding window* for each flight, i.e., the largest allowed departure hold. For instance, a maximum holding window of 1 hour implies that at most 7 copies of each flight can be created (associated with a departure hold from 0 to 60 minutes by intervals of 10 minutes). This information is then used to generate the ground arcs and flight arcs in the time-space network for the aircraft, time period, and disruption scenario under consideration.

The set of all time-space networks $\widehat{NW}_a^t$ for all aircraft a defines the input sets and parameters of the Aircraft Recovery Problem(ARP). The model is then solved using Mixed Integer Programming (line 11). From the model's solution, the state of the system R_t is then updated (lines 13 - 18). However, in instances where large disruptions happen, the problem may result in infeasible solutions due to the flow balance constraints, and if we cancel flights that cause infeasibility without increasing the maximum holding window it can result in an excessively large number of flight cancellations. This happens when the availability of any aircraft is further in the future (because of large delays) than allowed holding window for the flight it is scheduled to operate. Because of this, the supply node corresponding to the aircraft has no outgoing arc and thus the flow balance contrainst is unsatisfied at that node.

Indeed, in practice, the airlines need to balance the objectives of minimizing the deviations from the flight schedule (captured by the maximum holding window) and the objective of minimizing the number of cancellations. For this reason, when we get an infeasible solution, we first increase the maximum holding window using the procedure outlined above iteratively, to try mimize the number of cancellations which as a result imposes an upper bound to the number of flight cancellations, denoted by Γ. In our experiments, we set the maximum holding window expansion limit such that Γ is 5% of the number of flights considered in the ARP at each time period t.

Specifically, we start with a maximum holding window set to an initial value (line

4 in Algorithm 4). If the solution is feasible and results in less than Γ flight cancellations, then we update the state variable accordingly, and proceed to the next period (lines 12-18). In contrast, if the solution is infeasible or if it results in more than Γ cancellations (lines 19-21), then we increase the maximum holding window by increments of δ. As soon as a feasible solution that cancels less than Γ flights is found, we update our state variable and proceed to the next period. However, if no such solution is found once the maximum holding window reaches a pre-specified upper bound, we remove the restriction on the number of cancellations and re-solve the model (lines 23-35). We repeat this process throughout the decision-making window, until all flights of the day have been operated.

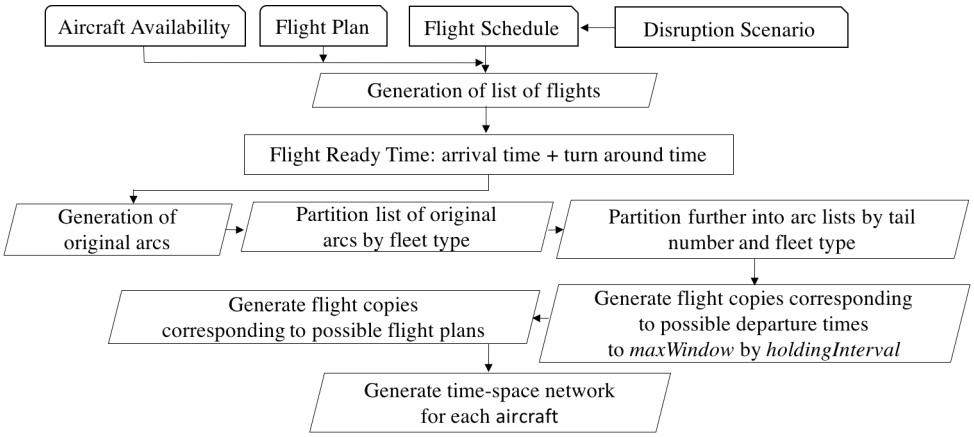

Figure 3.4: Process used to create time-space networks $\mathcal{NW}_a^t$.

3.3.6 Solution Approach Improvements: Special Ordered Sets and Warm Start

In this section, we describe two solution strategies we took to improve the runtime of the model. We used special branching strategies and warm start solution based on known initial solution to speed up the performance.

Algorithm 4 Solution algorithm for the Aircraft Recovery Problem (ARP).

get R_1 for $a \in \mathcal{A}$;
for each $t \in \{1, 2, \dots T\}$ **do**
  get $\mathcal{F}_t, \cdots, \mathcal{F}_{t+T_R}$
  maxWindow = initialHoldingWindow;
  holdingInterval = 10 minutes;
  set feasibleSolution = false;
  while feasibleSolution = false *and* maxWindow$\leq$ maxWindowLimit **do**
    for each $a \in \mathcal{A}$ **do**
      Generate $\mathcal{NW}_a^t$; ▷ See Figure 3.4
    end for
    Solve *aircraft recovery problem (ARP)*;
    if ARP feasible and less than Γ cancellations **then**
      feasibleSolution = true;
      for each $a \in \mathcal{A}$, each $f \in \mathcal{F}_t$, each $k \in \widehat{\mathcal{K}}_{fa}^t$ **do**
        if $x_{ka}^t \equiv x_{ka}^t = 1$ **then**
          Update $\boldsymbol{R^t}$ with new location and time of all aircraft $a \in \mathcal{A}$;
        end if
      end for
    else
      maxWindow=maxWindow+δ
    end if
  end while
  if feasibleSolution = false **then**
    $\tilde{A}$ = set of aircraft that cause infeasibility ;
    maxWindow = initialHoldingWindow;
    for each $a \in \mathcal{A} \setminus \tilde{A}$ **do**
      Generate $\mathcal{NW}_a^t$;
    end for
    Solve *aircraft recovery problem (ARP)*;
    for each $a \in \mathcal{A}$, each $f \in \mathcal{F}_t$, each $k \in \widehat{\mathcal{K}}_{fa}^t$ **do**
      if $x_{ka}^t = 1$ **then**
        Update $\boldsymbol{R^t}$ with new location and time of aircraft a;
      end if
    end for
  end if
end for

Special Ordered Sets.

Special ordered sets (SOS), which were first introduced by Beale and Tomlin (1970), are widely used in branch-and bound algorithms to alleviate the computational burden of branch-and-bound methods that do not take into account the structure of the constraints by branching on sets of variables, rather than individual variables. If we know a variable is part of a set which is ordered, it can help the branching strategies in branch-and bound.

Specifically, a Special Ordered Set of type 1 (SOS1) is defined to be a set of variables for which at most one of the variable from the set may be non-zero in a feasible solution. The special structure of our decision variables restricted by the flight coverage constraints (Equation 3.2), modeled as set-partitioning constraints in our formulation allows us to implement the SOS1.

Conventional branching on x_{lk} is basically dividing it by $x_{lk} = 0$ and $\sum_{j \neq k} x_{lj} = 0$, as the latter equality is implied by $x_{lk} = 1$. The $x_{lk} = 1$ branch will have relatively less solutions as compared to the $x_{lk} = 0$ branch. This will result in almost no progress from the parent node as the $x_{lk} = 0$ branch will end up containing almost the same feasible region as that of its parent. More efficient progress can be achieved by dividing the feasible region of the parent node in a more balanced way over the children nodes. The branching rule on SOS achieves this by branching on sets of variables rather than on the individual variables:

$$\sum_{j=1}^{\lfloor \frac{n_l}{2} \rfloor} x_{lj} = 0 \quad \text{or} \quad \sum_{j=\lfloor \frac{n_l}{2} \rfloor + 1}^{n_l} x_{lj} = 0.$$

The performance guarantees on this approach have been mathematically shown in Martin (1999) as follows. Let us first define k_i = number of free integer variables in SOS branching i, $i = 1, 2, 3, ..., p$ at node h. Now let S_h be the number of solutions yet to be enumerated at node h. Then $S_h = \prod_{i=1}^{p} k_i$. If the special ordered set $\sum_{j=1}^{n_l} x_{lj} = 1$ is selected for branching and that none of the x_{lj} are to be fixed at 0 or 1, then because $\min\{\frac{(n_l - \lfloor \frac{n_l}{2} \rfloor) S_h}{n_l}, \frac{\lfloor \frac{n_l}{2} \rfloor S_h}{n_l}\} > \min\{\frac{(n_l - 1) S_h}{n_l}, \frac{S_h}{n_l}\} = \frac{S_h}{n_l}$ for $n_l \geq 4$, SOS branching

enumerates more solutions with each fathom than the conventional branching and thus can enable faster progress towards an optimal solution.

Using Advanced Start.

In solving mixed integer programming problems (MIPs), warm start information provides additional input data that can allow the solver to quickly get "close" to optimality. We can add warm starts by either taking advantage of specific knowledge of the problem or by solving an easier instance of the problem (IBM 2015).

A warm start solution can provide a better initial point than what the algorithm can derive on its own, and heuristics in solvers may perform better in the presence of an initial solution. Because warm start options are processed first, the best of these solutions is treated as the incumbent solution. This allows the branch and bound to cut off larger portions of the search space.

3.4 Experimental Setup

3.4.1 Airline Network Description

We consider the flight network of Delta Air Lines, a major hub-and-spoke airline in the United States. The choice of airline is arbitrary, and is not specific to any airline's operating practices. Delta Air Lines leverages six airports as hubs of operations (New York's LaGuardia (LGA) and John F. Kennedy (JFK), Atlanta (ALT), Detroit (DTW), Minneapolis-Saint Paul (MSP), and Salt Lake City (SLC)). We obtain flight schedules and fleet assignments from the Aviation System Performance Metrics (ASPM) database maintained by the Federal Aviation Administration (FAA).

We use baseline flight schedules from four weekdays (July 15-18) in July 2014, shown in Table 3.1, which repeat on weekdays as per a daily schedule. In our experiments, the schedules from all fleet types are considered to model the entirety of the airline network,

and the passengers connecting across the different fleet types from origins to destinations. We also obtain passenger itinerary data for the same days as inputs to the schedule. We first extracted the itineraries that contain the flight legs that were present in the airlines schedule for or July 17, 2014. Passenger itineraries were then sorted in the descending order of the number of passengers and the top 10,000 ones are picked. This captures 16% of total passengers on July 17, 2014 to observe the major impact on passenger delays under climate change-related disruptions. We report passenger itinerary statistics in Table 3.2, corresponding to the flight network described in Table 3.1.

In terms of spatial concentration, the airline's network is tightly connected to the six hub airports—with around 50% of the arrivals and departures at a hub. We are interested in the airports (hubs) at which capacity is significantly affected due to warming, specifically, ATL, SLC, and LGA. While ATL and SLC experience capacity drops primarily due to rising temperatures, LGA is affected due to the combination of temperature increases and a short runway. We focus on the impact of climate change for operations at all the hubs and at PHX airport (specifically because its combination of temperature and altitude has shown significant vulnerability to rising temperatures).

Table 3.1: Summary statistics for the flight network.

Metric	July 15	July 16	July 17	July 18
# flights	2,324	2,330	2,348	2,379
# arr. – LGA	65	64	68	67
# arr. – ATL	640	632	625	647
# arr. – SLC	102	103	105	105
Total	807	799	798	819
# dep. – LGA	65	65	67	67
# dep. – ATL	636	634	627	642
# dep. – SLC	102	104	105	103
Total	803	803	799	812

Table 3.2: Summary statistics for the passenger itinerary network.

# Total passenger itineraries	10,000
# spoke-to-spoke	9,112
# connecting via a hub	9,071
# connecting via LGA, ATL, SLC or PHX	7,107
# spoke-to-hub	427
# destined to a hub	427
# destined to LGA, ATL, SLC or PHX	231
# hub-to-spoke	451
# originating at a hub	451
# originating at LGA, ATL, SLC or PHX	251

3.4.2 Inference and Classification of Disruption Instances

We first infer disruption realizations from historical real-world data, to compare their impacts in current times, and in the future under climate change. We use the departure delays from the Bureau of Transportation Statistics (BTS) database. Because these delays result from combined propagated (due to late arriving previous aircraft), as well as 'independent' disruptions at the systemic and contingent disruptions, using them directly would result in double-counting propagated disruptions (which would carry over from previous time periods as well as appear in the newly generated disruptions). We thus need to infer the "new" (systemic and contingent) disruptions by subtracting propagated disruptions.

To this end, we use the inference method from Lan et al. (2006a). We first sort the sequence of flight legs operated by each aircraft. We assume a minimum turnaround time of 30, 35 and 40 minutes for A319, A320 and B752 aircraft, respectively. For every pair of consecutive flights i and j operated by the same aircraft, we define the *slack* between i and j as the difference between the planned and minimum turnaround times between the two flights. The propagated delay of flight j is then computed as max(Arrival Delay of Flight i − Slack, 0). By subtracting this propagated delay from total delays, we obtain the newly created delays (from systemic and contingent disruptions). Additionally, for interpretability of our results, we classify all disruption instances into "small", "medium" and "large" disruptions, using a

classification procedure along similar lines as Lee et al. (2020).

Our testbed consists of 20 disruption scenarios, inferred from Delta Air Lines' historical operations in July 2014. These scenarios are categorized into small, medium and large disruptions based on the magnitude and extent of the disruption, as shown in Table 3.3.

Table 3.3: Disruption instance categories

Size	Small	Medium	Large
Num	7	7	6

3.4.3 Climate Change Parameter Settings

We perform our analysis for Boeing 737, Airbus A320 and Boeing 757 aircraft, using the Boeing 737-800 (B738), the A320-200 with CFM56 engines (A320), and the B757-200 (B752) as the archetypes of these aircraft. Each aircraft's manual of airplane characteristics for airport planning describes the relationship between the aircraft's maximum take-off weight, runway length, and ambient air temperature. These relationships appear as a series of graphs in each manual. We digitize the graphs and fit a linear model, which expresses the maximum take-off weight as a function of runway length and ambient temperature. The results of this analysis are summarized in Table 3.4 and equations (3.16), (3.17), and (3.18).

Table 3.4: Fitted Parameters for Allowable Payload for Different Aircraft Fleet Types (standard deviation in italics).

Variable	**B738**	**B757**	**A320**
(Intercept)	35	242	-116
	2.9	*50*	*3.5*
log(runway length in thousands of feet)	61	75	25
	0.79	*4.0*	*0.69*
Surface temperatures in degrees C	0.89	-18	-0.45
	0.16	*5.5*	*0.068*
(Surface temperatures in degrees C)^2	-0.023	0.60	0.037
	0.002	*0.19*	*0.006*
(Surface temperatures in degrees C)^3		-0.0067	-0.00082
		0.0021	*0.00013*
R^2	0.95	0.87	0.72

For the B738 aircraft, this relationship is best described by the following equation:

$$\begin{aligned} max\_takeoff\_weight = 60.8 * log(runway\_length) + \\ 0.9 * (ambient\_temperature) - \\ 0.02 * (ambient\_temperature)^2 + 35, \end{aligned} \tag{3.16}$$

where: (i) *max_takeoff_weight* is the aircraft's maximum take-off weight in thousands of pounds, (ii) *runway_length* is the runway length in thousands of feet. For airports with multiple runways, we run a separate analysis for each runway length. For example, Atlanta's Hartfield-Jackson airport has two runways that are each 9000 feet long, a third that is 10,000 feet long, and a fourth that is 12,400 feet long; (iii) ***ambient_temperature*** is the ambient air temperature, expressed in degrees centigrade, in the city in which the airport is located. As described in Section 3.2.1, we obtain 20 forecasts, which emerge from 20 climate models, of the ambient temperature at sea level for every hour of our years of interest (2035 and 2050). The aircraft performance curves from which the relationship above is derived are based on sea level temperature. In the case where the airport under consideration is not at sea level, we calculate an equivalent temperature by using earth's atmospheric lapse rate of 2 degrees C per 1000 feet(Hartmann 2015). That is, we assume that the air at an airport that is 1000ft above sea level and at a temperature of 20 degrees C has the same density as an airport that is at sea level and where the surface temperature is 22 degrees C.

For A320 aircraft, the relationship is described by

$$\begin{aligned} max\_takeoff\_weight = 24.7 * log(runway\_length) - \\ 0.45 * (ambient\_temperature) + \\ 0.037 * (ambient\_temperature)^2 - \\ 0.00082 * (ambient\_temperature)^3 - 116 \end{aligned} \tag{3.17}$$

For B757 aircraft, the relationship is described by

$$\begin{aligned} max\_takeoff\_weight = 74.5 * log(runway\_length) - \\ 18 * (ambient\_temperature) + \\ 0.6 * (ambient\_temperature)^2 - \\ 0.0067 * (ambient\_temperature)^3 + 242 \end{aligned} \tag{3.18}$$

Using these equations, we calculate the maximum takeoff weight for each hour of each year of interest, for each of the aircraft we are interested in, for each airport-runway combination. We calculate the mass of fuel needed for the aircraft to perform its journey using EUROCONTROL's Small Emitters Tool (EUROCONTROL 2018). In practice, we use the tool to calculate the fuel burn for each aircraft type for flight lengths from 100 miles to the maximum range of the aircraft in increments of 100 miles. For each flight, we estimate the fuel burn by rounding up the actual flight length and rounding up the nearest hundred. To account for the fact that the aircraft must carry some reserve fuel, we add the mass of fuel necessary for the aircraft to fly 200 miles to the mass of fuel that must be burned for it to complete the flight. This gives us an estimate of the total mass of fuel that the aircraft must carry. We subtract this fuel mass and the mass of the empty aircraft to estimate the maximum payload that the aircraft can carry. We assume that passengers (and their luggage and amenities) constitute the entire payload. As such, we divide the maximum available payload by 220lb (a scaled projection from 100kg used in 2019) to calculate the maximum number of passengers that the aircraft can carry, given its capabilities, the ambient temperature, and runway length. Where this number is less than the passenger capacity of the aircraft (assumed to be 175 for B738, 186 for A320 and 156 for A319) we calculate the maximum load factor of the aircraft as the ratio of the maximum number of passengers the aircraft can carry to the number of passengers on a full aircraft. Where this ratio is less than 0.86, we assume that the flight is disrupted. This is because the average load factor on U.S. domestic flights is 0.85 (BTS) and we assume that airlines

are likely reluctant to operate flights that are much emptier than that. Our threshold for interruption is in fact somewhat higher than this number because it is likely that the method described above somewhat overestimates the maximum capacity factor of the aircraft. For example, we ignore any cargo that the aircraft might be carrying in its belly, although it is known that about 40% of all airborne freight travels in the bellies of passenger flights (Bryant et al. 2016). We also ignore the practice of tankering, where—due to considerations of price or schedule optimization—an airplane may take off with enough fuel to complete the next several flights.

3.4.4 Classification of Climate Change Cases

We evaluate our model under multiple climate change models or cases corresponding to the RCP8.5 scenario for 2035 and 2050, based on different input parameters as discussed in Section 3.4.3. For this, we classify each climate change case into "mild", "medium" and "severe" categories. We use a multinomial logistic regression with two independent variables: average capacity drop and maximum capacity drop during the test day in July 2014. Our model is trained with selected cases that are *a priori* classified into the three categories, as a training step. We then perform a validation step, to predict the groups for all remaining cases. The proportional log-odds of a climate change case belonging to the mild and medium category, versus the severe category, is defined as the logarithm of the ratio of the two probabilities. The fitted logistic regression model is described in Equations (3.19) and (3.20), where P_{mild}, P_{med} and P_{severe} denote the probabilities of belonging to the mild, medium and severe categories, respectively.

$$\log\left(\frac{P_{mild}}{P_{severe}}\right) = \beta_0 + \beta_1^{mild} \text{ avg. capacity drop} + \beta_2^{mild} \text{ max capacity drop} \tag{3.19}$$

$$\log\left(\frac{P_{med}}{P_{severe}}\right) = \beta_0 + \beta_1^{med} \text{ avg. capacity drop} + \beta_2^{med} \text{ max capacity drop} \tag{3.20}$$

The coefficients corresponding to the classification based on logistic regression are

reported in Tables 3.5 and 3.6 for 2035 and 2050 respectively. The resulting classification of climate change cases into severe, medium and mild is presented in Table 3.7. Among the six hub airports of the airline's network, we are specifically interested in four airports at which capacity is significantly affected due to warming - ATL, SLC, PHX, and LGA. The chosen climate change models at these four hubs we consider for the experiments for 2035 and 2050, to be discussed in the next section, are summarized in Table 3.8.

Table 3.5: Parameter estimates for multinomial logistic regression for 2035.

	mild (vs. worst)		medium (vs. worst)	
Predictor	Coef.	p-value	Coef.	p-value
constant	1762.85	0.00014	850.01	0.0062
avg. cap drop	-2032.01	0.00015	-980.63	0.0063
max cap drop	-63.39	0.07321	-13.84	0.3366

Table 3.6: Parameter estimates for multinomial logistic regression for 2050.

	mild (vs. worst)		medium (vs. worst)	
Predictor	Coef.	p-value	Coef.	p-value
constant	1342.38	0.0027	597.71	0.0407
avg. cap drop	-1494.76	0.0028	-672.40	0.0409
max cap drop	-44.10	0.164	-10.48	0.275

3.4.5 Recovery Parameter Settings

Cost Parameters: We use the following cost parameters in our objective function. Aircraft swap costs (σ_k) are set to \$500 per intra-fleet swap and \$1000 per inter-fleet swap as described in Marla et al. (2017b). Cancellation costs (γ_f) are estimated as the cost to the airlines of re-accommodating passengers on the next available flight serving the same destination—to the airlines of re-accommodating passengers on the next available flight serving the same destination—assuming average 200 seats, a constant load factor of 85%, and a cost of \$37.5 per hour of passenger delays (including re-booking costs, goodwill cost) and average 4 hours of flight. Fuel costs (ρ_k) are set to \$0.73 per lb, according to the fuel

Table 3.7: Classification of climate change cases for 2035 and 2050

Climate change case	Classified category (2035)	Classified category (2050)
bcc-csm1-1_rcp85	Medium	Severe
bcc-csm1-1-m	Medium	Mild
BNU-ESM_rcp85	Mild	Severe
CanESM2_rcp85	Medium	Severe
CCSM4_rcp85	Severe	Mild
CNRM-CM5_rcp85	Mild	Medium
CSIRO-Mk3-6-0	Medium	Medium
GFDL-ESM2G_	Mild	Mild
GFDL-ESM2M_	Mild	Medium
HadGEM2-CC365_rcp85	Medium	Severe
HadGEM2-ES365_rcp85	Medium	Mild
inmcm4_rcp85	Severe	Mild
IPSL-CM5A-LR	Severe	Mild
IPSL-CM5A-MR	Mild	Mild
IPSL-CM5B-LR	Severe	Mild
MIROC-ESM_rcp85	Severe	Mild
MIROC-ESM-CHEM_rcp85	Severe	Medium
MIROC5_rcp85	Medium	Medium
MRI-CGCM3_rcp85	Mild	Medium
NorESM1-M_rcp85	Severe	Mild

Table 3.8: Representative climate change cases used in experiments

Category	**Case for 2035**	**Case for 2050**
Severe	IPSL-CM5B-LR	bcc-csm1-1_rcp85
Medium	CanESM2_rcp85	CNRM-CM5_rcp85
Mild	CNRM-CM5_rcp85	IPSL-CM5B-LR

price development charts. Finally, we use a baseline value for the flight delay cost (δ_k) of \$10 per minute of delay. Passenger re-accommodation cost is set to the fixed cost portion of \$400 per passenger (Jenkins and Marks 2011) plus the variable cost of passenger delay of \$1.09 per minute (Marla et al. 2017b). Disrupted passengers that are not able to be re-accommodated are assumed to be rebooked on another airline using a hypothetical itinerary in our model, with a penalty that is greater than the re-accommodation cost in our network. The penalty cost for aircraft ending the day of operations at a different location than originally planned (β_a^n), defined in Section 3.3.3 is set to be 1.5 times the cancellation cost,

because this potentially results in future operational and maintenance costs.

3.5 Computational Results

We now discuss our computational results for the 20 disruption instances extracted from a high traffic and high temperature timeframe in July as described in Section 3.4.2 and Table 3.3, over the representative climate change cases from 2035 and 2050 (Table 3.8). Our results compare aircraft and passenger recovery costs incurred *by the airline* under climate conditions in 2014 against 2035 and 2050. As described in Section 3.4, we assume similar network structures, engine properties and load factors for 2035 and 2050, as were seen in 2014. The metrics we present in our results are as follows. For the aircraft recovery component, we present the (i) total aircraft recovery costs ($), the total departure delay in minutes, over the entire network, (iii) the total arrival delay in minutes, over the entire network, (iv) the total fuel burnt to execute the chosen flight plans over the network, (v) the number of flight swaps executed to manage the disruption, (vi) the number of flights canceled on the network, (vii) the number of flights who speeds are changed to help manage the disruption, and (viii) the number of aircraft that are unbalanced, that is, they end operations at airports different from where they were intended, and cause disruptions for the future. For the passenger recovery component, we report (i) the delay minutes experienced by passengers whose itineraries are not broken or disrupted (*undisrupted pax delay min*), (ii) the delay minutes experienced by passengers who itineraries are disrupted and therefore they have to be reaccommodated onto alternative itineraries (*disrupted pax delay min*), (iii) the cost of the disrupted passenger delays, (iv) the number of passengers that need to be reaccommodated on itineraries not belonging to this airline (virtual itineraries), (v) reaccommodation costs for passengers that need to use another airline, (vi) the total passenger delay minutes, (vii) total passenger delay costs, (viii) sum of aircraft-related and passenger-related costs.

3.5.1 Impact of 20 years of climate change: 2014 vs. 2035

We compare aircraft recovery costs under mild, medium and severe climate cases in 2035 versus 2014 in Tables 3.9, 3.10 and 3.11. Corresponding passenger recovery costs are presented in 3.12, 3.13 and 3.14. Comparing first the aircraft recovery costs, our results show that the capacity drops induced by increased temperatures result in significant increase in both departure and arrival delays, number of swaps, and cancellations. Due to increased cancellations, we don't observe significant change in the fuel burn from 2014 to 2035. The combined effect of these aircraft recovery mechanisms results in increased total costs of 18.7% to 39.3% on average compared to 2014's costs under the severe climate change cases, 19.8% to 26.1% on average under the medium climate change cases, and 18 % to 38.7 % on average for mild medium climate change, compared to 2014's costs. We find that the costs of aircraft recovery over individual disruption instances increase by 6.6% to 68.9% for severe climate change cases, by 5.4% to 56.2 % for medium climate change cases, and by 8.5 % to 124.2 % for mild climate change.

The corresponding total passenger delay costs under 2035 climate change cases (Column 9 of Tables 3.12, 3.13 and 3.14) experienced by the airline increase by as much as 29% to 36.4% on average for mild climate change cases, 31.2% to 38.4% on average for medium climate change cases, and 29.3% to 33.6% on average for severe climate change cases over all sizes of disruptions. We observe that, over individual disruption instances, passenger-related recovery costs increase by as much as 19.1% to 55.6% for mild climate change cases, 18.9% to 47.4% for medium climate change cases, and 14.4% to 46.5% for severe climate change cases.

Combining the effect of aircraft and passenger-related delay costs to the airline, we find an increase of 26% to 36% on average for severe climate change cases, 28% to 50% on average for medium climate change cases, and 26% to 56% for mild climate change cases. Over individual disruption instances, we find that the total costs of aircraft and passenger-

related delay increase by as much as 18% to 178% for mild climate change cases, 13% to 165% for medium climate change cases, and 11.2% to 45% for severe climate change cases. We guess that the average percentage increase in combined aircraft and passenger-related delay costs as a percentage of existing costs do not significantly differ for the severe climate change cases from for the medium climate change cases, because the variation in capacity reductions due to climate-change imposed disruptions over the severe and medium climate change cases in 2035 is significantly lower than the difference in the size of original disruptions induced by airline or airport delays themselves.

As expected overall our experimental results show that the average total recovery costs, combined aircraft and passenger-related delay costs, increase over the size of the disruptions under the same climate change case as shown in Column 10 of Tables 3.12, 3.13 and 3.14. The most significant difference in terms of the average percentage increase as compared to 2014 is achieved when the disruption size is the smallest and the least average percentage increase is when the disruption size is the largest. This trend is consistent over different climate change cases. This indicates that for the year 2035, the relative impact of disruptions due to climate change is most noticeable in scenarios with small disruptions, as the capacity drops dominate the disruption itself.

Figure 3.5 shows that the recovery cost increases over all climate change cases projected for the year 2035 vs.the base year 2014. The largest cost increase is observed under the largest disruption scenarios, but the cost increase does not change significantly over the severity of the climate change case. Hence we observe that the difference in cost increase is mainly driven by the magnitude of disruptions. We also observe that, under all disruption sizes in 2035, the severe climate change cases have a neutral impact on the cost increase on average and we conclude that the size of the airline disruption has a significantly more dominant effect on the increase in recovery cost.

Table 3.9: Comparison of daily aircraft-related costs for recovery, 2014 versus 2035, under "Mild" climate change case, by disruption category.

Disruption Category	Year	Total Cost($)	Dep. Delay (min)	Arr. Delay Delay (min)	Fuel Burn (lb)	Num. Swaps	Num. Cancel.	Num. Speed Changes	Num. Unbalanced	Cost Increase
Small	2014 (min.)	1,423,586	2,855	3,364	1,690,290	23	1	38	0	–
	2014 (avg.)	1,575,194	4,289	4,815	1,792,383	66	8	45	0	–
	2014 (max.)	1,687,179	6,702	7,258	1,855,248	130	13	48	1	–
	2035 (min.)	1,667,498	4,444	4,961	1,420,119	187	7	27	0	11.8%
	2035 (avg.)	2,200,004	8,800	9,261	1,714,922	297	30	42	0	38.7%
	2035 (max.)	3,712,420	19,538	19,734	1,802,613	527	100	49	1	124.2%
Medium	2014 (min.)	1,632,927	5,736	6,330	1,668,951	57	7	40	0	–
	2014 (avg.)	1,770,040	8,185	8,689	1,770,186	86	16	44	0	–
	2014 (max.)	1,902,869	10,643	11,056	1,862,433	119	22	49	1	–
	2035 (min.)	1,984,489	7,467	7,982	1,627,763	229	18	40	0	8.5%
	2035 (avg.)	2,083,522	10,482	10,979	1,741,028	273	23	43	0	18.0%
	2035 (max.)	2,147,428	13,448	13,902	1,818,789	302	30	47	0	27.0%
Large	2014 (min.)	1,926,819	7,109	7,588	1,643,874	98	19	41	0	–
	2014 (avg.)	2,137,080	14,402	14,866	1,731,739	162	29	46	0	–
	2014 (max.)	2,448,624	22,023	22,367	1,795,621	256	40	53	1	–
	2035 (min.)	2,349,092	8,244	8,592	1,420,119	303	31	26	0	11.1%
	2035 (avg.)	2,944,520	15,476	15,867	1,589,257	432	62	36	0	33.6%
	2035 (max.)	3,712,420	20,314	20,510	1,739,695	530	100	46	2	63.2%

Table 3.10: Comparison of daily aircraft-related costs for recovery, 2014 versus 2035, under "Medium" climate change case, by disruption category.

Disruption Category	Year	Total Cost($)	Dep. Delay (min)	Arr. Delay Delay (min)	Fuel Burn (lb)	Num. Swaps	Num. Cancel.	Num. Speed Changes	Num. Unbalanced	Cost Increase
Small	2014 (min.)	1,423,586	2,855	3,364	1,690,290	23	1	38	0	–
	2014 (avg.)	1,575,194	4,289	4,815	1,792,383	66	8	45	0	–
	2014 (max.)	1,687,179	6,702	7,258	1,855,248	130	13	48	1	–
	2035 (min.)	1,778,884	4,574	5,163	1,664,032	202	10	35	0	5.4%
	2035 (avg.)	1,933,110	6,461	6,986	1,761,068	263	18	45	1	22.9%
	2035 (max.)	2,127,163	9,030	9,570	1,824,964	333	26	48	2	33.5%
Medium	2014 (min.)	1,632,927	5,736	6,330	1,668,951	57	7	40	0	–
	2014 (avg.)	1,770,040	8,185	8,689	1,770,186	86	16	44	0	–
	2014 (max.)	1,902,869	10,643	11,056	1,862,433	119	22	49	1	–
	2035 (min.)	1,969,998	7,561	8,119	1,711,654	235	18	39	0	6.9%
	2035 (avg.)	2,116,156	10,425	10,913	1,740,683	291	24	43	0	19.8%
	2035 (max.)	2,410,395	13,277	13,717	1,789,694	363	36	48	0	30.5%
Large	2014 (min.)	1,926,819	7,109	7,588	1,643,874	98	19	41	0	–
	2014 (avg.)	2,137,080	14,402	14,866	1,731,739	162	29	46	0	–
	2014 (max.)	2,448,624	22,023	22,367	1,795,621	256	40	53	1	–
	2035 (min.)	2,152,723	9,104	9,463	1,445,993	279	25	29	0	8.4%
	2035 (avg.)	2,692,414	16,027	16,416	1,596,231	396	51	39	0	26.1%
	2035 (max.)	3,306,135	23,128	23,436	1,774,854	510	79	49	0	56.2%

3.5.2 Impact of 35 years of climate change: 2014 vs. 2050

Tables 3.15, 3.16 and 3.17 compare the aircraft-related costs experienced by the airline during disruption management for the instances described in Table 3.3. The corre-

Table 3.11: Comparison of daily aircraft-related costs for recovery, 2014 versus 2035, under "Severe" climate change case, by disruption category.

Disruption Category	Year	Total Cost($)	Dep. Delay (min)	Arr. Delay Delay (min)	Fuel Burn (lb)	Num. Swaps	Num. Cancel.	Num. Speed Changes	Num. Unbalanced	Cost Increase
Small	2014 (min.)	1,423,586	2,855	3,364	1,690,290	23	1	38	0	–
	2014 (avg.)	1,575,194	4,289	4,815	1,792,383	66	8	45	0	–
	2014 (max.)	1,687,179	6,702	7,258	1,855,248	130	13	48	1	–
	2035 (min.)	1,672,638	4,023	4,497	1,691,358	204	7	39	0	6.6%
	2035 (avg.)	1,870,056	5,860	6,384	1,758,565	247	15	44	0	18.9%
	2035 (max.)	2,097,834	9,074	9,610	1,797,019	297	27	48	1	28.9%
Medium	2014 (min.)	1,632,927	5,736	6,330	1,668,951	57	7	40	0	–
	2014 (avg.)	1,770,040	8,185	8,689	1,770,186	86	16	44	0	–
	2014 (max.)	1,902,869	10,643	11,056	1,862,433	119	22	49	1	–
	2035 (min.)	2,105,144	6,601	6,940	1,600,730	257	22	32	0	12.8%
	2035 (avg.)	2,463,817	9,568	9,990	1,683,124	338	42	39	0	39.3%
	2035 (max.)	3,112,379	12,405	12,772	1,778,797	439	73	46	1	68.9%
Large	2014 (min.)	1,926,819	7,109	7,588	1,643,874	98	19	41	0	–
	2014 (avg.)	2,137,080	14,402	14,866	1,731,739	162	29	46	0	–
	2014 (max.)	2,448,624	22,023	22,367	1,795,621	256	40	53	1	–
	2035 (min.)	2,233,995	8,767	9,124	1,602,123	281	28	35	0	7.0%
	2035 (avg.)	2,567,439	16,185	16,563	1,640,796	392	43	40	1	18.7%
	2035 (max.)	2,867,304	24,185	24,498	1,710,085	494	53	44	2	41.2%

Table 3.12: Comparison of daily passenger-related costs for recovery, 2014 versus 2035, under "Mild" climate change case, by disruption category.

Disruption Category	Year	Undisrupted pax delay min	Disrupted pax delay min	Disrupted pax delay cost ($)	Virtual Itineraries (Num. pax.)	Reacc. cost on other airline($)	Total pax delay min	Total pax delay cost ($)	Aircraft plus Pax. cost ($)	Cost Increase
Small	2014 (min.)	1,166,678	2,975	3,243	13	19,500	1,169,653	1,445,555	2,869,141	–
	2014 (avg.)	1,207,059	17,567	19,148	125	187,286	1,224,626	1,584,471	3,159,665	–
	2014 (max.)	1,251,650	37,208	40,557	186	279,000	1,288,858	1,707,860	3,395,039	–
	2035 (min.)	1,244,564	18,562	20,233	251	376,500	1,298,895	2,033,948	3,839,919	23.6%
	2035 (avg.)	1,294,415	44,316	48,304	324	486,643	1,351,821	2,152,928	4,352,932	36.4%
	2035 (max.)	1,347,623	75,432	82,221	470	705,000	1,405,440	2,374,939	6,087,359	55.6%
Medium	2014 (min.)	1,198,841	19,591	21,354	123	184,500	1,218,432	1,763,589	3,396,516	–
	2014 (avg.)	1,270,637	33,675	36,706	225	336,857	1,304,312	1,856,557	3,626,597	–
	2014 (max.)	1,290,223	57,932	63,146	347	520,500	1,348,155	2,008,551	3,911,420	–
	2035 (min.)	1,326,992	28,089	30,617	344	516,000	1,343,491	2,430,767	4,415,256	19.1%
	2035 (avg.)	1,370,062	58,007	63,227	441	661,929	1,424,087	2,463,841	4,547,363	33.0%
	2035 (max.)	1,372,606	74,139	80,812	645	967,500	1,464,924	2,790,247	4,864,584	49.3%
Large	2014 (min.)	1,304,719	27,125	29,566	200	300,000	1,331,844	1,908,904	3,835,723	–
	2014 (avg.)	1,374,969	42,817	46,670	315	472,750	1,417,786	2,154,203	4,291,283	–
	2014 (max.)	1,490,596	83,497	91,012	454	681,000	1,574,093	2,212,310	4,660,934	–
	2035 (min.)	1,360,760	43,874	47,823	415	622,500	1,397,621	2,495,920	5,055,690	22.3%
	2035 (avg.)	1,471,726	81,065	88,361	548	822,500	1,534,924	2,775,634	5,720,153	29.0%
	2035 (max.)	1,566,558	116,628	127,125	785	1,177,500	1,668,174	2,920,507	6,160,487	35.0%

sponding passenger-related costs to the airline are described in Tables 3.18, 3.19 and 3.20 respectively. As with 2035, the decrease in capacities due to increasing temperatures result in increased flight cancellations, significantly increased flight departure delays and arrival delays, and a huge increase in the number of swaps. The huge increase in the number of swaps, while deviating from plan, results in increased ability to recover the schedule, and allows the airline to decrease propagation of delay despite the decreased resources. However,

Table 3.13: Comparison of daily passenger-related costs for recovery, 2014 versus 2035, under "Medium" climate change case, by disruption category.

Disruption Category	Year	Undisrupted pax delay min	Disrupted pax delay min	Disrupted pax delay cost ($)	Virtual Itineraries (Num. pax.)	Reacc. cost on other airline($)	Total pax delay min	Total pax delay cost ($)	Aircraft plus Pax. cost ($)	Cost Increase
Small	2014 (min.)	1,166,678	2,975	3,243	13	19,500	1,169,653	1,445,555	2,869,141	–
	2014 (avg.)	1,207,059	17,567	19,148	125	187,286	1,224,626	1,584,471	3,159,665	–
	2014 (max.)	1,251,650	37,208	40,557	186	279,000	1,288,858	1,707,860	3,395,039	–
	2035 (min.)	1,264,456	20,195	22,013	247	370,500	1,284,651	2,019,722	3,804,304	25.6%
	2035 (avg.)	1,315,948	44,489	48,493	339	508,286	1,360,437	2,189,733	4,122,844	38.4%
	2035 (max.)	1,335,671	76,092	82,940	454	681,000	1,411,763	2,331,248	4,422,315	46.5%
Medium	2014 (min.)	1,198,841	19,591	21,354	123	184,500	1,218,432	1,763,589	3,396,516	–
	2014 (avg.)	1,270,637	33,675	36,706	225	336,857	1,304,312	1,856,557	3,626,597	–
	2014 (max.)	1,290,223	57,932	63,146	347	520,500	1,348,155	2,008,551	3,911,420	–
	2035 (min.)	1,291,540	48,617	52,993	342	513,000	1,340,157	2,403,527	4,613,452	18.9%
	2035 (avg.)	1,367,433	61,003	66,493	473	709,714	1,428,436	2,497,910	4,614,066	35.0%
	2035 (max.)	1,378,159	104,646	114,064	647	970,500	1,482,805	2,755,326	4,826,782	47.4%
Large	2014 (min.)	1,304,719	27,125	29,566	200	300,000	1,331,844	1,908,904	3,835,723	–
	2014 (avg.)	1,374,969	42,817	46,670	315	472,750	1,417,786	2,154,203	4,291,283	–
	2014 (max.)	1,490,596	83,497	91,012	454	681,000	1,574,093	2,212,310	4,660,934	–
	2035 (min.)	1,363,014	47,497	51,772	355	532,500	1,410,511	2,482,278	4,978,415	21.6%
	2035 (avg.)	1,464,464	84,667	92,287	562	843,250	1,549,131	2,820,003	5,512,416	31.2%
	2035 (max.)	1,563,910	119,232	129,963	695	1,042,500	1,683,142	2,786,357	5,870,440	43.9%

Table 3.14: Comparison of daily passenger-related costs for recovery, 2014 versus 2035, under "Severe" climate change case, by disruption category.

Disruption Category	Year	Undisrupted pax delay min	Disrupted pax delay min	Disrupted pax delay cost ($)	Virtual Itineraries (Num. pax.)	Reacc. cost on other airline($)	Total pax delay min	Total pax delay cost ($)	Aircraft plus Pax. cost ($)	Cost Increase
Small	2014 (min.)	1,166,678	2,975	3,243	13	19,500	1,169,653	1,445,555	2,869,141	–
	2014 (avg.)	1,207,059	17,567	19,148	125	187,286	1,224,626	1,584,471	3,159,665	–
	2014 (max.)	1,251,650	37,208	40,557	186	279,000	1,288,858	1,707,860	3,395,039	–
	2035 (min.)	1,244,564	19,331	21,071	258	387,000	1,263,895	1,891,846	3,564,483	20.2%
	2035 (avg.)	1,294,415	39,863	43,451	319	478,071	1,334,278	2,112,206	3,982,262	33.6%
	2035 (max.)	1,347,623	67,397	73,463	427	640,500	1,415,020	2,309,050	4,406,885	42.0%
Medium	2014 (min.)	1,198,841	19,591	21,354	123	184,500	1,218,432	1,763,589	3,396,516	–
	2014 (avg.)	1,270,637	33,675	36,706	225	336,857	1,304,312	1,856,557	3,626,597	–
	2014 (max.)	1,290,223	57,932	63,146	347	520,500	1,348,155	2,008,551	3,911,420	–
	2035 (min.)	1,326,992	44,540	48,549	263	394,500	1,371,532	2,272,377	4,377,520	14.4%
	2035 (avg.)	1,370,062	61,408	66,935	439	658,071	1,431,470	2,461,860	4,925,676	32.9%
	2035 (max.)	1,372,606	84,264	91,848	624	936,000	1,456,870	2,739,191	5,851,569	46.5%
Large	2014 (min.)	1,304,719	27,125	29,566	200	300,000	1,331,844	1,908,904	3,835,723	–
	2014 (avg.)	1,374,969	42,817	46,670	315	472,750	1,417,786	2,154,203	4,291,283	–
	2014 (max.)	1,490,596	83,497	91,012	454	681,000	1,574,093	2,212,310	4,660,934	–
	2035 (min.)	1,360,760	53,267	58,061	355	532,500	1,414,027	2,365,570	4,599,565	15.9%
	2035 (avg.)	1,471,726	75,755	82,573	562	842,250	1,547,481	2,782,471	5,349,910	29.3%
	2035 (max.)	1,566,558	104,042	113,406	701	1,051,500	1,670,600	3,132,485	5,999,789	41.4%

because small-to-medium sized aircraft are more affected than large aircraft, we find a high increase in the number of swaps executed by the airline to simply maintain operations. Due to increased cancellations the fuel burn costs do not vary significantly or even decrease for some scenarios from 2014 to 2050, quite similar to the phenomenon observed for 2035. The combination of these effects results in increased aircraft recovery costs of 15.7% to 24% on average compared to 2014's costs under the severe climate change cases, 12.6% to 24.5% on average under the medium climate change cases, and 18 % to 20.7 % on average for mild medium climate change, compared to 2014's costs. We find that the costs of aircraft recovery

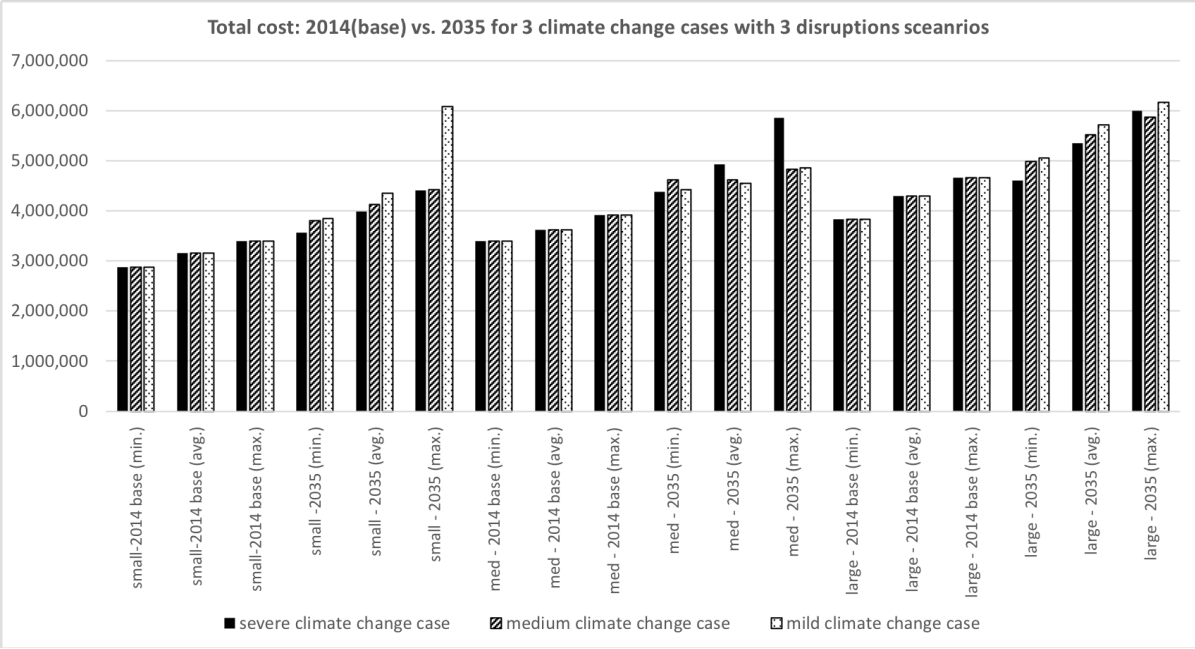

Figure 3.5: Total recovery cost comparison: 2014 base year vs. 2035, for 3 climate change cases with 3 disruption scenarios

over the individual instances increase by 3.9% to 36.2% for severe climate change cases, by 4.1% to 33 % for medium climate change cases, and by 9.3% to 39 % for mild climate change.

Moreover, due to increased swaps, many aircraft are placed in stations other than their planned stations at the end of the day, resulting in potentially even higher future costs arising from both operations and maintenance.

The passenger-related delay costs (Column 9 of Tables 3.18, 3.19,3.20) to the airline increase by as much as 33.1% to 49.4% on average for severe climate change cases, 30.5% to 40% on average for medium climate change cases, 29.6% to 37.9% on average for mild climate change cases, over all sizes of disruptions. Over individual disruption instances, we find that the costs of passenger recovery increase by as much as 18.1% to 74.3% for severe climate change cases, 18% to 56.6% for medium climate change cases, 17.4% to 52.7% for mild climate change. Considering combined aircraft and passenger-related delay costs to the airline, we find an increase of 25% to 36.9% on average for severe climate change cases, 30% to 49.3% on average for medium climate change cases, 25% to 47% on average for mild

climate change cases. Over individual disruption instances, we find that the costs of total recovery increase by as much as 10.6% to 54.8% for severe climate change cases, 16% to 144% for medium climate change cases, 17.4% to 52.7% for mild climate change.

We find that for small disruptions the average percentage increase in delay costs are higher as a percentage of existing costs, because the capacity reductions due to climate-change imposed disruptions are significantly higher than the size of the 'small' disruption itself. This is not observed in the case of medium or large disruptions, because they are more comparable in size to the costs of the climate-change-related disruptions. The implication of this observation is that even when disruptions caused independently due to airline or airport systemic delays are small, climate change alone imposes a significant cost burden on the airline network.

Table 3.15: Comparison of daily aircraft-related costs for recovery, 2014 versus 2050, under "Mild" climate change case, by disruption category.

Disruption Category	Year	Total Cost($)	Dep. Delay (min)	Arr. Delay Delay (min)	Fuel Burn (lb)	Num. Swaps	Num. Cancel.	Num. Speed Changes	Num. Unbalanced	Cost Increase
Small	2014 (min.)	1,423,586	2,855	3,364	1,690,290	23	1	38	0	–
	2014 (avg.)	1,575,194	4,289	4,815	1,792,383	66	8	45	0	–
	2014 (max.)	1,687,179	6,702	7,258	1,855,248	130	13	48	1	–
	2050 (min.)	1,750,662	4,303	4,777	1,734,655	194	10	44	0	12.3%
	2050 (avg.)	1,868,725	6,067	6,598	1,774,846	240	15	46	0	18.8%
	2050 (max.)	2,087,796	8,820	9,360	1,799,405	304	23	47	0	27.2%
Medium	2014 (min.)	1,632,927	5,736	6,330	1,668,951	57	7	40	0	–
	2014 (avg.)	1,770,040	8,185	8,689	1,770,186	86	16	44	0	–
	2014 (max.)	1,902,869	10,643	11,056	1,862,433	119	22	49	1	–
	2050 (min.)	2,013,283	8,205	8,769	1,627,763	229	18	40	0	9.3%
	2050 (avg.)	2,084,374	10,384	10,887	1,728,481	290	23	43	0	18.0%
	2050 (max.)	2,135,641	13,394	13,848	1,795,169	330	25	46	0	28.9%
Large	2014 (min.)	1,926,819	7,109	7,588	1,643,874	98	19	41	0	–
	2014 (avg.)	2,137,080	14,402	14,866	1,731,739	162	29	46	0	–
	2014 (max.)	2,448,624	22,023	22,367	1,795,621	256	40	53	1	–
	2050 (min.)	2,272,589	10,941	11,433	1,582,761	299	30	34	0	4.3%
	2050 (avg.)	2,631,319	16,461	16,868	1,646,097	385	46	40	1	20.7%
	2050 (max.)	2,929,625	23,605	23,882	1,729,444	463	60	45	3	39.0%

From a passenger perspective (see Table 3.20), we find that the passenger delay minutes experienced by passengers whose itineraries are not disrupted due to cancelations or misconnections but only delayed (column 3), are comparable from 2014 to 2050. However, significant increases are observed in the delay seen by disrupted passengers (column 4) after

Table 3.16: Comparison of daily aircraft-related costs for recovery, 2014 versus 2050, under "Medium" climate change case, by disruption category.

Disruption Category	Year	Total Cost($)	Dep. Delay (min)	Arr. Delay Delay (min)	Fuel Burn (lb)	Num. Swaps	Num. Cancel.	Num. Speed Changes	Num. Unbalanced	Cost Increase
Small	2014 (min.)	1,423,586	2,855	3,364	1,690,290	23	1	38	0	–
	2014 (avg.)	1,575,194	4,289	4,815	1,792,383	66	8	45	0	–
	2014 (max.)	1,687,179	6,702	7,258	1,855,248	130	13	48	1	–
	2050 (min.)	1,720,605	4,712	5,301	1,726,796	205	8	43	0	14.0%
	2050 (avg.)	1,960,454	6,555	7,090	1,790,587	259	18	47	0	24.5%
	2050 (max.)	2,182,963	9,042	9,595	1,824,964	336	24	49	0	33.0%
Medium	2014 (min.)	1,632,927	5,736	6,330	1,668,951	57	7	40	0	–
	2014 (avg.)	1,770,040	8,185	8,689	1,770,186	86	16	44	0	–
	2014 (max.)	1,902,869	10,643	11,056	1,862,433	119	22	49	1	–
	2050 (min.)	2,005,007	8,195	8,725	1,653,243	251	20	37	0	9.9%
	2050 (avg.)	2,138,660	10,633	11,111	1,702,203	293	27	42	0	21.0%
	2050 (max.)	2,347,165	13,169	13,591	1,785,025	344	35	46	1	27.4%
Large	2014 (min.)	1,926,819	7,109	7,588	1,643,874	98	19	41	0	–
	2014 (avg.)	2,137,080	14,402	14,866	1,731,739	162	29	46	0	–
	2014 (max.)	2,448,624	22,023	22,367	1,795,621	256	40	53	1	–
	2050 (min.)	2,167,959	10,246	10,702	1,657,575	268	21	43	0	4.1%
	2050 (avg.)	2,402,996	16,799	17,262	1,704,495	348	34	46	1	12.6%
	2050 (max.)	2,819,032	23,659	24,078	1,779,004	422	49	49	1	16.9%

Table 3.17: Comparison of daily aircraft-related costs for recovery, 2014 versus 2050, under "Severe" climate change case, by disruption category.

Disruption Category	Year	Total Cost($)	Dep. Delay (min)	Arr. Delay Delay (min)	Fuel Burn (lb)	Num. Swaps	Num. Cancel.	Num. Speed Changes	Num. Unbalanced	Cost Increase
Small	2014 (min.)	1,423,586	2,855	3,364	1,690,290	23	1	38	0	–
	2014 (avg.)	1,575,194	4,289	4,815	1,792,383	66	8	45	0	–
	2014 (max.)	1,687,179	6,702	7,258	1,855,248	130	13	48	1	–
	2050 (min.)	1,794,336	5,733	6,217	1,674,532	226	12	44	0	6.4%
	2050 (avg.)	1,953,681	7,679	8,259	1,749,957	264	18	48	0	24.0%
	2050 (max.)	2,155,315	9,974	10,937	1,800,854	359	25	65	0	35.6%
Medium	2014 (min.)	1,632,927	5,736	6,330	1,668,951	57	7	40	0	–
	2014 (avg.)	1,770,040	8,185	8,689	1,770,186	86	16	44	0	–
	2014 (max.)	1,902,869	10,643	11,056	1,862,433	119	22	49	1	–
	2050 (min.)	2,000,122	8,685	9,220	1,656,151	248	16	40	0	13.6%
	2050 (avg.)	2,169,961	11,893	12,374	1,729,701	304	26	44	0	22.8%
	2050 (max.)	2,354,249	15,368	15,801	1,790,085	360	36	49	1	34.3%
Large	2014 (min.)	1,926,819	7,109	7,588	1,643,874	98	19	41	0	–
	2014 (avg.)	2,137,080	14,402	14,866	1,731,739	162	29	46	0	–
	2014 (max.)	2,448,624	22,023	22,367	1,795,621	256	40	53	1	–
	2050 (min.)	2,267,736	10,843	11,336	1,634,296	295	29	41	0	3.9%
	2050 (avg.)	2,501,097	17,598	18,014	1,725,892	356	38	46	0	15.7%
	2050 (max.)	2,708,065	25,354	25,639	1,779,686	421	42	51	1	36.2%

re-accommodation on the airline's network. Passenger delay minutes are seen, on average, to increase by 2-3 times over all disruption sizes. Moreover, the number of passengers that need to be accommodated on other airlines, modeled as a virtual itinerary, increases significantly both on average as well as for the maximum observed over all disruption sizes. Because

Table 3.18: Comparison of daily passenger-related costs for recovery, 2014 versus 2050, under "Mild" climate change case, by disruption category.

Disruption Category	Year	Undisrupted pax delay min	Disrupted pax delay min	Disrupted pax delay cost ($)	Virtual Itineraries (Num. pax.)	Reacc. cost on other airline($)	Total pax delay min	Total pax delay cost ($)	Aircraft plus Pax. cost ($)	Cost Increase
Small	2014 (min.)	1,166,678	2,975	3,243	13	19,500	1,169,653	1,445,555	2,869,141	–
	2014 (avg.)	1,207,059	17,567	19,148	125	187,286	1,224,626	1,584,471	3,159,665	–
	2014 (max.)	1,251,650	37,208	40,557	186	279,000	1,288,858	1,707,860	3,395,039	–
	2050 (min.)	1,264,327	19,820	21,604	247	370,500	1,284,147	2,014,550	3,796,204	22.7%
	2050 (avg.)	1,302,584	42,794	46,645	352	528,214	1,345,377	2,184,104	4,052,829	37.9%
	2050 (max.)	1,329,663	86,672	94,472	561	841,500	1,416,335	2,490,019	4,378,534	52.7%
Medium	2014 (min.)	1,198,841	19,591	21,354	123	184,500	1,218,432	1,763,589	3,396,516	–
	2014 (avg.)	1,270,637	33,675	36,706	225	336,857	1,304,312	1,856,557	3,626,597	–
	2014 (max.)	1,290,223	57,932	63,146	347	520,500	1,348,155	2,008,551	3,911,420	–
	2050 (min.)	1,336,139	24,865	27,103	328	492,000	1,361,004	2,430,174	4,443,457	23.0%
	2050 (avg.)	1,364,603	57,447	62,617	443	663,857	1,422,050	2,446,691	4,531,066	32.1%
	2050 (max.)	1,388,620	77,996	85,016	530	795,000	1,466,616	2,553,977	4,689,618	41.4%
Large	2014 (min.)	1,304,719	27,125	29,566	200	300,000	1,331,844	1,908,904	3,835,723	–
	2014 (avg.)	1,374,969	42,817	46,670	315	472,750	1,417,786	2,154,203	4,291,283	–
	2014 (max.)	1,490,596	83,497	91,012	454	681,000	1,574,093	2,212,310	4,660,934	–
	2050 (min.)	1,414,392	59,670	65,040	342	513,000	1,474,062	2,396,146	4,798,780	17.4%
	2050 (avg.)	1,467,183	81,010	88,301	555	832,250	1,548,193	2,787,380	5,418,699	29.6%
	2050 (max.)	1,578,363	105,151	114,615	658	987,000	1,683,514	3,047,780	5,977,405	41.2%

Table 3.19: Comparison of daily passenger-related costs for recovery, 2014 versus 2050, under "Medium" climate change case, by disruption category.

Disruption Category	Year	Undisrupted pax delay min	Disrupted pax delay min	Disrupted pax delay cost ($)	Virtual Itineraries (Num. pax.)	Reacc. cost on other airline($)	Total pax delay min	Total pax delay cost ($)	Aircraft plus Pax. cost ($)	Cost Increase
Small	2014 (min.)	1,166,678	2,975	3,243	13	19,500	1,169,653	1,445,555	2,869,141	–
	2014 (avg.)	1,207,059	17,567	19,148	125	187,286	1,224,626	1,584,471	3,159,665	–
	2014 (max.)	1,251,650	37,208	40,557	186	279,000	1,288,858	1,707,860	3,395,039	–
	2050 (min.)	1,272,697	23,456	25,567	243	364,500	1,296,153	1,938,199	3,861,888	18.0%
	2050 (avg.)	1,320,304	41,354	45,076	367	551,143	1,361,658	2,218,665	4,179,119	40.0%
	2050 (max.)	1,320,304	70,705	77,068	586	879,000	1,425,674	2,641,776	4,824,739	54.7%
Medium	2014 (min.)	1,198,841	19,591	21,354	123	184,500	1,218,432	1,763,589	3,396,516	–
	2014 (avg.)	1,270,637	33,675	36,706	225	336,857	1,304,312	1,856,557	3,626,597	–
	2014 (max.)	1,290,223	57,932	63,146	347	520,500	1,348,155	2,008,551	3,911,420	–
	2050 (min.)	1,343,724	24,865	27,103	431	646,500	1,368,589	2,408,309	4,452,524	19.9%
	2050 (avg.)	1,371,804	66,878	72,897	498	746,571	1,438,682	2,557,021	4,695,681	38.3%
	2050 (max.)	1,388,388	107,613	117,298	623	934,500	1,496,001	2,767,235	4,772,242	56.6%
Large	2014 (min.)	1,304,719	27,125	29,566	200	300,000	1,331,844	1,908,904	3,835,723	–
	2014 (avg.)	1,304,719	42,817	46,670	315	472,750	1,417,786	2,154,203	4,291,283	–
	2014 (max.)	1,490,596	83,497	91,012	454	681,000	1,574,093	2,212,310	4,660,934	–
	2050 (min.)	1,369,249	52,730	57,476	419	628,500	1,421,979	2,585,936	4,753,895	22.1%
	2050 (avg.)	1,465,541	75,762	82,580	581	871,500	1,541,303	2,810,120	5,213,116	30.5%
	2050 (max.)	1,465,541	110,374	120,308	799	1,198,500	1,699,154	2,959,257	5,395,767	35.5%

many more passengers need to be re-booked on new itineraries or with other airlines, the costs imposed on the airline increase non-linearly (compared to the non-disrupted but delayed itineraries). This indicates significant deterioration in recoverability, and consequently the

Table 3.20: Comparison of daily passenger-related costs for recovery, 2014 versus 2050, under "Severe" climate change case, by disruption category.

Disruption Category	Year	Undisrupted pax delay min	Disrupted pax delay min	Disrupted pax delay cost ($)	Virtual Itineraries (Num. pax.)	Reacc. cost on other airline($)	Total pax delay min	Total pax delay cost ($)	Aircraft plus Pax. cost ($)	Cost Increase
Small	2014 (min.)	1,166,678	2,975	3,243	13	19,500	1,169,653	1,445,555	2,869,141	–
	2014 (avg.)	1,207,059	17,567	19,148	125	187,286	1,224,626	1,584,471	3,159,665	–
	2014 (max.)	1,251,650	37,208	40,557	186	279,000	1,288,858	1,707,860	3,395,039	–
	2050 (min.)	1,295,002	33,407	36,414	292	438,000	1,328,409	2,064,766	3,859,102	38.0%
	2050 (avg.)	1,333,123	47,676	51,967	427	641,143	1,380,798	2,360,785	4,314,466	49.4%
	2050 (max.)	1,374,557	64,558	70,368	535	802,500	1,439,115	2,493,383	4,648,698	74.3%
Medium	2014 (min.)	1,198,841	19,591	21,354	123	184,500	1,218,432	1,763,589	3,396,516	–
	2014 (avg.)	1,270,637	33,675	36,706	225	336,857	1,304,312	1,856,557	3,626,597	–
	2014 (max.)	1,290,223	57,932	63,146	347	520,500	1,348,155	2,008,551	3,911,420	–
	2050 (min.)	1,328,160	49,902	54,393	398	597,000	1,378,062	2,476,275	4,476,397	32.8%
	2050 (avg.)	1,407,367	63,676	69,407	558	837,000	1,471,043	2,699,694	4,869,655	45.7%
	2050 (max.)	1,450,971	78,479	85,542	692	1,038,000	1,529,450	2,838,542	5,192,792	56.8%
Large	2014 (min.)	1,304,719	27,125	29,566	200	300,000	1,331,844	1,908,904	3,835,723	–
	2014 (avg.)	1,374,969	42,817	46,670	315	472,750	1,417,786	2,154,203	4,291,283	–
	2014 (max.)	1,490,596	83,497	91,012	454	681,000	1,574,093	2,212,310	4,660,934	–
	2050 (min.)	1,366,770	40,273	43,898	397	595,500	1,407,043	2,410,458	4,678,194	18.1%
	2050 (avg.)	1,466,321	72,993	79,563	591	886,250	1,539,314	2,872,102	5,373,199	33.1%
	2050 (max.)	1,581,445	110,192	120,109	867	1,300,500	1,691,637	3,571,389	6,279,454	52.7%

loss of resilience in the airline's network.

We also observe that recovery costs for passengers incurred by the airline increases significantly more, up to 74.3%; as compared to the recovery costs for aircraft, up to 39%. We observe only few number of unbalanced aircraft ending up at a station other than the original one. This is due to the high penalty cost of such endings that can potentially result in future operational and maintenance costs. Hence, the cost-minimizing decisions involve canceling flights than incurring the costs of unbalanced aircraft.

Figures 3.6 shows that the recovery cost increases over all climate change cases projected for the year 2050 vs.the base year 2014. The largest cost increase is observed when the severe climate change case is superimposed on the largest disruption scenarios. Specifically, we observe that the difference in cost increase is mainly driven by the magnitude of disruptions. We also observe that, under all disruption sizes, the severe climate change cases have a significantly negative impact on the cost increase on average.

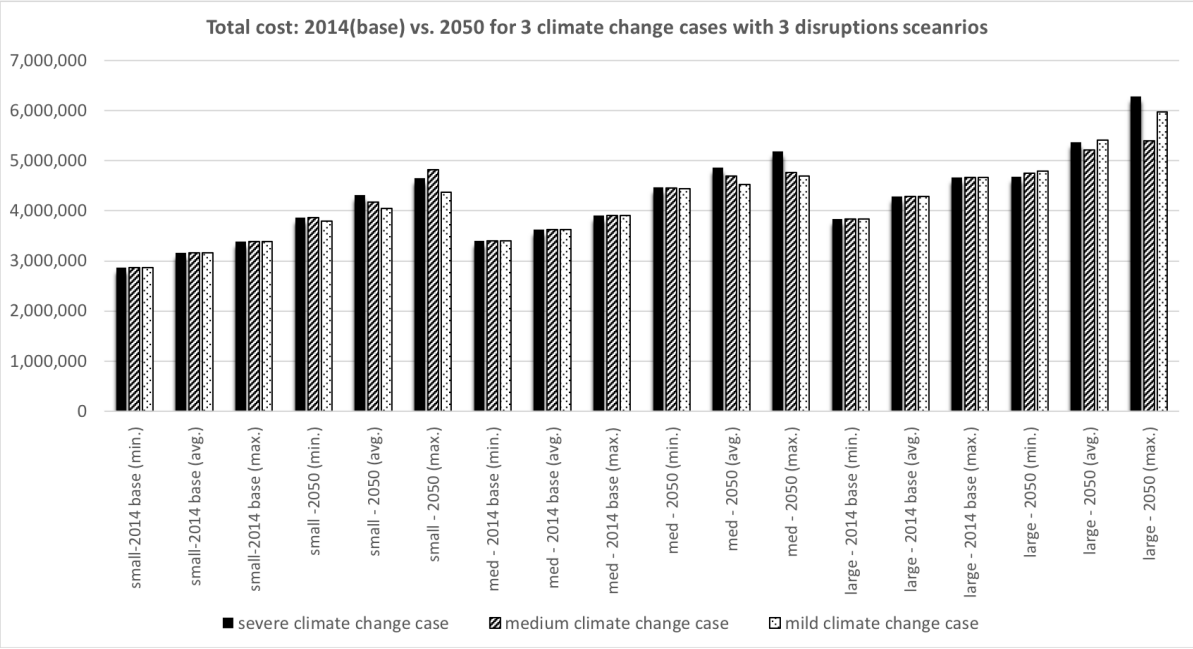

Figure 3.6: Total recovery cost comparison: 2014 base year vs. 2050, for 3 climate change cases with 3 disruption scenarios

3.5.3 The evolution of recovery costs from 2035 to 2050

We find that the significant increase in recovery costs from 2035 to 2050 is best observed when the effect of the climate-change-induced capacity reductions dominates the size of the original disruption (induced by the airline or airport). In other words, the costs of aircraft recovery increase most significantly for small disruptions under the severe climate change cases, over all disruptions sizes under the mild, medium or severe climate change case. Moreover, the cost increase is mostly driven by the passenger recovery from the delayed itineraries disrupted due to cancellations or misconnections, number of passengers that need to be accommodated other airlines. For example, comparing the results for the small disruptions under the severe climate change case in 2035 (Table 3.14) vs 2050 (Table 3.20), we observe that passenger-related recovery costs to the airline increases significantly more, by 15.8% from 33.6% to 49.4%, as compared to the aircraft-recovery related costs, by 5.1%, from 18.9% to 24% . This increase in aircraft recovery costs is driven by the decrease in capacities due to increasing temperatures, which result in increased flight cancellations and

swaps and increased flight departure delays and arrival delays.

We find that for medium or large sized disruptions under severe climate change cases the average percentage increase in combined aircraft and passenger-related delay costs, as a percentage of existing costs, increase although the average aircraft-recovery related costs alone decrease from 2035 to 2050. That indicates that the significant increase in passenger-related recovery costs from 2035 to 2050 solely contributes to the overall increase in combined aircraft and passenger-related delay costs. Specifically, in some medium or large sized disruption case, the number of swaps and cancellations decrease from 2035 to 2050 while the fuel burn costs increase from 2035 to 2050. The combined effect from each of these mechanisms results in comparable overall costs in aircraft-recovery from 2035 to 2050. On the other hand, from a passenger perspective, the primary driver in passenger-related cost increases is the missed connections, leading re-accommodation on the same or other airlines, which occurs in all sizes of the disruption cases in any climate change case. This indicates that the cost increase in passenger-related metric is mainly from an increased number of passengers re-accommodated to other airlines, comprising up to 90% of the total cost, due to the capacity drops due to increased temperature and/or serious airline-related disruptions.

3.6 Discussion and Conclusions

In this chapter, we studied the impact of climate change on the ability of airlines to recover from everyday disruptions. Increasing temperatures caused by climate change, impose constraints on aircrafts' ability to generate enough lift to take off as planned. This is a function of the specific airport, temperatures and pressure, the runway length being used and the type of aircraft. Smaller aircraft are disproportionately affected compared to larger aircraft. Because sufficient lift cannot be generated at high temperatures, aircraft payloads and capacities will decrease significantly. Depending on airline policies, aircraft

whose capacity drops below a threshold load factor can also be grounded and operated only when temperatures have dropped later in the day.

In this work, we compare the performance of a large hub-and-spoke airline's operations and recoverability in the years 2014 and 2035 as well as 2050 assuming similar disruption types and load factors and aircraft mix. We construct a modeling and algorithmic framework that allows for simultaneous aircraft and passenger recovery while explicitly modeling payload-range-related capacity changes at various (increased) temperatures. We study the 2035 and 2050 settings, which are the current trend temperatures have been following, for climate change cases that are representative of mild, medium and severe cases. We study these settings on traffic and disruptions for the summer month of July for both 2035 and 2050. Our experimental results indicate that daily total costs on airline networks increase on average from 2014 to 2035, by 25% to 55.9% and from 2014 to 2050, 25% to 49.3%. Over individual disruption instances, we find that the costs of recovery increase by 11.2% to 178.4% in 2035 and by 10.6% to 156 % in 2050.

We observe that the increase in the passenger recovery costs comprises a significantly higher proportion of the total cost increase, as compared to the aircraft recovery component. In our experiments, passenger-related cost increases for the airline are seen to increase by 33.1% to 49.4% on average for the severe climate change case in 2050, driven primarily by passengers whose connections are missed or flights are canceled, necessitating re-accommodation on the same or other airlines, and secondarily by passengers whose originally booked itineraries are delayed at the destination. Specifically, one of the main reasons for the increase in operating costs can be attributed to re-accommodating costs for passengers. These re-accommodations are mostly because of capacity drops and cancellations due to disruptions caused by global warming.

Our experimental results show two points. First, the higher the disruptions, the higher the increase in cost. Second, we also observed that a mild climate change case can have a larger cost increase than a medium climate change case. This can be explained as follows:

First, the dominant factor in cost increase in terms of the aircraft component is the increase in cancellations. This cancellations lead to the passengers to be re-accommodated to other airline, which comprises the dominant cost factor in the passenger recovery cost. Second, the significance of airline-related disruptions directly triggers these two component; that is, the more disruptions, the more number of cancellations and the more it incurs the number of passengers re-accommodated to other airlines. On the other hand, the climate change case (if it's not in conjunction with airline disruptions) is related to the capacity drops, rather than directly related to the cost increase. Under small disruptions, these climate change effects would be solely responsible for the capacity drops (even to zero), as there will be fewer cancellations (that usually incur the significant cost increase in re-accommodating to other airlines in addition to the cancellation cost itself).

Overall, these results indicate that an airline's network properties such as recoverability and resilience, which impact its ability to perform as a service network for passengers, are deteriorated to a great extent through the impacts of climate change-caused warming in conjunction with the airline-related disruptions. While these are mostly observed during the months with higher temperatures, note that those months also correspond to higher traffic.

Our observations indicate that airlines need to systematically and consistently begin to account for the impacts of climate change, both through re-design and consolidation of network operations in terms of schedules, aircraft routes and operations; as well as design aircraft that are more resistant to the impacts of climate change, or use larger aircraft that accommodate consolidated demands with lower frequencies. The timeline between our baseline (2014) and the projected years (2050) also indicate that the next 30 years are crucial in focusing not only on the impacts on aviation on climate change, but also the impacts of climate change on aviation operations and the worldwide economy.

Chapter 4

CONCLUSION

As discussed in Chapter 1, operating delays and network wide disruptions propagated across airline system result in billions of dollars of lost revenue for airlines. These disruptions can be caused by various reasons such as unfavorable weather, airport congestion due to demand-capacity imbalance, and contingent disruptions such as aircraft maintenance, crew sickness, and passenger boarding delay. In this thesis, we first focused on airline's short-term disruption management using a joint reactive and proactive optimization approach that leverages future anticipated disruptions. We design an efficient solution procedure that can help airlines enhance recovery decisions in response to disruptions and reduce expected disruption costs. We present extensive experimental results with real world data to demonstrate the effectiveness of the proposed approaches. Next, we are interested in understanding an airline's long-term disruption management costs, in light of the impact of climate change on airline operations. We model the disruptions due to climate change on airline operations by putting restrictions on flight take-off weights and payloads, based on the temperature and airport. We demonstrate the effects of climate change on aviation through extensive experiments using data from a major hub-and-spoke airline. We aim for these insights to motivate airlines in designing better fleeting and scheduling practices.

In Chapter 2, we discuss a jointly reactive and proactive approach to airline dis-

ruption management. This approach leverages partial and probabilistic forecasts of future disruptions in optimizing disruption recovery decisions. Specifically, these forecasts arise from predictions of airport congestion-caused delays at the hub airports (based on Jacquillat and Odoni (2015a)), and hence the forecasts are partial and probabilistic. We formulate a Stochastic Reactive and Proactive Disruption Management (SRPDM) model to optimize network-wide airline disruption recovery under this model of airport queuing stochasticity. SRPDM is formulated as a stochastic integer program using a probabilistic time-space network representation. Because capturing future stochasticity into the model increases the computational burden significantly, we design an efficient solution algorithm based on a look-ahead approximation procedure. This enables the model's implementation at any decision point in reasonable computational times, consistent with earlier recovery models and with practical airline requirements. Experimental results show that our jointly reactive and proactive approach to disruption management can significantly enhance recovery decisions, as compared to purely reactive approaches. When compared to myopic baseline approach (that uses realized disruptions alone), it shows that leveraging even partial and probabilistic estimates of future disruptions can reduce expected recovery costs by 1-2%. These benefits are mainly driven by the deliberate introduction of departure holds to reduce expected fuel costs, fight cancellations and aircraft swaps. Highly concentrated flight networks, for example at hub airports, can benefit further from our scenario-based look-ahead approach especially where hub airports are highly congested. Further cost savings could potentially be achieved by real-time sharing of operating conditions, congestion, and delay forecasts, which could reduce system-wide uncertainty on future operations, thus permitting more effective recovery.

While Chapter 2 focused on aircraft recovery problem under current operating conditions, Chapter 3 studied the impact of climate change on the ability of airlines to recover from everyday disruptions, explicitly considering both aircraft and passenger recoveries. Airline operations are sensitive to weather and thus directly affected by climate change. Increasing

temperatures caused by climate change impose constraints on aircraft's ability to generate enough lift to take off as planned. These result in reduced aircraft payload capacity and causes flight cancellations and passenger itinerary re-accommodations. In this work, we evaluated the impact of climate change by comparing the recovery cost associated with airline's operations and recoverability in the years 2014, 2035 and 2050. We compared the costs across these three years under worst, medium, and mild climate change cases. Comparing our results for 2035 and 2050 against the 2014 baseline, we find that the higher the disruptions due to climate change, the higher the increase in cost. Experimental results indicate that daily total costs of airline networks increase on average from 2014 to 2035, by 25% to 55.9%; and from 2014 to 2050, by 25% to 49.3%. Over individual disruption instances, we find that the costs of recovery increase by 11.2% to 178.4% in 2035 and by 10.6% to 156% in 2050. Passenger-related cost increases for the airline are seen in our experiments to increase by 29 % to 38.4% on average from 2014 to 2035, and 33.1% to 49.4% on average for the worst climate change case from 2014 to 2050. Although the impacts of climate change cannot be avoided, airlines can try to mitigate the impact. Airlines can save these unnecessary extra costs associated with passenger re-accommodations and cancellations by provisioning for itinerary re-routing and reductions in aircraft capacity as a result of global warming.

REFERENCES

Load factor. https://www.transtats.bts.gov/Data_Elements.aspx?Data=5, year=2019.

Khaled Abdelghany, Sharmila Shah, Sidhartha Raina, and Ahmed Abdelghany. A model for projecting flight delays during irregular operation conditions. *Journal of Air Transport Management*, 10(6):385–394, 2004.

Khaled Abdelghany, Ahmed Abdelghany, and Goutham Ekollu. An integrated decision support tool for airlines schedule recovery during irregular operations. *European Journal of Operational Research*, 185(2):825–848, 2008.

Shervin Ahmadbeygi, Amy Cohn, and Marcial Lapp. Decreasing airline delay propagation by re-allocating scheduled slack. *IIE transactions*, 42(7):478–489, 2010.

Mazhar Arıkan, Vinayak Deshpande, and Milind Sohoni. Building reliable air-travel infrastructure using empirical data and stochastic models of airline networks. *Operations Research*, 61(1): 45–64, 2013.

Hamsa Balakrishnan and Bala Chandran. Algorithms for Scheduling Runway Operations Under Constrained Position Shifting. *Operations Research*, 58(6):1650–1665, 2010.

M. Ball, C. Barnhart, M. Dresner, M. Hansen, K. Neels, A. Odoni, E. Peterson, L. Sherry, A. Trani, and B. Zou. Total Delay Impact Study. Technical report, National Center of Excellence for Aviation Operations Research, College Park, MD, 2010.

C. Barnhart, T Kniker, and Lohatepanont M. Itinerary-Based Airline Fleet Assignment. *Transportation Science*, 36(2):149–269, 2002.

Cynthia Barnhart and Vikrant Vaze. Irregular operations: Schedule recovery and robustness. *The Global Airline Industry*, pages 253–274, 2015.

E.. Beale and J. Tomlin. Special Facilities in a General Mathematical Programming System for Non-Convex Problems Using Ordered Sets of Variables. *Proceedings of the Fifth International Conference on Operations Research*, pages 447–454, 1970.

D. Bertsekas. *Dynamic Programming and Optimal Control*, volume I. Athena Scientific, 3rd edition, 2005.

D. Bertsekas. *Dynamic Programming and Optimal Control*, volume II. Athena Scientific, 4th edition, 2012.

D. Bertsimas, G. Lulli, and A. Odoni. An integer optimization approach to large-scale air traffic flow management. *Operations Research*, 59(1):211–227, 2011.

S. Bisaillon, J.F. Cordeau, G. Laporte, and F. Pasin. A large neighbourhood search heuristic for the aircraft and passenger recovery problem. *4OR:A Quarterly Journal of Operations Research*, 9 (2):139–157, 2011.

Ralf Borndörfer, Ivan Dovica, Ivo Nowak, and Thomas Schickinger. Robust tail assignment. 2010.

S. Bratu and C. Barnhart. Flight Operations Recovery: New Approaches Considering Passenger Recovery. *Journal of Scheduling*, 9(3):279–298, 2006a.

Stephane Bratu and Cynthia Barnhart. Flight operations recovery: New approaches considering passenger recovery. *Journal of Scheduling*, 9(3):279–298, 2006b.

Michelle Bryant, Thomas Nesthus, and Rowley. Evaluation of fatigue andresponsibilities of cargo-supervisors and flightmechanic cargo supervisors. Technical report, 2016.

Luis Cadarso and Ángel Marín. Integrated robust airline schedule development. *Procedia-Social and Behavioral Sciences*, 20:1041–1050, 2011.

JiaâMing Cao and Adib Kanafani. Realâtime decision support for integration of airline flight cancellations and delays Part II: algorithm and computational experiments. *Transportation Planning and Technology*, 20(3):201–217, 1997.

Michael Clarke and Yudi Naryadi. The Airline Operation Control Centre : an overview of Garuda's Operation Control (EM) at Cengkereng Jakarta, Indonesia : final report to PT Garuda Indonesia. Technical report, Massachusetts Institute of Technology, Flight Transportation Laboratory, 1995.

Ethan Coffel, Terence Thompson, and Radley Horton. The impacts of rising temperatures on aircraft takeoff performance. *Climatic Change*, 144:381–388, 2017.

A. Cook and G. Tanner. Dynamic Cost Indexing: Airline costs of delayed passengers and how to estimate full network delay costs. Technical report, Innovative Cooperative Actions of R&D in EUROCONTROL Programme CARE INO III, 2008a.

J. Cook and G. Tanner. Innovative Cooperative Actions of Research & Development in EUROCONTROL Programme CARE INO III: Dynamic Cost Indexing: Airline costs of delayed passengers and how to estimate full network delay costs. Technical report, Transport Studies Group, University of Westminster, London, 2008b.

Michelle Dunbar, Gary Froyland, and Cheng-Lung Wu. Robust Airline Schedule Planning: Minimizing Propagated Delay in an Integrated Routing and Crewing Framework. *Transportation Science*, 46(2):204–216, 2012.

Michelle Dunbar, Gary Froyland, and Cheng-Lung Wu. An integrated scenario-based approach for robust aircraft routing, crew pairing and re-timing. *Computers & Operations Research*, 45: 68–86, 2014.

N. Eggenberg, M. Salani, and M. Bierlaire. Constraint-specific recovery network for solving airline recovery problems. *Computers & Operations Research*, 37(6):1014–1026, 2010.

EUROCONTROL. Small emitters tool. `https://www.eurocontrol.int/tool/small-emitters-tool`, 2018.

Federal Aviation Administration. Airport Capacity Benchmark Report. Technical report, 2004.

Gary Froyland, Stephen J Maher, and Cheng-Lung Wu. The recoverable robust tail assignment problem. *Transportation Science*, 48(3):351–372, 2013.

Dennis Hartmann. *Global Physical Climatology*. Elsevier Science, 2015.

Y. Hu, B. Xu, J. F. Bard, H. Chi, and M. Gao. Optimization of multi-fleet aircraft routing considering passenger transiting under airline disruption. *Computers & Industrial Engineering*, 80:132 – 144, 2015. doi: https://doi.org/10.1016/j.cie.2014.11.026.

Y. Hu, Y. Song, K. Zhao, and B. Xu. Integrated recovery of aircraft and passengers after airline operation disruption based on a GRASP algorithm. *Transportation Research Part E: Logistics*

and Transportation Review, 87:97–112, 2016. URL https://doi.org/10.1016/j.tre.2016.01.002.

IBM. IBM ILOG CPLEX Optimization Studio CPLEX Userâs Manual. https://www.ibm.com/support/knowledgecenter/SSSA5P_12.6.2/ilog.odms.studio.help/pdf/usrcplex.pdf, 2015.

ICAO Report. 2016 Environmental Report (Aviation and Climate Change). https://www.icao.int/environmental-protection/Documents/ICAO_EnvironmentalReport2016.pdf, 2016.

International Air Transport Association. Jet Fuel Price Development. Technical report, 2010.

IPCC Report. Climate Change 2014 Synthesis Report Summary for Policymakers. https://www.ipcc.ch/site/assets/uploads/2018/02/AR5_SYR_FINAL_SPM.pdf, 2014.

A. Jacquillat and A. Odoni. An Integrated Scheduling and Operations Approach to Airport Congestion Mitigation. *Operations Research*, 63(6):1390–1410, 2015a.

A. Jacquillat and A. Odoni. Endogenous Control of Arrival and Departure Service Rates in Dynamic and Stochastic Queuing Models with Application at JFK and EWR. *Transportation Research Part E: Logistics and Transportation Review*, 73(1):133–151, 2015b.

Alexandre Jacquillat and Amedeo Odoni. A New Airport Demand Management Approach Based on Targeted Scheduling Interventions. *Journal of Transport Economics and Policy*, 51(2): 115–138, 2017.

Alexandre Jacquillat, Amedeo R Odoni, and Mort D Webster. Dynamic control of runway configurations and of arrival and departure service rates at JFK airport under stochastic queue conditions. *Transportation Science*, 51(1):155–176, 2016.

N. Jafari and S. Zegordi. Simultaneous Recovery Model for Aircraft and Passengers. *Journal of the Franklin Institute*, 348(7):1638–1655, 2011.

Niloofar Jafari and Seyed Hessameddin Zegordi. The airline perturbation problem: considering disrupted passengers. *Transportation Planning and Technology*, 33(2):203–220, 2010.

Ahmad Jarrah, Gang Yu, Nirup Krishnamurthy, and Ananda Rakshit. A Decision Support Framework for Airline Flight Cancellations and Delays. *Transportation Science*, 27(3):266–280, 1993.

Darryl Jenkins and Joshua Marks. Consumer Regulation and Taxation of the U.S. Airline Industry: Estimating the Burden for Airlines and the Local Impact. Technical report, 2011.

N. Jozefowiez, C. Mancel, and F. Mora-Camino. A heuristic approach based on shortest path problems for integrated flight, aircraft, and passenger rescheduling under disruptions. *Journal of the Operational Research Society*, 64:384–395, 2013.

Anton J Kleywegt, Alexander Shapiro, and Tito Homem-de Mello. The sample average approximation method for stochastic discrete optimization. *SIAM Journal on Optimization*, 12(2): 479–502, 2002.

S. Lan, J. Clarke, and C. Barnhart. Planning for Robust Airline Operations: Optimizing Aircraft Routings and Flight Departure Times to Minimize Passenger Disruptions. *Transportation Science*, 40(1):15–28, 2006a.

Shan Lan, John-Paul Clarke, and Cynthia Barnhart. Planning for Robust Airline Operations: Optimizing Aircraft Routings and Flight Departure Times to Minimize Passenger Disruptions. *Transportation Science*, 40(1):15–28, 2006b.

Jane Lee, Lavanya Marla, and Alexandre Jacquillat. Dynamic disruption management in airline networks under airport operating uncertainty. *Transportation Science*, 2020.

L. Lettovsky. *Airline operations recovery: an optimization approach*. PhD thesis, Georgia Institute of Technology, 1997.

Ladislav Lettovský, Ellis Johnson, and George Nemhauser. Airline Crew Recovery. *Transportation Science*, 34(4):337–348, 2000.

S. Maher. A Novel Passenger Recovery Approach for the Integrated Airline Recovery Problem. *Computers and Operations Research*, 57:123–137, 2015.

S. J. Maher. Solving the integrated airline recovery problem using column-and-row generation. *Transportation Science*, 50(1):216–239, 2016.

Lavanya Marla, Bo Vaaben, and Cynthia Barnhart. Integrated Disruption Management and Flight Planning to Trade Off Delays and Fuel Burn. *Transportation Science*, 51(1):88–111, 2017a.

Lavanya Marla, Bo Vaaben, and Cynthia Barnhart. Integrated Disruption Management and Flight Planning to Trade Off Delays and Fuel Burn. *Transportation Science*, 51(1):88–111, 2017b.

Lavanya Marla, Vikrant Vaze, and Cynthia Barnhart. Robust optimization: Lessons learned from aircraft routing. *Computers & Operations Research*, 98:165–184, 2018.

R. Martin. *Large Scale Linear and Integer Optimization: A Unified Approach*. Springer Science Business Media, 1st edition, 1999.

L. A. McCarty and A. E. M. Cohn. Preemptive rerouting of airline passengers under uncertain delays. *Comput. Oper. Res.*, 90:1–11, 2018. doi: 10.1016/j.cor.2017.09.001. URL `https://doi.org/10.1016/j.cor.2017.09.001`.

Gerald A. Meehl, George J. Boer, Curt Covey, Mojib Latif, and Ronald J. Stouffer. The coupled model intercomparison project (cmip). *Bulletin of the American Meteorological Society*, 81 (2):313–318, 2000.

C. Meloni, D. Pacciarelli, and M. Pranzo. A Rollout Metaheuristic for Job Shop Scheduling Problems. *Annals of Operations Research*, 131:215–235, 2004.

Richard Moss, Jae Edmonds, Kathy Hibbard, Martin Manning, Steven Rose, Detlef van Vuuren, Timothy Carter, Seita Emori, Mikiko Kainuma, et al. The next generation of scenarios for climate change research and assessment. *Nature*, 463(7282):747–756, 2010.

J. Petersen, G. Solveling, E. Johnson, J. Clarke, and S. Shebalov. An optimization approach to airline integrated recovery. *Transportation Science*, 46(4):482–500, 2012a.

J. Petersen, G. SÃ¶lveling, J.P. Clarke, E. Johnson, and S. Shebalov. An Optimization Approach to Airline Integrated Recovery. *Transportation Science*, 46(4):439–546, 2012b.

J. Pita, C. Barnhart, and A. Antunes. Integrated Flight Scheduling and Fleet Assignment under Airport Congestion. *Transportation Science*, 47(4):477–492, 2012.

W. B. Powell. *Approximate Dynamic Programming: Solving the Curses of Dimensionality*. Wiley-Interscience, 2nd edition, 2007.

N. Pyrgiotis, K. Malone, and A. Odoni. Modelling Delay Propagation within an Airport Network. *Transportation Research Part C: Emerging Technologies*, 27:60–75, 2013.

David Reidmiller, Christopher Avery, and Kunkel. USGCRP, 2018: Impacts, Risks, and Adaptation in the United States: Fourth National Climate Assessment, Volume II. Technical report, 2018.

Keywan Riahi, Shilpa Rao, Volker Krey, Cheolhung Cho, Vadim Chirkov, Guenther Fischer, Georg

Kindermann, Nebojsa Nakicenovic, and Peter Rafaj. RCP 8.5—A scenario of comparatively high greenhouse gas emissions. *Climatic Change*, 109(1):33, 2011.

N. Ribeiro, A. Antunes, A. Jacquillat, A. Odoni, and J. Pita. An optimization approach for airport slot allocation under IATA guidelines. *Transportation Research Part B: Methodological*, 112: 132–156, 2017.

J. M. Rosenberger, E. L. Johnson, and G. L. Nemhauser. Rerouting aircraft for airline recovery. *Transportation Science*, 37(4):408–421, 2003.

Jay M Rosenberger, Ellis L Johnson, and George L Nemhauser. A robust fleet-assignment model with hub isolation and short cycles. *Transportation science*, 38(3):357–368, 2004.

Santer B. D. et.al. A search for human influences on the thermal structure of the atmosphere. *Nature*, 382, 1996.

Andrew J Schaefer, Ellis L Johnson, Anton J Kleywegt, and George L Nemhauser. Airline crew scheduling under uncertainty. *Transportation science*, 39(3):340–348, 2005.

N. Secomandi. A Rollout Policy for the Vehicle Routing Problem with Stochastic Demands. *Operations Research*, 49(5):796–802, 2001.

Sergey Shebalov and Diego Klabjan. Robust airline crew pairing: Move-up crews. *Transportation science*, 40(3):300–312, 2006.

I. Simaiakis. *Analysis, Modeling and Control of the Airport Departure Process*. PhD thesis, Massachusetts Institute of Technology, 2012.

Ioannis Simaiakis, Harshad Khadilkar, Hamsa Balakrishnan, Tom Reynolds, and John Hansman. Demonstration of reduced airport congestion through pushback rate control. *Transportation Research Part A: Policy and Practice*, 66:251–267, 2014.

K. Sinclair, J-F. Cordeau, and G. Laporte. Improvements to a large neighborhood search heuristic for an integrated aircraft and passenger recovery problem. *European Journal of Operational Research*, 233(1):234 – 245, 2014a.

K. Sinclair, J.F. Cordeau, and G. Laporte. A large neighbourhood search heuristic for the aircraft and passenger recovery problem. *European Journal of Operational Research*, 233(1):234–245, 2014b.

Barry C Smith and Ellis L Johnson. Robust airline fleet assignment: Imposing station purity using station decomposition. *Transportation Science*, 40(4):497–516, 2006.

Milind Sohoni, Yu-Ching Lee, and Diego Klabjan. Robust airline scheduling under block-time uncertainty. *Transportation Science*, 45(4):451–464, 2011.

Dušan Teodorović. Optimal dispatching strategy on an airline network after a schedule perturbation. *European Journal of Operational Research*, 15(2):178–182, 1984.

B. G. Thengvall, J. F. Bard, and G. Yu. Balancing user preferences for aircraft schedule recovery during irregular operations. *IIE Transactions*, 32(3):181–193, 2000.

T. Vossen, R. Hoffman, and A. Mukherjee. Air Traffic Flow Management. In *Quantitative Problem Solving Methods in the Airline Industry*, volume 169 of *International Series in Operations Research & Management Science*, pages 385–453. Springer US, 2012.

Guo Wei, Gang Yu, and Mark Song. Optimization Model and Algorithm for Crew Management During Airline Irregular Operations. *Journal of Combinatorial Optimization*, 1(3):305–321, 1997.

Wired. Why phoenix's airplanes can't take off in extreme heat. `https://www.wired.com/story/phoenix-flights-canceled-heat/`, 2017.

Chiwei Yan and Jerry Kung. Robust aircraft routing. *Transportation Science*, 52(1):118–133, 2016.

Shangyao Yan and Dah Hwei Yang. A decision support framework for handling schedule perturbation. *Transportation Research Part B: Methodological*, 30(6):405–419, 1996.

Joyce W Yen and John R Birge. A stochastic programming approach to the airline crew scheduling problem. *Transportation Science*, 40(1):3–14, 2006.

Gang Yu, Michael Argüello, Gao Song, Sandra McCowan, and Anna White. A New Era for Crew Recovery at Continental Airlines. *Interfaces*, 33(1):5–22, 2003.

D. Zhang, H. H. Lau, and C. Yu. A two stage heuristic algorithm for the integrated aircraft and crew schedule recovery problems. *Computers & Industrial Engineering*, 87:436–453, 2015.

D. Zhang, C. Yu, J. Desai, and H. H. Lau. A math-heuristic algorithm for the integrated air service recovery. *Transportation Research Part B: Methodological*, 84:211–236, 2016.

Y. Zhang and M. Hansen. Real-Time Intermodal Substitution: Strategy for Airline Recovery from

Schedule Perturbation and for Mitigation of Airport Congestion. *Transportation Research Record*, 2052(1):90–99, 2008.

K. Zografos, Y. Salouras, and M. Madas. Dealing with the Efficient Allocation of Scarce Resources at Congested Airports. *Transportation Research Part C: Emerging Technologies*, 21(1):244–256, 2012.